MODULATING INSULIN-DEGRADING ENZYME ACTIVITY: IMPLICATIONS FOR IDENTIFYING ACTIVATORS THROUGH HIGH-THROUGHPUT SCREENING

by

SAYALI SHRIKANT KUKDAY

(Under the Direction of Walter K. Schmidt)

ABSTRACT

The insulin-degrading enzyme (IDE), a Zn^{2+}-dependent metalloprotease, degrades several physiologically important peptides including Aβ, a peptide involved in the pathogenesis of Alzheimer's disease. Enhancing IDE activity may be therapeutically beneficial because it would lead to increased clearance of Aβ thereby minimizing its toxic effects. In this study, small-molecule activators of IDE were identified by means of a high-throughput screen, using rat IDE and a synthetic fluorogenic reporter. The results demonstrate that IDE activators exhibit substrate and species specificity, which was observed upon comparing the effects of activators on various IDE orthologs and in the context of distinct reporters. The results of a high-throughput screen aimed at identifying small-molecule activators of human IDE using a novel Aβ synthetic fluorogenic reporter are also discussed. This study provides insight into the various considerations that should be taken into account during the design of high-throughput screens aimed at identifying IDE activators. This study also indicates that activators can be substrate-specific thereby minimizing the impact on other IDE substrates including insulin.

INDEX WORDS: Alzheimer's disease, Aβ, insulin-degrading enzyme, activator, protease, high-throughput screen, fluorescence, yeast, **a**-factor

MODULATING INSULIN-DEGRADING ENZYME ACTIVITY: IMPLICATIONS FOR IDENTIFYING ACTIVATORS THROUGH HIGH-THROUGHPUT SCREENING

by

SAYALI SHRIKANT KUKDAY

B.S., K.C. College, India 2005

M.S., The Institute of Science, India 2007

A Dissertation Submitted to the Graduate Faculty of The University of Georgia in Partial Fulfillment of the Requirements for the Degree

DOCTOR OF PHILOSOPHY

ATHENS, GEORGIA

2012

MODULATING INSULIN-DEGRADING ENZYME ACTIVITY: IMPLICATIONS FOR IDENTIFYING ACTIVATORS THROUGH HIGH-THROUGHPUT SCREENING

by

SAYALI SHRIKANT KUKDAY

Major Professor:	Walter K. Schmidt
Committee:	Claiborne V.C. Glover Marcus Fechheimer Lance Wells

Electronic Version Approved:

Maureen Grasso
Dean of the Graduate School
The University of Georgia
August 2012

DEDICATION

I dedicate this thesis to my parents, Mrs. Vaishali Kukday and Justice (Retd.) Shrikant Kukday, for believing in me and for their tremendous support and encouragement.

ACKNOWLEDGEMENTS

There are several people who have made significant contributions to this work. I would like to thank my advisor, Dr. Walter Schmidt for his constant support and guidance throughout my time in the PhD program. Other members on my committee, Dr. Claiborne Glover, Dr. Marcus Fechheimer and Dr. Michael Tiemeyer have always guided me in the right direction in research. I would also like to thank all the current and past members of the Schmidt lab, particularly, Dr. Surya Manandhar, Dr. Emily Hildebrandt, Betsy Burriss, Samar Aldrugh for their experimental contributions and stimulating intellectual discussions. I am grateful to Dr. Zachary Wood and the employees at the Bioexpression and Fermentation Facility (UGA) for access to instrumentation and technical guidance. Lastly, I would like to thank my family and friends for their constant and unrelenting support and encouragement without which this journey could not have been completed.

TABLE OF CONTENTS

Page

LIST OF TABLES

Page

LIST OF FIGURES

Page

CHAPTER 1

INTRODUCTION AND LITERATURE REVIEW

BACKGROUND

Alzheimer's Disease

Alzheimer's disease (AD) is a neurodegenerative disorder that is characterized by the progressive accumulation of the amyloid β (Aβ) peptide in the cerebral cortex and hippocampus. Patients suffering from AD present clinical symptoms such as progressive cognitive decline, memory loss, and neurodegeneration [1]. The German psychiatrist and neuropathologist, Alois Alzheimer, first discovered the disease in a 51-year old patient [2]. This patient displayed unique behavioral symptoms that could not be explained by the known diseases at the time. Upon further analysis of the brain sections after the patient's death, Alzheimer found significant neuronal loss and fibrillar deposits in places where the neurons were present [2]. These deposits were later found to consist of Aβ (extracellular and cerebrovascular) and Tau protein (intracellular). The Aβ peptide accumulates in the form of discrete structures known as amyloid plaques. These extracellular plaques were, for the longest time, thought to be the underlying cause for neurodegeneration and subsequent memory loss. It has been recently found that low molecular weight oligomers (aggregates) of Aβ are the neurotoxic species whereas deposition of Aβ into fibrillar forms may be a protective mechanism that guards against oligomer toxicity [3-5].

The incidence of the Alzheimer's disease in the United States is 5.4 million in 2012 and is predicted to double by 2050. AD ranks sixth as a leading cause of death in the United States [6]. Deaths related to AD have been on the increase over the years, in contrast with deaths due to other causes like heart disease and prostrate cancer. AD cases can be classified as Early Onset Alzheimer's Disease (EOAD) and Late Onset Alzheimer's Disease (LOAD). Mutations in the Amyloid Precursor Protein (APP) and presenilin genes PS1/PS2 are associated with EOAD and lead to increased production of Aβ [1]. EOAD typically affects individuals that are younger than 65 years of age and is sometimes diagnosed as early as at 30 years. Currently, approximately 200,000 people are living with EOAD. LOAD is thought to result from an imbalance between Aβ production and clearance [7]. LOAD cases represent more than 95% of the total AD cases and therefore, the underlying mechanisms that contribute to LOAD have been the focus of research for the past two decades.

The amyloid hypothesis

The amyloid hypothesis suggests that AD results from the progressive accumulation of Aβ into plaques and the formation of neurofibrillary tangles in the brain of patients [7, 8]. Aggregation of Aβ peptides into diffuse plaques followed by formation of fibrils was thought to cause progressive synaptic injury and neuronal loss. These plaques and tangles were also seen in boxers with dementia-pugilistica (DP) syndrome drawing a link between head trauma and AD [9]. The amyloid hypothesis was further supported by the discovery of mutations that increase production of pathogenic $A\beta_{1-42}$ in the *APP* gene on chromosome 21 followed by *PSEN1* and *PSEN2* on chromosomes 14 and 1, respectively [10]. So far, 32 mutations in *APP*, 185 in *PSEN1,* and 13 in *PSEN2* have been identified, most of which lead to an increase in Aβ production [11]. Recently it has been found, however, that soluble low molecular weight

oligomers of Aβ and not plaques are likely responsible for damage to neurons in Alzheimer's disease [3]. Although controversial, deposition into plaques is considered to be a clearance mechanism that prevents neuronal damage inflicted by Aβ oligomers [12]. Providing partial evidence in support of this clearance pathway, Giannakopoulos et al. found that there is no significant correlation between the number of amyloid plaques and neuronal loss or the degree of cognitive decline [13]. Oligomer toxicity has also been observed for other amyloidogenic proteins such as α-synuclein [14].

Aβ production

Aβ is generated through the sequential proteolytic processing of APP by the β- and γ-secretases. APP is a single pass transmembrane protein that is processed into three distinct fragments by the action of multiple proteases. The predominant pathway involves cleavage of APP by α-secretase within the Aβ sequence to generate soluble APPα (sAPPα) followed by the action of γ-secretase, which cleaves in the transmembrane region of APP to release small peptides 21-24 amino acids long and a large C-terminal fragment known as the APP Intracellular Domain (AICD). The peptides generated as a result of this processing pathway do not have a tendency to aggregate; hence this pathway is considered non-pathogenic. In an alternate pathway, β-secretase cleaves APP to release sAPPβ. This is followed by a second proteolytic step mediated by γ-secretase, which generates Aβ peptides that are 39-42 amino acids in length that are released into extracellular space, and AICD [15, 16]. The pathways that contribute to the production of Aβ are depicted in Figure 1.1.

For a long time, the widely accepted view was that APP processing is a random detrimental process that results in the formation and subsequent aggregation of Aβ into plaques. Recently though, the cleavage products have been found to serve specific physiological functions [17, 18].

This is exemplified by the finding that a triple knockout of APP and its homologs APLP1 and APLP2 is lethal in mice [19].

Aβ clearance

Soluble Aβ is normally cleared from the brain through one of three routes. First, the low-density lipoprotein receptor-related protein (LRP) binds Aβ directly or indirectly by binding Aβ in complex with apolipoprotein E (ApoE) or α2 macroglobulin (α2M). Aβ is thus transported across the blood-brain barrier (BBB) into peripheral circulation. Second, and somewhat controversial, the Aβ peptides deposit into plaques and fibrils that act as a sink to prevent neuronal damage caused by the Aβ oligomers. Last, the Aβ monomer can be degraded by several proteases, the most notable of which are the insulin-degrading enzyme (IDE) and neprilysin (NEP) [12]. The pathways that contribute to the production and clearance of Aβ are depicted in Figure 1.1. Degradation of the Aβ monomer can prevent oligomerization of the peptide, precluding subsequent neurotoxicity. Facilitating IDE-mediated degradation of Aβ is the main focus of this study.

Aβ aggregation

Aβ forms oligomers/ annular aggregates, protofibrils, and fibrils. In addition to these, multiple sub-species have been reported including paranuclei, globulomers, Aβ*56, and Aβ-derived diffusible ligands. Aβ oligomers or annular aggregates are spherical as seen by electron microscopy and can generally be distinguished from fibrils based on their antiparallel cross-β-sheet pattern where the angle between the adjacent β-strands (θ) is > 0° [20]. High-molecular weight oligomers have been known to form pore-like structures similar to bacterial toxins that can disrupt membranes and cause cell death due to the loss of calcium homeostasis [21].

Protofibrils are intermediates between oligomers and mature fibrils. They are usually < 400 nm long and < 10 nm wide and more curvilinear than mature fibrils. Protofibrils also lack the high order and periodic symmetry that mature fibrils possess. Mature fibrils are long, straight structures with very regular morphology that is visible by transmission electron microscopy. They also have a cross β-sheet structure with spacing between sheets ranging from 4.7-10 Å, although $\theta = 0°$. Fibrils are several micrometers in length and 10-20 nm in width. The axis is twisted at regular intervals; these areas are known as crossovers. Dyes such as Congo Red and Thioflavin T stain fibrils enabling them to be visualized by microscopy [20].

The conversion of Aβ from the oligomeric state to the fibrillar state has been a matter of debate for several years and is still unclear. Recent evidence suggests that fibril formation begins via a nucleation event in which Aβ peptides assemble into a spherical conformation. This stage is called seeding. Once a seed is formed, there is a slow nucleated conformational change that leads to the formation of fibrils [22]. Other reports have described nucleation as a rare event that occurs when three or four molecules expose their amyloid forming segments at the same time. This is followed by a rapid growth phase during which single molecules are added to the growing fibril one at a time [23].

AD therapies

Presently, there is no known cure for AD. Therapies that are currently prescribed to patients include drugs that alleviate disease symptoms such as memory loss, cognitive decline, and problems associated with thinking and reasoning. Symptomatic AD treatments fall into two categories: cholinesterase inhibitors and N-methyl-D-aspartate (NMDA) receptor antagonists. Donepezil (Aricet), rivastigmine (Exelon) and galantamine (Razadyne) work by inhibiting cholinesterase-mediated breakdown of cholinergic neurotransmitters, thus, prolonging their

action. Memantine (Namenda), an NMDA receptor antagonist, reduces calcium-mediated apoptosis caused by excessive release of glutamate. Vitamin E is also sometimes prescribed in combination with other therapies because its antioxidant properties slow the loss of normal cognitive function in AD patients. Although helpful, the effectiveness of these therapies lasts only for 6 to 12 months, and they work in only 50% of AD patients [6]. These numbers emphasize the importance of finding new treatments that could slow or even halt the progression of this devastating disease.

Immunotherapy as a novel treatment strategy for AD has been investigated over the past few years. This field was initiated by ELAN Pharmaceuticals when they reported a significant increase in antibody titers in PDAPP mice (overexpress a human APP carrying the mutation Val717Phe) that were immunized with human fibrillar Aβ in Freund's adjuvant compared to non-vaccinated controls. Since then, several mouse models have been evaluated for the effect of different forms of the Aβ vaccine, adjuvants, and vaccination routes. These studies have yielded similar results [1]. Another active immunization trial (Phase I) has been carried out by ELAN Pharmaceuticals in which they injected mild-to-moderate AD patients with $A\beta_{1-42}$ aggregates (AN1792). Increase in anti-Aβ titers was observed in more than 50% of the 80 patients after 1-3 inoculations with no obvious adverse effects. This study progressed to Phase II but was discontinued prematurely because 6% of the patients developed aseptic meningoencephalitis [24, 25]. Passive immunization strategies involving injection with anti-Aβ antibodies are also in clinical trials and have reached Phase III (e.g., Bapineuzumab, ELAN Pharmaceuticals). In phase II, Bapineuzumab had no significant effect on cognitive and functional endpoints in individuals who completed the study. The study is now in Phase III because it was unclear whether treatment with Bapineuzumab led to a negative or positive outcome [26]. Although

efforts to identify viable immunotherapeutic strategies to combat AD are ongoing, the field has met with limited success.

Another approach involves modulating the activity of apolipoprotein E (apoE) in the brain. The ε4 allele of apoE is considered to be a risk factor for AD [27]. Several strategies that target Aβ-dependent effects of apoE4 have been investigated including increasing expression of apoE in the brain in order to facilitate Aβ clearance thereby reducing brain Aβ levels. Other strategies are aimed at disrupting the interaction between apoE and Aβ by peptide analogs. Treatment with $A\beta_{12\text{-}28P}$, a non-toxic peptide that can cross the BBB results in reduced amyloid deposition in human APP transgenic mice. This peptide works by blocking the apoE/Aβ interaction [28]. Bexarotene, a Food and Drug Administration-approved retinoid X receptor (RXR) agonist, decreases Aβ levels in several transgenic mouse models of AD. The drug can cross the BBB and has a favorable safety profile. Bexarotene treatment leads to RXR-mediated increase in expression of apoE and its transporters ABCA1 and ABCG1. This results in increased formation of high-density lipoprotein particles that clear Aβ [29]. Bexarotene is currently in Phase I safety trial (http://gel-server1.cwru.edu/) and although the results seem promising, information on the drug's efficacy in humans remains unknown. Also, the effect of bexarotene on ApoEε4 needs to be investigated since this isoform is a risk factor for AD [30].

Several treatment strategies aimed at reducing Aβ production are also being pursued. Aβ is produced by the action of the aspartic proteases β- and γ-secretase. OM99-2, a transition-state analog of a β-secretase substrate and a potent inhibitor has been studied for its Aβ-lowering properties. Structure-based design of OM99-2 derivatives has led to the development of inhibitors that can cross the BBB and reduce brain Aβ production in mice. Although many inhibitors have been discovered through structural design and many other strategies, their

efficacy has been hindered by problems such as oral availability and brain penetration [31]. A γ-secretase inhibitor LY411575 (Eli Lilly) is active at low to subnanomolar range in cell-based assays. Aβ levels in the brain decreased in transgenic mice when given a dose as low as 0.3 mg/kg [32]. The greatest reduction was observed in plasma Aβ levels, followed by cerebrospinal fluid (CSF) and brain. LY450139, a related compound, showed positive effect in Phase I and Phase II clinical trials although less than that seen with LY411575. In non-transgenic guinea pigs, LY450139 treatment resulted in a dose-dependent decrease in level of Aβ in plasma, CSF, and brain was observed [33]. Although effective, treatment with these drugs leads to adverse side effects. These effects include thymic atrophy and deterioration of intestinal epithelium due to a negative impact on lymphocyte and intestinal cell differentiation, respectively [34]. Similar effects are observed with genetic inhibition of the Notch signaling pathway, which suggests that they are associated with loss of γ-secretase activity.

Table 1.1 summaries the different strategies that have been assessed for the treatment of AD. The concern that other physiological functions of β- and γ-secretase would be affected if these activities were inhibited limits the utility of these approaches in the treatment of AD. Another viable AD treatment strategy involves facilitating clearance of the Aβ peptide through direct degradation by Aβ-cleaving proteases, especially the insulin-degrading enzyme.

Insulin-Degrading Enzyme (IDE)

IDE is a ~110 kDa protein and a member of the M16A subfamily of metalloproteases. IDE orthologs are widely distributed among prokaryotes and eukaryotes including bacteria (pitrilysin), yeast (Ste23p and Axl1p), invertebrates (*Ce*IDE), and mammals (*Rn*IDE and *Hs*IDE). The enzyme was first described almost 60 years ago as a protease from rat liver that inactivated insulin [35]. IDE is expressed in all tissues including pancreas, liver, muscle, kidney,

breast, and brain [36]. The reported subcellular localization of IDE varies widely. IDE is primarily present in the cytosol, but is also present in peroxisomes and endosomes and can be secreted [37]. Recently, the Aβ-cleaving activity of IDE has been detected in human serum [38]. IDE has an unusual inverted zinc-binding motif HXXEH, typical of proteases belonging to the M16A subfamily, that coordinates a catalytic Zn^{2+} ion. The enzyme has four homologous domains that contain alternating α-helices and β-strands [39]. The N- and C-terminal halves are shaped like a clam-shell enclosing the catalytic chamber and are connected via a 28 residue loop that acts like a hinge. The opening and closing of IDE-N and IDE-C is considered the rate-limiting step during peptide cleavage. The crystal structure of IDE is depicted in Figure 1.2. Mutations in residues that promote a constitutively open conformation, result in a 30- to 40-fold increase in IDE activity. IDE-N houses the active site that consists of the HXXEH motif and an exosite that binds and stabilizes the N-termini of substrates in a conformation suitable for cleavage [39].

IDE degrades a large number of small peptides that are diverse in both sequence and function. Some examples of IDE substrates include insulin, Aβ, glucagon, atrial natriuretic factor, transforming growth factor-α (TGF-α), amylin, and insulin-like growth factor II (IGF II) [37, 39, 40]. Although these substrates are diverse in sequence, they share certain features that make them conducive for cleavage by IDE. First, they possess the ability to form β-sheet interactions with the catalytic site of the enzyme. Second, the N-terminus of the substrates interacts with the exosite to facilitate binding of substrate in the right conformation. Third, most IDE substrates are <50 amino acids long because of the relatively small size of the catalytic chamber (~13000 $Å^3$). Last, negatively charged peptides make excellent substrates for IDE, whereas positively charged peptides encounter repulsive forces exerted by the positively charged

IDE-C [39]. Certain cleavage site preferences have been predicted for IDE. The enzyme cleaves on the amino side of basic or hydrophobic residues [41].

In solution, IDE exists in equilibrium between monomer, dimers and tetramers, the most active form being the dimer, which has 1.6-fold more activity than the tetramer [42]. Substrates of IDE activate the enzyme by binding to one subunit of the dimer and thus increasing the affinity of the other subunit for the substrate [42]. This allosteric activation can occur in a homotropic manner (substrate activation) or heterotropic manner (activation by molecules and peptides other than substrates). The individual subunits of the IDE dimer are capable of independent activity, although there is communication between the subunits. This communication can occur through either a cis mechanism at a distal site within the same subunit or a trans mechanism involving the other subunit. Structural changes are at the base of these interactions, which require the enzyme to be in its dimeric form since a monomeric variant of IDE loses its allosteric properties [42-45].

IDE and AD

A link between IDE and AD was discovered when the locus for the IDE gene (10q25) was implicated in the pathogenesis of AD [46]. Subsequently, other studies have demonstrated that loss-of-function mutations in IDE correlate with increased Aβ levels in type 2 diabetic rats [47]. IDE knockout mice have significantly reduced ability to degrade Aβ (50% of wildtype) and increased cerebral accumulation of $A\beta_{1-40}$ and $A\beta_{1-42}$ [48]. Suggestive of therapeutic potential, a two-fold overexpression of IDE in APP transgenic mice increases insulin-inhibitable Aβ degrading activity by ~100% and decreases plaque burden by ~50% [49]. There is also inverse correlation between IDE levels and intracellular Aβ levels in CHO cells expressing a 695 amino acid isoform of APP. IDE overexpression significantly reduces secreted and intracellular

levels of Aβ in CHO-695 cells [50]. Collectively, the evidence described above suggests that enhancing IDE activity has potential to attenuate Alzheimer's disease pathology.

Enzyme activators

Research efforts generally focus on discovery of enzyme inhibitors as therapeutic agents in disease. Discovery of enzyme activators as therapeutic agents is a new and challenging field, and hit-rates from high-throughput screens tend to be lower than those of traditional inhibitor screens [51]. Interest in the discovery of pharmacological activators has gained momentum, with the earliest reports of such agents published within the past decade [52]. To date, about a dozen enzyme activators have been discovered either fortuitously or through high-throughput screening efforts.

These activators fall into one of four general categories depending on the mechanism of activation [51]. The first category includes small molecules that directly bind and activate the enzyme monomer via allosteric binding sites. These sites are more difficult to predict in comparison to inhibitors, which are most commonly substrate analogs or compounds that bind to an enzyme's active site leading to inhibition. The glucokinase activator, compound A, binds to an allosteric site thus stabilizing the enzyme in an active conformation [53]. The second category includes small molecules that bind the proenzyme and induce auto-proteolysis leading to formation of active enzyme. On binding to the proenzyme form, procaspase-3 activator 1541 promotes the auto-proteolysis of some molecules, which in turn activate other procaspase molecules through a positive feedback mechanism [54]. Activators that fall into the third category bind and displace a regulatory subunit on the enzyme leading to exposure of the active site. A-769662, an AMPK activator, binds to the β- and γ-subunits of the kinase preventing the dephosphosphorylation of an important residue (Thr-172) that is essential for its activation [55].

The fourth category includes small molecules that modulate the oligomerization state of an enzyme leading to activation. For example, RNase L activators, C1 and C2, increase enzyme activity by inducing dimerization [56]. The activators mentioned above have EC_{50} values ranging from 2 to 99 μM and have been shown to be effective in cell-based assays [51].

Most drug discovery research on Alzheimer's disease is focused on developing β- and γ-secretase inhibitors, but there are problems associated with this approach. For example, inhibiting γ-secretase could impact γ-secretase-dependent Notch signaling that is important for lymphocyte development [34]. An alternate approach involves activating IDE to cleave and neutralize the toxic Aβ species. We hypothesize that agents that can enhance the ability of IDE to cleave and neutralize Aβ toxicity could provide an alternative therapeutic avenue for drug discovery.

Current efforts to develop activators of IDE have led to the discovery of compounds like Suramin, an anti-trypanosomal drug that has been patented as an activator of IDE [57] though no data on its IDE-activating properties has been published so far. Anti-hypertensive drugs like Valsartan have also recently been reported as having IDE activating properties in primary neuron cultures as well as in AD mice [58]. ATP also activates IDE, though this effect is mediated by the triphosphate moiety rather than the ATP molecule as a whole [59]. Recently, two small molecule activators of IDE have been reported [60]. These activators require the presence of ATP for activation. In addition, the activators fail to enhance cleavage of Aβ unless the original non-Aβ substrate used for compound identification is present in the reaction [60]. The study also lacks data concerning specificity of the activators or their effect *in vivo*. These observations suggest a need for better design of Aβ-based reporters so that the results from a high-throughput screen can be translated to the native peptide.

Yeast as a model system for the study of M16A metalloproteases

The budding yeast *Saccharomyces cerevisiae* has long been used in various industrial processes involving fermentation. Over the years, yeast has gained increasing importance as a model system in the fields of genetics, cell biology, and metabolism. Several unique characteristics make this organism ideal for use in research. First, it is a unicellular eukaryote having signaling pathways that are present in more complex eukaryotes. Second, yeast have a short doubling time (1.5 hours), making it easy to grow and maintain cultures. Lastly, genetic manipulation in yeast is straightforward due to the ability to propogate the haploid form of the organism.

Yeast can exist as both haploid as well as diploid forms. Haploid yeast can either reproduce asexually through mitotic division or sexually through mating [61]. The two haploid mating types (**a** and α) secrete mating pheromones (**a**- and α-factor, respectively). These pheromones bind to Ste2p and Ste3p receptors present on **a** and α cells, respectively, and lead to cell cycle arrest in the G1 phase. Following this arrest, genes that are required for the fusion process are transcribed. The cells develop projections toward each other leading to contact and eventual fusion of the two cells to form a diploid. Diploid cells are stable and cannot mate, though they can undergo meiosis to form four haploid cells through a process called sporulation [61]. The stages of the yeast life cycle are shown in Figure 1.3.

a-Factor is encoded as a 36 amino acid precursor (encoded by the *MFA1* gene) that undergoes several post-translational modifications to form the mature pheromone, which is a dodecapeptide. The first step in **a**-factor precursor processing involves addition of a farnesyl moiety to the cysteine of the C-terminal *CaaX* motif (C-cysteine, a-aliphatic amino acid, X-one of several amino acids). The aaX tripeptide is then cleaved by one of two proteases, Rce1p and

Ste24p. The C-terminal cysteine gets carboxymethylated by Ste14p. There are also two successive cleavages that occur at the N-terminus. The first of these cleavages is mediated by Ste24p, while the yeast M16A metalloproteases Axl1p and Ste23p mediate the second cleavage to produce mature **a**-factor, which is then secreted via an ABC transporter protein Ste6p [62-64].

IDE homologues, from species as diverse as bacteria (pitrilysin), eukaryotes such as *Caenorhabditis elegans* (*Ce*IDE), and mammals like rat (*Rn*IDE), can recognize the **a**-factor precursor as a substrate [65, 66] (Burriss and Schmidt, unpublished observation). This observation makes yeast a convenient cellular system to monitor the activities of these enzymes. A typical assay involves measuring the amount of **a**-factor produced by the recombinant strain through genetic methods or bioassays (e.g., the ability to mate or cause growth arrest in α cells) [65]. The processing pathway of the **a**-factor precursor is depicted in Figure 1.4. IDE orthologs can substitute for the yeast M16A enzymes Axl1p and Ste23p at step 5.

SUMMARY AND HYPOTHESIS

Alzheimer's disease is considered a devastating neurodegenerative disorder that currently has no cure. There is great need for treatments that could prevent or slow the progression of the disease. The Aβ hypothesis proposes that AD results from an imbalance of the production and clearance of the Aβ peptides. Therapies aimed at reducing Aβ production, however, have certain inherent problems associated with them. IDE represents a novel attractive therapeutic target due to its ability to degrade the Aβ monomer and thus prevent the formation of toxic aggregates of the peptide.

In these studies, we have identified several small-molecule activators of *Rn*IDE, characterized these molecules in terms of their specificity for and interaction with IDE, their effect on IDE activity *in vivo*, and on IDE isolated from other species (*Ce*IDE). We have also attempted to identify activators of human IDE (*Hs*IDE). These studies provide a better understanding about the process of identifying IDE activators using a high-throughput screening approach and also inform the design of synthetic reporters used to measure IDE activity.

REFERENCES

1. Jakob-Roetne, R. and H. Jacobsen, *Alzheimer's disease: From pathology to therapeutic approaches.* Angew Chem Int Ed, 2009. **48**: p. 3030-3059.
2. Stelzmann, R.A., H.N. Schnitzlein, and F.R. Murtagh, *An english translation of Alzheimer's 1907 paper, "Über eine eigenartige Erkankung der Hirnrinde".* Clin Anat, 1995. **8**: p. 429-431.
3. Walsh, D.M., et al., *Naturally secreted oligomers of amyloid β protein potently inhibit hippocampal long-term potentiation in vivo.* Nature, 2002. **416**(6880): p. 535-539.
4. Mucke, L., et al., *High-level neuronal expression of $A\beta_{1-42}$ in wild-type human Amyloid Protein Precursor transgenic mice: Synaptotoxicity without plaque formation.* J Neurosci, 2000. **20**(11): p. 4050-4058.
5. Walsh, D.M., et al., *The oligomerization of Amyloid β-protein begins intracellularly in cells derived from human brain.* Biochemistry, 2000. **39**(35): p. 10831-10839.
6. Association, A.s., *Alzheimer's Disease Facts and Figures.* Alzheimers Dement, 2011. **7**(2): p. 208-244.
7. Hardy, J. and D.J. Selkoe, *The amyloid hypothesis of Alzheimer's disease: Progress and problems on the road to therapeutics.* Science, 2002. **297**: p. 353-356.
8. Hardy, J.A. and G.A. Higgins, *Alzheimers disease: The amyloid cascade hypothesis.* Science, 1992. **256**(5054): p. 184-185.
9. Roberts, G.W., D. Allsop, and C. Bruton, *The occult aftermath of boxing.* J Neurol Neurosurg Psychiatry, 1990. **53**: p. 373-378.

10. Tanzi, R.E. and L. Bertram, *Twenty years of the Alzheimer's disease amyloid hypothesis: A genetic perspective.* Cell, 2005. **120**: p. 545-555.

11. Cruts, M. and C. Van Broeckhoven, *Molecular genetics of Alzheimer's disease.* Ann Med, 1998. **30**(6): p. 560-565.

12. Tanzi, R.E., R.D. Moir, and S.L. Wagner, *Clearance of Alzheimer's Aβ peptide: The many roads to perdition.* Neuron, 2004. **43**: p. 605-608.

13. Giannakopoulos, P., et al., *Tangle and neuron numbers, but not amyloid load, predict cognitive status in Alzheimer's disease.* Neurology, 2003. **60**: p. 1495-1500.

14. Cremades, N., et al., *Direct observation of the interconversion of normal and toxic forms of α-synuclein.* Cell, 2012. **149**: p. 1048-1059.

15. Selkoe, D.J., *Deciphering the genesis and fate of amyloid-β protein yields novel therapies for Alzheimer's disease.* J Clin Invest, 2002. **110**: p. 1375-1381.

16. Zhang, Y., et al., *APP processing in Alzheimer's disease.* Mol Brain, 2011. **4**(3): p. 1-13.

17. Laurén, J., et al., *Cellular prion protein mediates impairement of synaptic plasticity by amyloid-β oligomers.* Nature, 2009. **457**(7233): p. 1128-1132.

18. Nikolaev, A., et al., *APP binds DR6 to trigger axon pruning and neuron death via distinct caspases.* Nature, 2009. **457**: p. 981-989.

19. Heber, S., et al., *Mice with combined gene knock-outs reveal essential and partially redundant functions of Amyloid Precursor Protein family members.* J Neurosci, 2000. **20**(21): p. 7951-7963.

20. Fändrich, M., *Oligomeric intermediates in amyloid formation: Structure determination and mechanisms of toxicity.* J Mol Biol, 2012.

21. Lashuel, H.A., et al., *Amyloid Pores from pathogenic mutations.* Nature, 2002. **418**: p. 291-291.

22. Lee, J., et al., *Amyloid-β forms fibrils by nucleated conformational conversion of oligomers.* Nat Chem Biol, 2012. **7**(9): p. 602-609.

23. Eisenberg, D. and M. Jucker, *The amyloid state of proteins in human diseases.* Cell, 2012. **148**: p. 1188-1203.

24. Hawkes, C.A. and J. Mclaurin, *Immunotherapy as treatment for Alzheimer's disease.* Expert Rev Neurother, 2007. **7**(11): p. 1535-48.

25. Nicoll, J.A.R., et al., *Neuropathology of human Alzheimer disease after immunization with amyloid-β peptide: a case report.* Nat Med, 2003. **9**(4): p. 448-452.

26. Salloway, S., et al., *A phase 2 multiple ascending dose trial of bapineuzumab in mild to moderate Alzheimer disease.* Neurology, 2009. **73**: p. 2061-2070.

27. Cedazo-Mínguez, A., *Apolipoprotein E and Alzheimer's disease: molecular mechanisms and therapeutic opportunities.* J Cell Mol Med, 2007. **11**(6): p. 1227-1238.

28. Yang, J., et al., *Blocking the apolipoprotein E/amyloid-β interaction reduces fibrillar vascular amyloid deposition and cerebral microhemorrhages in TgSwDI mice.* J Alzheimers Dis, 2011. **24**: p. 269-285.

29. Cramer, P.E., et al., *ApoE-directed therapeutics rapidly clear β-amyloid and reverse deficits in AD mouse models.* Science, 2012. **335**: p. 1503-1506.

30. Cedago-Minguez, A., *Apolipoprotein E and Alzheimer's disease: molecular mechanisms and therapeutic opportunities.* J Cell Mol Med, 2007. **11**(6): p. 1227-1238.

31. Ghosh, A.K., M. Brindisi, and J. Tang, *Developing β-secretase inhibitors for treatment of Alzheimer's disease.* J Neurochem, 2012. **120**(Suppl s1): p. 71-83.

32. Best, J.D., et al., *Quantitative measurement of changes in Amyloid-β(40) in the rat brain and cerebrospinal fluid following treatment with the γ-secretase inhibitor LY-411575 [N2-[(2S)-2-(3,5- Difluorophenyl)-2-hydroxyethanoyl]-N1-[(7S)-5-methyl-6-oxo- 6,7-dihydro-5H-dibenzo[b,d]azepin-7-yl]-L-alaninamide]*. J Pharmacol Exp Ther, 2005. **313**(2): p. 902-908.

33. Lanz, T.A., et al., *Concentration-dependent modulation of Amyloid-β in vivo and in vitro using the γ-secretase inhibitor, LY-450139.* J Pharmacol Exp Ther, 2006. **319**(2): p. 924-933.

34. Wong, G.T., et al., *Chronic treatment with the γ-secretase inhibitor LY-411,575 inhibits β-amyloid peptide production and alters lymphopoiesis and intestinal cell differentiation.* J Biol Chem, 2004. **279**(13): p. 12876-12882.

35. Vaughan, M., *The inactivation of insulin by an enzyme from rat liver.* Biochim Biophys Acta, 1954. **15**(3): p. 432-433.

36. Yfanti, C., et al., *Expression of metalloprotease insulin-degrading enzyme insulysin in normal and malignant human tissues.* Int J Mol Med, 2008. **22**: p. 421-431.

37. Duckworth, W.C., R.G. Bennett, and F.G. Hamel, *Insulin degradation: Progress and potential.* Endocr Rev, 1998. **19**(5): p. 608-624.

38. Liu, Z., et al., *Characterization of insulin degrading enzyme and other amyloid-β degrading proteases in human serum: A role in Alzheimer's disease?* J Alzheimers Dis, 2012. **29**(2): p. 329-340.

39. Shen, Y., et al., *Structures of human insulin-degrading enzyme reveal a new substrate recognition mechanism.* Nature, 2006. **443**: p. 870-874.

40. Guo, Q., et al., *Molecular basis for the recognition and cleavages of IGF-II, TGF-α and amylin by human insulin-degrading enzyme.* J Mol Biol, 2010. **395**: p. 430-443.

41. Song, E.S., et al., *Analysis of the subsite specificity of rat insulysin using fluorogenic peptide substrates.* J Biol Chem, 2001. **276**(2): p. 1152-1155.

42. Song, E.S., et al., *Substrate activation of insuling-degrading enzyme (insulysin).* J Biol Chem, 2003. **278**(50): p. 49789-49794.

43. Song, E.S., D.W. Rodgers, and L.B. Hersh, *A monomeric variant of insulin degrading enzyme (IDE) loses its regulatory properties.* PLoS One, 2010. **5**(3): p. e9719.

44. Noinaj, N., et al., *Identification of allosteric regulatory site of insulysin.* PLoS One, 2011. **6**(6): p. e20864.

45. Song, E.S., D.W. Rodgers, and L.B. Hersh, *Mixed dimers of insulin-degrading enzyme reveal a cis activation mechanism.* J Biol Chem, 2011. **286**(16): p. 13852-13858.

46. Bertram, L., et al., *Evidence for genetic linkage of Alzheimer's disease to chromosome 10q.* Science, 2000. **290**(5500): p. 2302-2303.

47. Farris, W., et al., *Partial loss-of-function mutations in insulin-degrading enzyme that induce diabetes also impair degradation of amyloid β-protein.* Am J Pathol, 2004. **164**(4): p. 1425-1434.

48. Farris, W., et al., *Insulin-degrading enzyme regulates the levels of insulin, amyloid β-protein, and the β-amyloid precursor protein intracellular domain in vivo.* Proc Natl Acad Sci USA, 2003. **100**(7): p. 4162-4167.

49. Leissring, M.A., et al., *Enhanced proteolysis of β-Amyloid in APP transgenic mice prevents plaque formation, secondary pathology, and premature death.* Neuron, 2003. **40**: p. 1087-1093.

50. Sudoh, S., M.P. Frosch, and B.A. Wolf, *Differential effects of proteases involved in intracellular degradation of amyloid β-protein between detergent-soluble and -insoluble pools in CHO-695 cells.* Biochemistry, 2002. **41**(4): p. 1091-1099.

51. Zorn, J.A. and J.A. Wells, *Turning enzymes ON with small molecules.* Nat Chem Biol, 2010. **6**: p. 179-188.

52. Grimsby, J., et al., *Allosteric activators of Glucokinase: Potential role in diabetes therapy.* Science, 2003. **301**: p. 370-373.

53. Kamata, K., et al., *Structural basis for allosteric regulation of the monomeric allosteric enzyme human glucokinase.* Structure, 2004. **12**: p. 429-438.

54. Wolan, D.W., et al., *Small-molecule activators of a proenzyme.* Science, 2009. **326**: p. 853-858.

55. Sanders, M.J., et al., *Defining the mechanism of activation of AMP-activated protein kinase by the small molecule A-769662, a member of the thienopyridone family.* J Biol Chem, 2007. **282**(45): p. 32539-32548.

56. Thakur, C.S., et al., *Small-molecule activators of RNase L with broad-spectrum antiviral activity.* Proc Natl Acad Sci USA, 2007. **104**(23): p. 9585-9590.

57. Adessi, C., et al., *Activator for Insulin Degrading Enzyme*, W.I.P. Organization, Editor. 2006.

58. Wang, J., et al., *Valsartan lowers brain β-amyloid protein levels and improves spatial learning in a mouse model of Alzheimer disease.* J Clin Invest, 2007. **117**(11): p. 3393-3402.

59. Song, E.S., et al., *ATP effects on insulin-degrading enzyme are mediated primarily through its triphosphate moiety.* J Biol Chem, 2004. **279**(52): p. 54216-54220.

60. Cabrol, C., et al., *Small-molecule activators of insulin-degrading enzyme discovered through high-throughput compound screening.* PLoS One, 2009. **4**(4): p. e5274.

61. Herskowitz, I., *Life cycle of the budding yeast Sacchromyces cerevisiae.* Microbiol Rev, 1988. **52**(4): p. 536-553.

62. Adames, N., et al., *Role of yeast insulin-degrading enzyme homologs in propheromone processing and bud site selection.* Science, 1995. **270**(5235): p. 464-467.

63. Chen, P., et al., *Biogenesis of Saccharomyces cerevisiae mating pheromeone **a**-factor.* J Cell Biol, 1997. **136**(2): p. 251-269.

64. Fujimura-Kamada, K., F.J. Nouvet, and S. Michaelis, *A novel membrane-associated metalloprotease, Ste24p, is required for the first step of NH2-terminal processing of the yeast **a**-factor precursor.* J Cell Biol, 1997. **136**(2): p. 271-285.

65. Kim, S., et al., *Yeast as a tractable genetic system for functional studies of the insulin-degrading enzyme.* J Biol Chem., 2005. **280**(30): p. 27481-27490.

66. Alper, B.J., T.E. Nienow, and W.K. Schmidt, *A common genetic system for functional studies of pitrilysin and related M16A proteases.* Biochem J, 2006. **398**(1): p. 145-52.

67. Michaelis, S. and W.K. Schmidt, *Axl1p protease*, in *Handbook of Proteolytic Enzymes*. 2004, Elsevier Academic Press. p. 879-882.

Table 1.1. *Strategies for the treatment of AD.*

Class of drugs	Examples	Mode of action	Reference
Acetylcholinesterase inhibitors	Donepezil, Rivastigmine, Galantamine	Inhibit the enzyme that breaks down cholinergic neurotransmitters	Alzheimer's Association, 2012
NMDA receptor antagonist	Memantine	Prevents excessive release of glutamate by blocking the NMDA receptor	Alzheimer's Association, 2012
Immunotherapeutics	AN1792, Bapineuzumab	Active (Aβ peptide) or passive (Aβ antibody) immunization for AD patients	Hawkes et al., 2007 Nicoll et al., 2003 Salloway et al., 2009
β-secretase inhibitors	OM99-2, GRL-8234	Inhibit the enzyme responsible for the first of two cleavages needed to release Aβ	Ghosh et al., 2012 Chang et al., 2011
γ-secretase inhibitors	LY450139	Inhibit the enzyme responsible for the second cleavage that releases Aβ	Imbimbo, 2008
IDE activators	Valsartan	Activate the protease that degrades and clears the Aβ monomer	Wang et al., 2007
ApoE	Bexarotene $A\beta_{12\text{-}28P}$	Induces ApoE expression Blocks ApoE/Aβ interaction	Cramer et al., 2012 Yang et al., 2011

Figure 1.1. *Pathways involved in the production and clearance of Aβ.*

A) Aβ is generated as a result of sequential processing of the amyloid precursor protein (APP) by β- and γ-secretases. The predominant pathway, however, involves cleavage of APP by α-secretase leading to generation of non-toxic peptides. Mem: membrane; AICD: APP Intracellular Domain.

B) Aβ is normally cleared through one of three pathways: receptor uptake facilitating transport across the blood-brain barrier, oligomerization leading to formation of plaques and fibrils, and direct proteolytic degradation of the Aβ monomer. LRP: Low density lipoprotein receptor-related protein; ApoE: Apolipoprotein E; IDE: Insulin-Degrading Enzyme; NEP – Neprilysin. Figure 1.1 has been adapted from Tanzi *et al* (2004) [12].

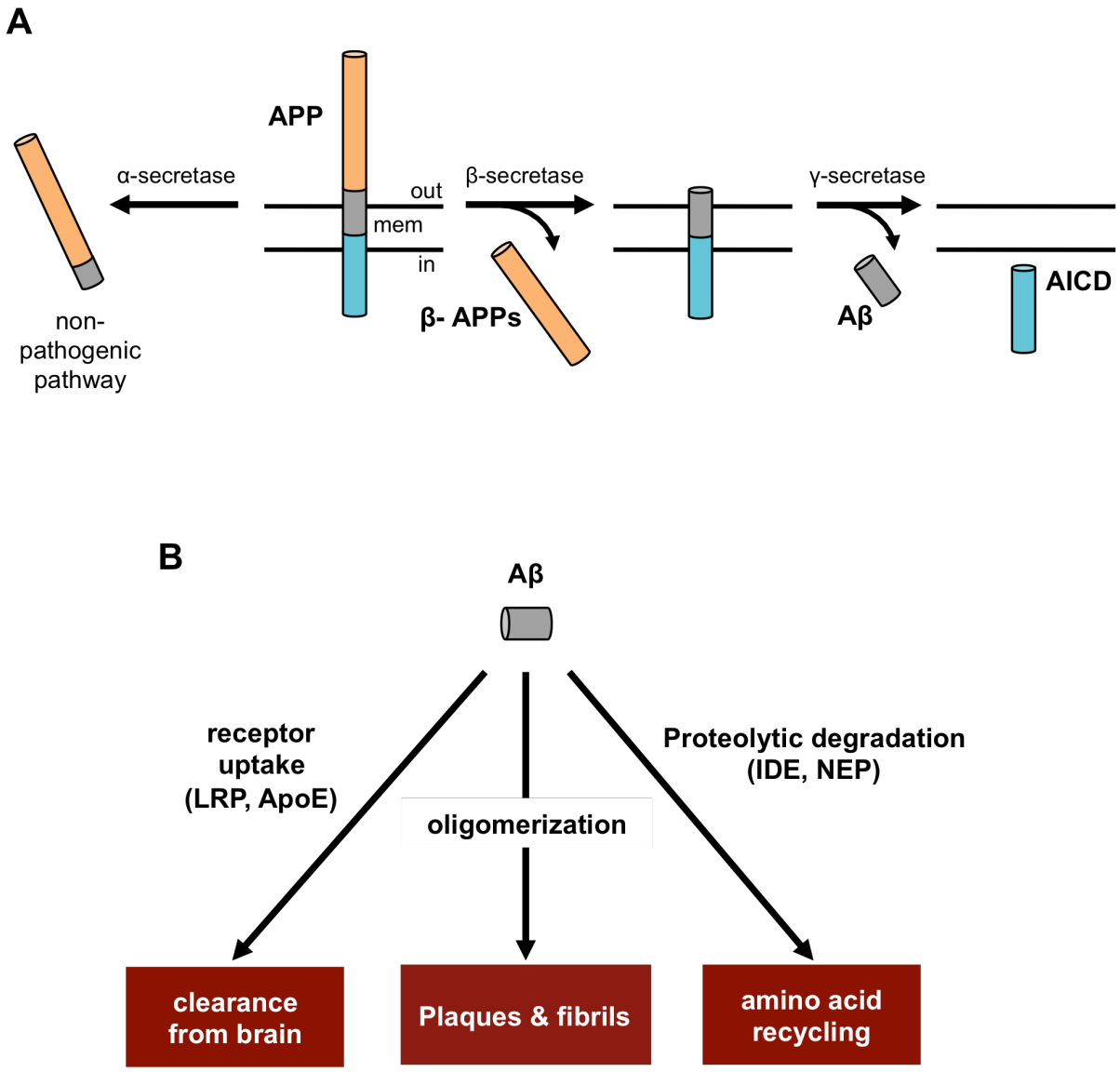
A
APP
α-secretase
out
mem
in
β-secretase
γ-secretase
non-
pathogenic
pathway
β- APPs
Aβ
AICD
B
Aβ
receptor
uptake
(LRP, ApoE)
oligomerization
Proteolytic degradation
(IDE, NEP)
clearance
from brain
Plaques & fibrils
amino acid
recycling

Figure 1.2. *Structure of IDE.*

IDE is a Zn^{2+}-dependent metalloprotease that is shaped like a clam-shell with its N-terminal and C-terminal halves enclosing a catalytic chamber that is about 1100 $Å^3$ in size. Substrate proteolysis occurs in the following sequence: The chamber opens to let substrates into the catalytic site, closes to allow for degradation, opens again to release proteolytic fragments. The N-terminal half contains an exosite that binds to and stabilizes the N-termini of substrates in a position that aligns the cleavage site (P1-P1´) with the catalytic site (S1-S1´). This image of *Rn*IDE was obtained by modifying the PDB file 3P7L using PyMOL molecular visualization software [44]. N: N-terminus, C: C-terminus.

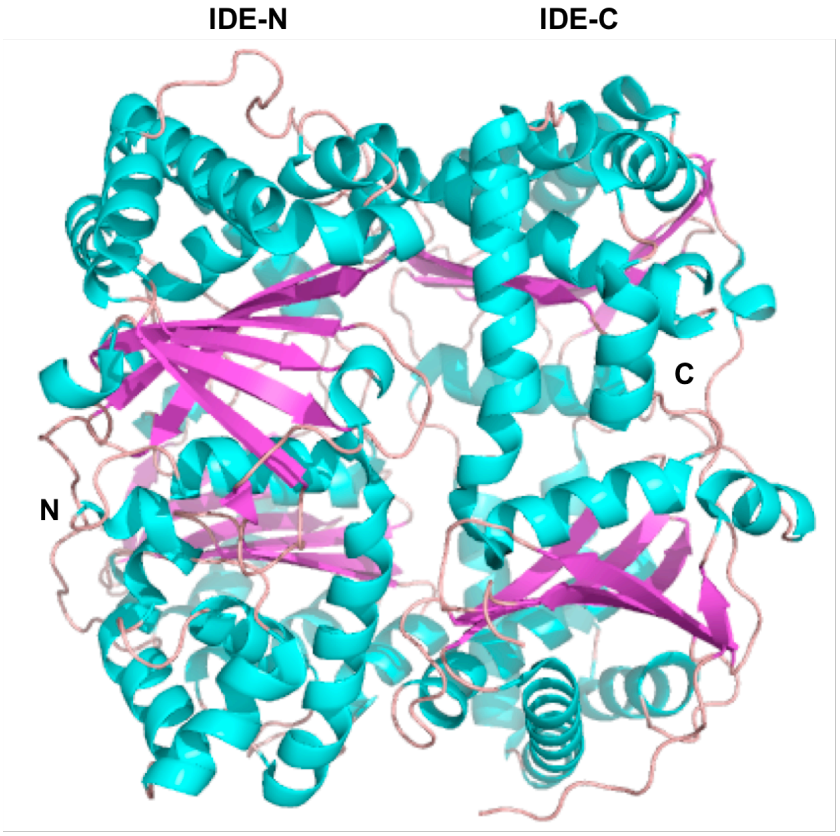
IDE-N
IDE-C
C
N

Figure 1.3. *Life cycle of Saccharomyces cerevisiae.*

Saccharomyces cerevisiae is a budding yeast that can exist in the haploid or diploid state. The haploid cells (**a** and α) secrete mating pheromones (**a**-factor and α-factor, respectively). These pheromones are received by receptors on the opposite cell type that trigger signaling pathways resulting in several changes. The two cells develop projections toward one another and subsequently fuse to form a diploid. The diploid can undergo meiosis to form haploid cells through a process called sporulation.

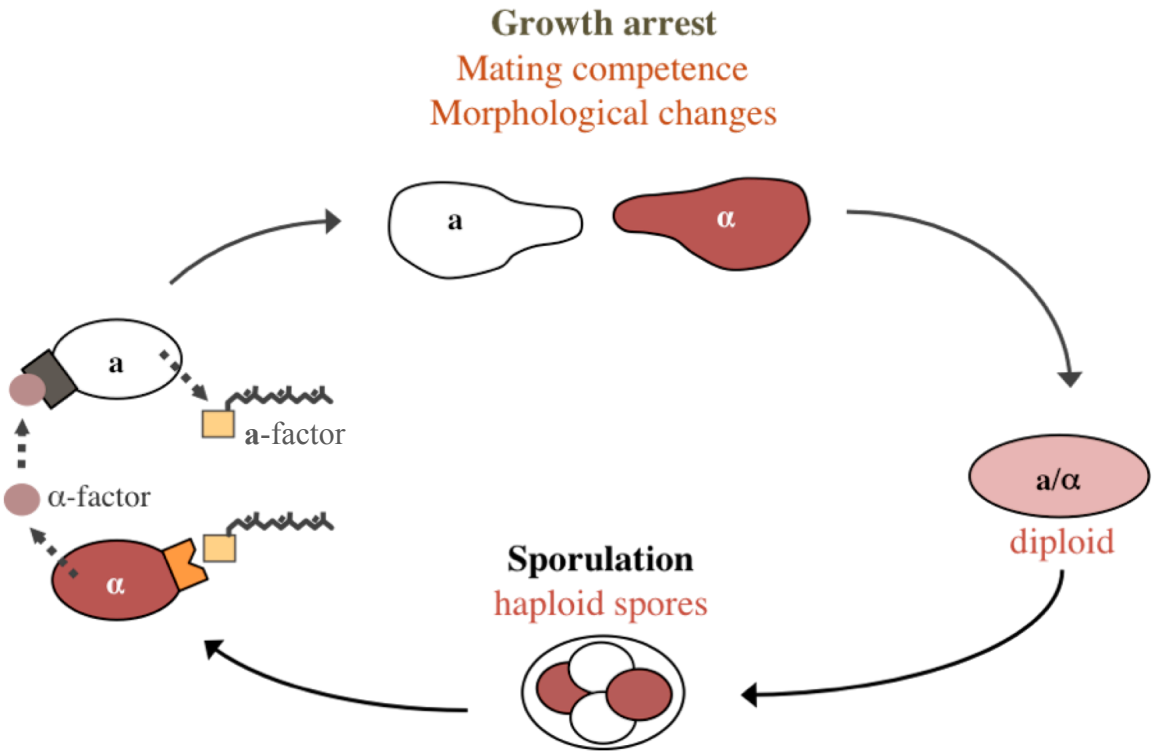
Growth arrest
Mating competence
Morphological changes
a
α
a
a-factor
α-factor
α
a/α
diploid
Sporulation
haploid spores

Figure 1.4. *Steps in the **a**-factor precursor processing pathway.*

The yeast **a**-factor precursor (P0) undergoes a series of post-translational modifications before being secreted as a mature pheromone (M). These modifications include farnesylation, aaX cleavage, and carboxylmethylation (steps 1-3) directed by a *CaaX* motif present at the C-terminal end, and proteolytic removal of an N-terminal extension (steps 4-5). The mature **a**-factor obtained as a result of these modifications is exported out of the cell through a dedicated pheromone transporter (step 6). The enzymes that catalyze each step of the pathway and their respective functions are indicated. P0*, P1, P2: **a**-factor intermediates; M: mature pheromone. This figure has been modified from Michaelis and Schmidt (2004) [67].

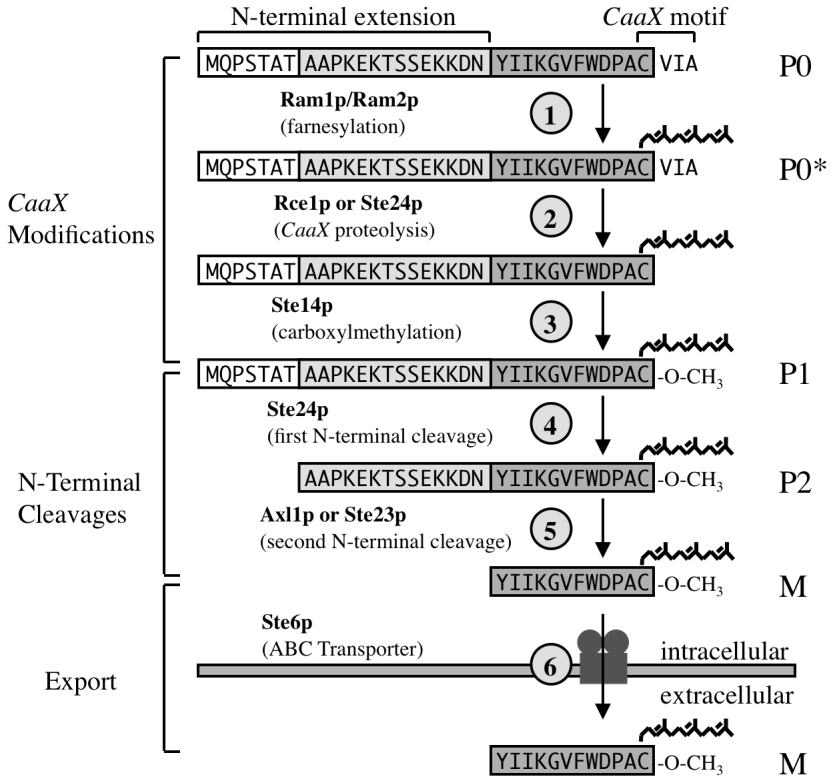
N-terminal extension
CaaX motif
MQPSTAT
AAPKEKTSSEKKDN
YIIKGVFWDPAC
VIA
P0
Ram1p/Ram2p
(farnesylation)
1
P0*
CaaX
Modifications
Rce1p or Ste24p
(CaaX proteolysis)
2
Ste14p
(carboxylmethylation)
3
-O-CH3
P1
Ste24p
(first N-terminal cleavage)
4
P2
N-Terminal
Cleavages
Axl1p or Ste23p
(second N-terminal cleavage)
5
M
Ste6p
(ABC Transporter)
6
intracellular
extracellular
Export
M

CHAPTER 2

CELL-PERMEABLE, SMALL MOLECULE ACTIVATORS OF THE INSULIN-DEGRADING ENZYME[1]

[1] Kukday, S.S.*, Manandhar, S.P.*, Ludley, M.C., Burriss, M.E., Alper, B.J. and W.K. Schmidt. 2012. Accepted by *Journal of Biomolecular Screening*. Reprinted here with permission of publisher.
*Equal contribution by these authors

ABSTRACT

The insulin-degrading enzyme (IDE) cleaves numerous small peptides, including biologically active hormones and disease-related peptides. The propensity of IDE to degrade neurotoxic Aβ peptides marks it as a potential therapeutic target for Alzheimer's disease. Using a synthetic reporter based on the yeast **a**-factor mating pheromone precursor, which is cleaved by multiple IDE orthologs, we identified seven small-molecules that stimulate rat IDE activity *in vitro*. Half-maximal activation of IDE by the compounds is observed *in vitro* in the range of 43-198 μM. All compounds decrease the K_M of IDE. Four compounds activate IDE in the presence of the competing substrate insulin, which disproportionately inhibits IDE activity. Two compounds stimulate rat IDE activity in a cell-based assay, indicating that they are cell permeable. The compounds demonstrate specificity for rat IDE since they do not enhance the activities of IDE orthologs, including human IDE, and they appear specific for **a**-factor-based reporters since they do not enhance rat IDE-mediated cleavage of Aβ-based reporters. Our results suggest that IDE activators function in the context of specific enzyme-substrate pairs, indicating that the choice of substrate must be considered in addition to target validation in IDE activator screens.

INTRODUCTION

According to the Aβ hypothesis, Aβ peptides contribute to Alzheimer's disease (AD) by serving as a source of neurotoxicity. It remains unclear whether neurotoxicity stems from accumulation of the monomeric, oligomeric (ADDLs), and/or fibrillar forms of Aβ [1]. Independent of the neurotoxic species, strategies aimed at reducing Aβ levels hold promise for the treatment of AD. Since biosynthetic and clearance activities regulate steady state Aβ levels, either or both activities could be manipulated to reduce Aβ. While most research on Aβ has centered on its production (i.e. the α, β, and γ secretases), several mechanisms are known to clear Aβ [2].

One prominent Aβ clearance mechanism involves proteolytic cleavage of the Aβ monomer, which eliminates its ability to form higher order structures. The insulin-degrading enzyme (IDE; EC 3.4.24.56) is one of several Aβ-cleaving enzymes; others include neprilysin, plasmin, matrix metalloprotease-9, angiotensin converting enzyme, and endothelin converting enzyme [2]. In animal models, IDE deficiency correlates with increased Aβ levels and increased risk of Alzheimer's disease (AD), while IDE over-expression appears to protect against AD [3, 4]. Genetic linkage and biochemical analyses also strongly support a connection between IDE and AD [5, 6]. IDE also cleaves other small molecules (e.g. insulin, glucagon, and amylin) that can adopt β secondary structure and form amyloid fibrils [7].

IDE belongs to the M16A family of zinc-dependent metalloproteases, which are evolutionarily widespread and highly conserved in sequence and structure [8, 9]. An inverted zinc-binding motif is characteristic of this family. The recent elucidation of several M16A enzyme structures, including that of human IDE, pitrilysin (*E. coli*), and the related M16C

enzyme PreP1 (*A. thaliana*), reveals a structure resembling that of a clamshell in which substrates form b-sheet contacts with β-strands of IDE [8, 9]. Members of the M16A family can recognize each others' substrates as evident by the ability of mammalian IDE and pitrilysin to substitute for the yeast M16A enzymes Axl1p and Ste23p in production of the yeast **a**-factor mating pheromone [10, 11] and the ability of Ste23p and pitrilysin to cleave Aβ [12, 13].

The proposed physiological role of IDE in Aβ clearance has led to the hypothesis that its hyperactivation could be therapeutically beneficial. Studies of IDE involving under and over-expression in transgenic mice support this hypothesis [3, 4]. Small molecule activators of IDE can thus be considered potential therapeutic agents, and several such molecules have been reported [14, 15]. Nucleotide triphosphates (i.e. ATP) activate IDE to cleave certain small substrates other than Aβ. This effect occurs at ATP concentrations (i.e. 0.1-1 mM) much higher than that thought to exist physiologically in the extracellular environment where Aβ is supposedly proteolyzed by IDE (i.e. 5-50 nM) but within the range expected intracellularly (4-5 mM) [16, 17]. ATP-dependent enhancement of IDE activity does not involve ATP hydrolysis; the effect is also buffer dependent [14]. High throughput screening (HTS) has identified two additional small molecule activators of IDE [15]. Curiously, these molecules enhance IDE-mediated cleavage of an Aβ reporter only when the synthetic non-Aβ HTS substrate is also present. The synthetic compound suramin has also been indicated as an IDE activator [18]. To date, data pertaining to its effectiveness as an IDE activator or AD therapeutic has not been released.

In this study, we report seven chemical activators of IDE that were identified by HTS from a pharmacophore-rich small molecule library provided by the NIH Developmental Therapeutics Program. We demonstrate the ability of identified compounds to enhance the activity of rat IDE

toward both synthetic and natural peptides based on the yeast **a**-factor mating pheromone. We also describe a novel internally quenched Aβ-based reporter useful for direct measurement of Aβ-cleaving activity. The results we present in this study collectively demonstrate the existence of cell permeable, substrate and species-specific activators of IDE.

EXPERIMENTAL

Peptides

Two synthetic substrates were used to monitor the *in vitro* activities of the IDE orthologs evaluated in this study. One was an internally quenched, fluorogenic peptide Abz-SEKKDNYIIKGV-NitroY-OH (AnaSpec, Inc., San Jose, CA; CHI Scientific, Inc., Maynard, MA), where Abz is aminobenzoic acid and NitroY is 3-nitro-tyrosine. The peptide is based on the sequence flanking the M16A cleavage site found in the yeast **a**-factor precursor. It was used for the activator screen and for monitoring activities since it is recognized by multiple IDE orthologs, including rat IDE, yeast Ste23p, worm IDE, bovine trypsin, and Pronase E; human IDE does not recognize this substrate. The second IDE substrate was the internally quenched, fluorogenic peptide H_2N-DAEFRHDSGYEVHHQK^{DABCYL}LVFFAE^{EDANS}DVGSNK-OH (CHI Scientific, Maynard, MA), where K^{DABCYL} is ε-DABCYL-L-lysine and E^{EDANS} is EDANS-L-glutamate. The peptide, based on the $A\beta_{1-28}$ sequence, was used for monitoring activities of rat, human, and worm IDE. Powder forms of both peptides were resuspended in DMSO (10 mM) and stored at -80 °C. Diluted 2X working stock solutions (100 μM) were heated to 65 °C for 3 min then cooled to room temperature prior to use. Product formation was measured using a BioTek Synergy microtiter plate reader equipped with 320/420 nm and 320/485 nm

excitation/emission filter sets, respectively.

The substrates used to monitor activities of yeast Rce1p and yeast Ste24p were internally quenched, fluorogenic, farnesylated peptide substrates that are based on the K-Ras C-terminus [19, 20]. Product formation for these substrates was measured using a 320/420 nm excitation/emission filter set.

Recombinant enzymes and other reagents

Plasmids encoding rat and yeast Ste23p have been described [13, 21]. The plasmid encoding human IDE was constructed by amplifying the human IDE open reading frame from plasmid IDE-pSRα using oligos designed to encode a 6X-His tag at the N-terminus and restriction sites for subcloning the PCR product into the *Xba*I and *Not*I sites of pET30b(+) (Novagen) [22]. The plasmid encoding *C. elegans* IDE was constructed by amplifying the cDNA sequence of F44E7.4 from the RB1 cDNA library by PCR and subcloning into the *Xba*I and *Not*I sites of pET30b(+) [23]. Recombinant rat, human, *C. elegans*, and yeast IDE were inducibly expressed in BL21 (DE3) *E. coli* and recovered by immobilized nickel affinity chromatography (IMAC) essentially as previously described [13, 21]. Purified IDE was stored at -80 °C as 1 mg/ml aliquots in Storage Buffer (50 mM HEPES, 140 mM NaCl, 20% glycerol, pH 7.4 or 25 mM KPi, 200 mM NaCl, 20% glycerol, pH 7.6). Membranes containing yeast Rce1p or yeast Ste24p activity were prepared as previously described [20]. Bovine trypsin, Pronase E, Proteinase K, ATP, BSA, and human recombinant insulin were all from Sigma-Aldrich. Ia1 and Ia2 were from Key Organics (London, UK).

Chemical library

The Diversity Set compound library was obtained through the NIH Developmental

Therapeutics Program (DTP) [24]. This compound library contains 1,981 compounds with unique pharmacophore characteristics that were reduced from a parent set of over 70,000 compounds with the use of the 3D structure generation program Chem-X (Chemical Design Ltd.; Mahwah, NJ).

High-throughput screen

Assays were conducted in the wells of a black, clear bottom, 96-well microtiter plate (Costar, Corning Inc., NY) in 0.1 M potassium phosphate buffer (KPi), pH 7.6. The fully assembled reactions contained rat IDE (10 μg/ml), compound (100 μM), and **a**-factor-based substrate (50 μM). The assay protocol involved mixing the enzyme and substrate in a 1:1 ratio after the enzyme was preincubated for 10 min at 37 °C with a unique compound from the DTP library. Product fluorescence was monitored for each well over a 60 min timecourse. The 15-30 min window of the assay was typically used to determine rate of reaction. Compounds yielding IDE activity ≥150% relative to the DMSO-treated control were preliminarily assigned as activators (n = 33; 1.67% hit rate). Detailed examination of hits identified compounds that altered the baseline fluorescence and/or enhanced the fluorescence intensity of the fluorophore, generating false positives. Thus, observed fluorescence values were normalized by first subtracting the baseline fluorescence of the substrate in the presence of compounds then dividing observed rates of reaction by the maximum fluorescence of the sample observed after complete digestion of the substrate by a mixture of trypsin (5 μg/ml) and pronase E (10 μg/ml). Compounds yielding ≥150% activity relative to a DMSO-treated control after normalization were designated as activators for follow-up studies (n=8; 0.4% hit rate). One of these compounds (**4**) was subsequently dropped from analysis due to no observed impact on the kinetic parameters of rat IDE and inconsistency between experiments.

Chemical analyses

The structures of the identified IDE activators were rendered in ChemBioDraw Ultra (v. 11.0, CambridgeSoft, Cambridge, MA). Molecular weight, Log *P*, and other QSAR values were calculated using the Analysis and Chemical Properties tools of ChemBioDraw. Additionally, molecular weights of the compounds were confirmed by ESI analysis (Proteomic and Mass Spectrometry Core Facility, University of Georgia) using an API I Plus, PE Sciex, mass spectrometer (Perkin Elmer, Waltham, MA) in positive or negative ion mode depending on the biophysical properties of the compounds. All samples were dissolved in methanol for ESI analysis.

Target specificity analyses

The effects of compounds on the activities of other enzymes were assessed using methods similar to that outlined above for HTS. Reaction rates were determined in triplicate after a 10 min preincubation with 100 μM compound. Single dose effects on rat IDE (10 μg/ml), Ste23p (10 μg/ml), trypsin (0.5 μg/ml), and pronase E (0.5 μg/ml) were determined using the **a**-factor-based peptide using conditions outlined above, with the exception that Ste23p activity was assayed at 30 °C. Effects on Rce1p and Ste24p activities were determined using yeast-derived microsomes (250 μg/ml) enriched for these enzymes and a K-Ras-based peptide [20]. In all cases, activity values were normalized using the trypsin/pronase approach described above and are reported relative to a DMSO-treated control that was set at 100% within each enzyme set.

Dose-response, kinetic, and other assays

Values for dose-response curves were determined according to the conditions outlined above (i.e. KPi buffer) using a range of activator concentrations (up to 1 mM) and trypsin/pronase

normalization. Half-maximal activating concentration values (AC_{50}) were derived from best-fit curves obtained by plotting the data points in Prism 4.0 (GraphPad Software, Inc.). For compounds lacking sigmoidal dose response curves, the concentration resulting in half-maximal activation ($[Max]_{50}$) was used.

Data for kinetic analyses was determined over a range of substrate concentrations (0-750 μM) in the absence and presence of activator (100 μM). Data collected was subjected to non-linear regression analysis in Prism 4.0 to extract kinetic parameters. Curves were fitted using the equation $Y = V_{max}*X/[K_M+X]$. Because internal quenching effects were observed with the **a**-factor based substrate at concentrations ≥30 μM, activities observed at these concentrations were multiplied by a correction factor for the purposes of kinetic analysis (Figure 2.S1).

The effects of BSA, ATP, insulin, and buffer composition were determined in the context of 50 μM **a**-factor-based substrate. BSA assays were performed in 0.1 M KPi, pH 7.6 containing 0.01% BSA; dose response curves contained 0-0.5% BSA [25]. ATP assays were performed in 50 mM Tris, pH 7.5 containing 1 mM ATP and 0.1% BSA; dose response curves contained 0-10 mM ATP in either 0.1 M KPi, pH 7.6 or 50 mM Tris, pH 7.5 containing 0.1% BSA [15]. Insulin competition experiments were performed in 0.1 M KPi, pH 7.6 containing 0.92 μM human recombinant insulin; dose response curves contained 0-17.4 μM insulin). The effect of activators on $A\beta_{1-28}$ cleavage was determined using 50 μM substrate in the presence of 100 μM of activator. In this case, Proteinase K was used to obtain complete cleavage of the $A\beta_{1-28}$ to obtain the maximum fluorescence amplitude. Human and *C. elegans* IDE were used at a concentration of 100 μg/ml and 10 μg/ml, respectively.

The activating properties of two previously reported IDE activators (Ia1 and Ia2) were also evaluated for comparison to the hits obtained in this study [15]. They were evaluated as for the

single-dose target specificity studies described above using previously reported concentrations of Ia1 (50 μM) and Ia2 (10 μM).

Enzyme-chemical interaction studies

For determining thermal melt profiles, a solution of recombinant rat IDE (0.5 μM) and SYPRO Orange (5x working solution diluted from a 5000x stock solution; Sigma) was prepared in 0.1 M KPi, pH 7.6 and dispensed as 100 μl aliquots into a 96-well plate (HSP-9601; MJ Research) containing DMSO or a candidate activator (100 μM). The wells were overlayed with 10 μl of mineral oil and incubated in the dark at room temperature for 60 min. Samples were heated from 28 to 70 °C (Δt increment = 1-3 °C) and fluorescence measured (465 nm excitation, 590 nm emission) at appropriate intervals using a FluoDia T70 high temperature fluorescence plate reader (Photon Technology International). Thermal melt mid-points (T_m) were determined from a fluorescence vs. temperature plot that was fit to a 4-parameter sigmoidal dose response (variable slope) equation using PRISM software. Similar results were obtained when IDE was evaluated in 0.1 M HEPES buffer, pH 7.5 containing 150 mM NaCl.

For native PAGE profiles, rat IDE (0.5 μg) was preincubated with compound (100 μM) for 60 min at 37 °C, mixed with equal volume of 2X native gel sample buffer (0.1% bromophenol blue, 20% glycerol, 0.6 M Tris-HCl, pH 6.8), and analyzed by 10% native-PAGE at 4 °C. Gels were stained with silver and scanned using a flat bed scanner.

Yeast strains and plasmids

The yeast strains used in this study were IH1783 (*MAT***a** *trp1 leu2 ura3 his4 can1*), y272 (*MAT***a** *trp1 leu2 ura3 his4 can1 axl1::LEU2 ste23::LEU2*), and RC757 (*MAT*α *sst2-1*) [26-28]. Plasmid-bearing versions of these strains were generated according to published methods [29].

Strains were grown at 30 °C using YEPD or synthetic complete dropout (SC-) medium [27]. Plasmids pRS316 (*CEN URA3*), pWS192 (*2μ TRP1 MFA1*), pWS491 (*2μ URA3* P_{PGK}*-RnIDE),* and pWS496 (*2μ URA3* P_{PGK}*-RnIDE::2HA*) have been reported [10, 30, 31].

Yeast toxicity assay

To determine whether compounds could exert their activating effects *in vivo*, it was first critical to determine whether any were cytotoxic, which would complicate *in vivo* analyses. The effect of compounds on yeast growth was assessed by determining the density of compound-treated cultures after incubation for 44 hours at 30 °C. Briefly, a saturated starter culture of yeast y272 co-transformed with pWS192 and pWS496 was diluted (1:2000) into SC-UW, split into equal volume aliquots (1 ml), and aliquots treated with DMSO or compound (100 μM). Each condition was evaluated in triplicate, and the average absorbance observed for each condition after 44 hours was calculated as a percentage of that observed for the DMSO-treated condition, which was set at 100%. To obtain accurate measurements of culture densities, saturated cultures were typically diluted ten-fold, and A_{600} values obtained were expressed as percent of untreated. Where toxicity was observed, a lower dose allowing for saturated growth after 44 hours of incubation at 30 °C was empirically determined. For compounds that retained toxicity at these lower concentrations, the yeast cultures were grown for 72 hrs to allow saturated growth.

a-Factor production assay

A bioassay was used to assess the impact of compounds on the ability of IDE to promote **a**-factor production [10]. The assay entails the recovery and enrichment of secreted **a**-factor from cultures of *MAT***a** yeast (y272 co-transformed with pWS192 and pWS496) followed by an assessment of bioactivity to judge potency of the recovered pheromone. Cultures were grown to

saturation (72 hrs at 30 °C) as described above in the presence of DMSO or compound (100 μM or highest non-toxic dose), except that 5 ml volumes were used. The recovered pheromone was spotted as a 2-fold serial dilution on a thin lawn of RC757 (*MATα sst2-1*) yeast. The amount of **a**-factor activity observed for each sample was normalized to the cell density of the original culture as determined from A_{600} absorbance measurements of appropriately diluted cultures. **a**-factor production for the DMSO-treated control was set at 100%. Culture densities did not vary significantly between compound and DMSO-treated cultures (Kukday and Schmidt, unpublished observation).

RESULTS

An a-factor-based internally quenched fluorogenic peptide is cleaved by IDE

The yeast mating pheromone **a**-factor is synthesized as a precursor that undergoes extensive post-translational processing, including isoprenylation, multiple proteolytic cleavages, and carboxylmethylation (Figure 2.1A). One of the cleavage events is mediated by the yeast M16A proteases, with Axl1p having a predominant role in this process relative to Ste23p [13, 28]. We have previously documented that yeast is a convenient system for functional studies of heterologously expressed M16A enzymes [10, 11]. In this system, the *in vivo* activity of an M16A enzyme is monitored by the production of the bioactive **a**-factor mating pheromone, which is measured using straightforward biological assays (Figure 2.1B). Given our observations, we hypothesized that an internally quenched fluorogenic peptide centered on the M16A cleavage site found within the **a**-factor precursor could serve as a suitable substrate for monitoring the *in vitro* activity of IDE and other M16A enzymes (Figure 2.1C). Indeed,

recombinant rat IDE cleaves such a peptide with a specific activity of 1.33 nmol/min/mg under our standard assay conditions (Figure 2.1D).

Identification of IDE activators by HTS

The assay described above was optimized for a 96-well format and used to screen the NIH Developmental Therapeutics Program (DTP) Diversity Set library for modulators of IDE activity [24]. Under the conditions of the screen, the assay had a calculated Z′-factor of 0.86 and a signal-to-noise ratio of 7.0. The compounds of the library had a variety of effects on IDE activity. Of the 1981 compounds within the DTP library, 451 partly inhibited IDE (<50% activity relative to untreated), and 1495 had minor impact on activity (50-150% activity observed). Two compounds could not be assessed due to strong quenching effects exerted on the substrate. Of specific interest were 33 compounds (1.7% hit rate) that enhanced the rate of fluorescence output ≥150% relative to that observed for DMSO-treated IDE; DMSO represents the solvent for the library collection and was used as a control. The set of hits was further reduced to 8 compounds after elimination of autofluorescing and fluorescence-enhancing compounds. An additional compound (**4**) was later removed for lack of an effect on the kinetic parameters of rat IDE and inconsistent behavior between experiments (Manandhar, Kukday and Schmidt, unpublished observation). The structures of the final seven hits (Figure 2.2) are represented by a variety of chemical scaffolds incorporating aromatics, heterocycles, charged groups, and aromatic systems.

The compounds all adhere to Lipinski's rule of 5 and have other drug-like characteristics [32]. The compounds range in mass from 188 to 472 Da (associated counterions excluded) (Table 2.S1). The most potent *in vitro* acting compound **3** had the lowest CLogP value (-6.04) and highest tPSA value (179.58). Although the hits were not re-synthesized or purchased

commercially through other sources, largely due to their unavailability, the activating potential of each hit was further confirmed in samples obtained through an independent request from the DTP. In all cases, HPLC revealed a single peak fraction, and subsequent LC-MS analyses revealed the major species to be of expected mass, with some minor species detected for compounds **1** and **8** (Figures 2.S2 and 2.S3).

Activators are IDE-specific

The impact of compounds (100 μM) on the activities of IDE and a select group of other proteases was examined (Table 2.1). The maximum activation of IDE observed was 356% (compound **3**), and several other compounds activated >200% (compounds **5**, **6** and **8**). By comparison, two previously reported IDE activators (Ia1 and Ia2) enhanced IDE activity to a lesser extent. The specificity of compounds was investigated by examining their ability to stimulate the activities of other proteases. Our analysis revealed no compound-induced activation of the yeast M16A enzyme Ste23p, bovine trypsin, or Pronase E. Similarly, no compound-induced activation was observed for the yeast *CaaX* proteases Rce1p and Ste24p, which catalyze a distinct proteolytic cleavage on the **a**-factor precursor [33]. While our enzyme panel was clearly not exhaustive, the inability of compounds to activate five other proteases, including a closely related ortholog, suggests that the compounds do not promiscuously activate enzymes. By contrast, partial inhibition (≤75% residual activity) was observed in a limited number of instances for Pronase (compound **5**) and the *CaaX* proteases (compounds **3** and **8**).

Dose-response and kinetic studies

The HTS screen for IDE activators used a fixed concentration of compound. To determine the optimal activating concentration of compounds, dose-response assays were performed.

Compounds **1**, **2**, **6**, and **7** yielded classic sigmoidal dose-responses from which AC_{50} values were calculated and found to be in the range 43-198 μM (Figure 2.2). Saturation with compound **1** was not achieved at the highest concentration tested (1 mM), but the data was sufficient for curve fitting. Compounds **3** and **8**, and possibly **5**, exhibited an inverted bell-shaped activation curve with an observable peak concentration and less activation at both lower and higher doses (i.e. a hormetic dose response). For these compounds, the lowest half maximal effective dose (i.e. $[Max]_{50}$) is reported. These values were in the range 62.5-125 μM.

Enzyme kinetic studies were performed in the presence of 100 μM compound. All compounds reduced the K_M of IDE, and all but compound **5** increased the V_{max} of IDE compared to that observed for a DMSO-treated control (Table 2.2). Compound **6** had the largest impact on K_M while compound **3** had the largest impact on V_{max}.

Compounds 3, 6 and 8 physically interact with IDE

To determine whether the activators interact with IDE to exert their effects, we performed two types of studies. First, we hypothesized that ligand binding would alter the biophysical properties of IDE in some manner. Thermal melt analyses revealed a substantial shift in the melting profile of IDE in the context of compound **3** only (Figure 2.3A). Second, we hypothesized that binding of activators might induce structural changes in the enzyme. Native PAGE analyses did not reveal a mobility shift in the context of compound **3** but did reveal a noticeable shift with compounds **6** and **8**, suggestive of a physical interaction (Figure 2.3B). The nature and strength of this interaction remains unknown and open for future investigation. We did not observe a mobility shift with ATP, which induces a measurable conformational change in IDE [34]. The differing results may be due to differences in the native-gel protocols.

Effect of assay conditions on activator potency

Promiscuous activation has been reported for certain enzyme/activator combinations [25]. Often, the activating effects of such compounds are mitigated in the presence of BSA or low concentrations of detergent. In the presence of low amounts of BSA (≤0.02%), a modest increase in IDE activity was observed (Figure 2.4A). The reason for this effect is unknown and could reflect stabilization of a more active form of IDE or better substrate/enzyme availability (i.e. less non-specific adsorption by plasticware). Importantly, all of the compounds retained their ability to activate IDE in the presence of an optimal dose of BSA (Figure 2.4B). The relative amount of activation observed was less than that observed in the absence of BSA (Table 2.1), which is due to the higher baseline activity of the BSA-treated control. Similarly, detergent treatment (0.1% CHAPS) also reduced, but did not completely neutralize compound-induced activation of IDE (Manandhar and Schmidt, unpublished observation).

Based on the fact that IDE can cleave multiple substrates, we investigated the ability of our compounds to hyperactivate IDE under mixed substrate conditions. The compounds were evaluated in the presence of insulin, which disproportionately inhibits IDE-mediated Aβ degradation [21]. The effect of insulin on degradation of the **a**-factor-based substrate was also disproportionate. Dose-response studies revealed that 10 μM insulin was sufficient to fully inhibit IDE activity in the presence of 50 μM **a**-factor-based substrate (Figure 2.4C). The observed IC_{50} for insulin was approximately 0.92 μM. We evaluated our compounds at the IC_{50} concentration of insulin and observed that only four compounds (**1**, **3**, **5**, **7**) retained their ability to stimulate IDE activity (Figure 2.4D).

Lastly, we examined whether our compounds were activating IDE in an ATP-like manner [14]. We expected this to be unlikely since ATP-dependent activation was not observed under

the assay conditions used for HTS. To resolve whether the lack of ATP-dependent activation was due to our substrate or assay conditions, we evaluated the effect of ATP under assay conditions where effects had been observed [14, 15]. The switch from a KPi buffering system to one containing Tris/BSA resulted in ATP-dependent activation of IDE, indicating that using KPi buffer indeed neutralizes ATP-dependent activation of IDE (Figure 2.4E). The maximum activating concentration in the Tris/BSA buffering system was approximately 1 mM. Evaluation of the activators under these conditions revealed that all the compounds, with the exception of compound **2**, displayed a significant additive effect in the presence of ATP (Figure 2.4F). Compound **5** was associated with the highest additive effect (>250% activity relative to ATP-only condition). Despite having the highest activating effect under KPi-buffered conditions, compound **3** marginally activated IDE in the presence of ATP (approximately 25% over ATP-only condition). Since a majority of the compounds displayed additive effects in the presence of ATP, we deduce that these compounds likely activate IDE by a mechanism distinct from that utilized by ATP. Our results also indicate that our compounds function in a buffer independent manner, unlike ATP, whose use is restricted to certain buffering systems.

Effect of activators on yeast growth and IDE-mediated production of a-factor

The ability of compounds to enhance IDE-mediated cleavage of an **a**-factor-based substrate *in vitro* led to the hypothesis that these compounds would enhance **a**-factor production *in vivo* when IDE is expressed heterologously as the only M16A enzyme in yeast. Prior to testing this hypothesis, we first evaluated whether compounds negatively impacted the viability of yeast. At a dose of 100 μM, compounds **1** and **3** did not substantially impact yeast saturation density (>90% relative to DMSO-treated control). Compounds **2**, **5** and **7** modestly decreased density (61-87% relative to DMSO-treated). Compound **6** and **8** completely inhibited growth. Dose

response studies revealed that treating cultures with lower concentrations of compounds (i.e. **5**, **6** and **8**) resulted in saturation after 44 hours (>90% relative to DMSO-treated culture). Compound **7** did not exhibit a dose-dependent response, and treated cultures did not achieve saturated growth at the lowest concentration evaluated (12.5 μM). In this case, extending the incubation period to 72 hours led to near saturation of the treated culture (>85% relative to DMSO-treated culture) (Kukday, Manandhar and Schmidt, unpublished observation).

Using conditions guided by the toxicity data, we next addressed whether any of the compounds could stimulate IDE-mediated **a**-factor production when added to yeast cultures. After 72 hours of incubation in the presence of 100 μM compound, most cultures achieved a saturated culture density; compounds **5**, **6** and **8** were used at 12.5 μM, 50 μM and 25 μM, respectively. The **a**-factor produced was isolated at the end of the treatment period and assayed for biological activity (Figure 2.5A). Quantification of amounts of **a**-factor produced revealed that compounds **3**, **5**, **6** and **8** enhanced **a**-factor production *in vivo* (Figure 2.5B), with compound **3** bringing about the most significant change. Unexpectedly, compounds **2** and **7** reduced the yield of **a**-factor produced.

Where changes in net **a**-factor production were observed, there were no significant differences in final culture density, thus ruling out this trivial explanation for the effect of compound treatment (Kukday and Schmidt, unpublished observation). To rule out the possibility that the activators were non-specifically enhancing **a**-factor recovery or mimicking **a**-factor biological activity, untreated cultures were grown to saturation and then treated with activators and incubated for an additional 24 hours. At the end of this incubation period, the cultures were processed for **a**-factor recovery. None of the compound-treated cultures showed a net increase in

a-factor production by comparison to a DMSO-treated control (Kukday and Schmidt, unpublished observation).

Substrate and species specificity of IDE activators

Although the synthetic and *in vivo* **a**-factor-based substrates described above are convenient reporters of IDE activity, we sought to examine the ability of compounds to enhance cleavage of a more physiologically relevant substrate. Hence, we designed a novel FRET-based reporter to evaluate *in vitro* cleavage of $A\beta_{1-28}$ (Figure 2.6A). Under the same reaction conditions used to evaluate our **a**-factor-based reporter (0.1 M KPi, pH 7.6), the K_M observed for rat IDE with the fluorogenic $A\beta_{1-28}$ substrate was 142.3 μM. All of the compounds identified as rat IDE activators in the context of the **a**-factor-based reporter, as well as Ia1 and Ia2 identified by Cabrol *et al*, failed to enhance rat IDE-mediated cleavage of this Aβ reporter (Figure 2.6B; Kukday and Schmidt, unpublished observation). Our compounds also failed to stimulate human and *C. elegans* IDE. Moreover, the compounds were unable to enhance rat IDE-mediated degradation of full-length $A\beta_{1-40}$ (Kukday and Schmidt, unpublished observation). The compounds were further unable to enhance *Ce*IDE-mediated cleavage of the **a**-factor reporter (Figure 2.6C). Human IDE did not recognize the **a**-factor-based substrate and could not be evaluated. Together, these findings indicate that the rat IDE activators reported here display substrate and species specificity.

DISCUSSION

IDE cleaves small amyloidogenic peptides [35]. Thus, the activation of IDE has been viewed as therapeutic for the clearance of Aβ [36]. Indeed, IDE over-expression reduces amyloid

deposits in the brain of APP transgenic mice [4]. IDE can also be rendered hyperactive through mutations that expose the active site for a longer period of time [9]. As documented by our findings and related studies, chemical activation of IDE is also feasible [15, 18]. We have identified seven small molecule activators of rat IDE that lower K_M of IDE, retain activation in the presence of a competing substrate (insulin), and are effective in an *in vivo* assay. The activators are structurally distinct from previously reported IDE activators, consistent with the possibility that there may be multiple modes of IDE activation.

An important and critical outcome of our study revolves around the use of non-native IDE substrates as reporters (i.e. **a**-factor). The fact that M16A enzymes have reciprocal substrate specificity suggested that any IDE substrate might have utility in identifying IDE activators. This observation drove our initial choice of **a**-factor-based reporters because of the potential for both *in vitro* and *in vivo* assay development. This direction, however, yielded rat IDE activators that did not enhance cleavage of an $A\beta_{1-28}$ reporter. The finding that Ia1 and Ia2 enhance IDE-mediated cleavage of the **a**-factor-based reporter but not the $A\beta_{1-28}$ reporter further lends support to the idea of substrate-specific activation. In the original study, these activators enhanced IDE-mediated Aβ degradation only when the non-native, high-throughput synthetic substrate was included in the reaction [15]. We posit that failure of compounds to enhance Aβ cleavage is an indication that compounds are substrate-specific. Should this indeed be the case for IDE activators in general, it may be feasible to identify activators that specifically enhance cleavage of Aβ over that of insulin and other IDE substrates, thereby limiting the potential negative impact on glucose homeostasis and other physiological pathways impacted by IDE.

We expect our current findings to provide guidance for future studies aimed at identifying IDE activators. Foremost, the observation that the compounds identified in this study do not

generally activate IDE orthologs emphasizes the importance of using the appropriate target enzyme (i.e. human IDE) in future high throughput screens aimed at generating therapeutic agents. Our study also provides evidence that a hormetic *in vitro* dose-response profile (e.g. compounds **3** and **5**) should not necessarily exclude an agent from being evaluated in cell-based assays. The underlying reason for the observed hormetic effect is unknown, but could reflect an issue as straightforward as solubility (i.e. precipitation at high concentrations) or as complicated as multiple binding sites (i.e. a high affinity activating site and a low affinity inhibitory site). We have also provided evidence that insulin affects the properties of IDE activators. In our case, several of our hits were adversely affected when insulin was present in the assay mixture. The impact of insulin and possibly other competing substrates on the activating potential of compounds should therefore be considered an important component of future activators screens. We have also provided the first example of potentially non-toxic activators of IDE, albeit toxicity was gauged against yeast cells. Nevertheless, we are encouraged by the observation that relatively non-toxic compounds exert positive effects on IDE activity both *in vitro* and in a cell-based system (e.g. compound **3**). By comparison, suramin is broadly toxic and non-specific, both activating and inactivating other enzymes [37, 38]. It also displays a hormetic response under our assay conditions (Manandhar and Schmidt, unpublished observation).

Perhaps the most important impact of our study will be on the design of future IDE reporters, which our study suggests should resemble Aβ as closely as possible. A key step toward this goal is our development of a FRET-based Aβ reporter. Our reporter is based on $A\beta_{1-28}$ with a strategically positioned quencher (DABCYL) and fluorophore (EDANS) on K16 and E22, respectively. Choice of the 1-28 peptide vs. a longer Aβ species was driven by the technical issues frequently reported for syntheses and storage of longer forms of Aβ [39]. Moreover,

residues beyond E23 lack ordered density in the IDE/$A\beta_{1-40}$ co-crystal structure (PDB 2g47), suggesting that they do not impact substrate binding [9]. K16 and E22 were chosen for side-chain modification because our analysis of the IDE/$A\beta_{1-40}$ co-crystal structure suggested that these residues are in reasonable proximity and could be modified without impairing interactions between Aβ and IDE. Importantly, the $A\beta_{1-28}$ reporter has a free N-terminus and thus retains an important exosite binding capability that is not found on other IDE HTS-compatible reporters (e.g. FAβB) [40]. An $A\beta_{1-28}$ reporter having an N-terminal fluorophore has been reported as a relatively poor IDE substrate, but specific data was not reported and direct comparison between the reporters is thus not possible [40]. We contend that N-terminal modifications may lead to binding interference at the IDE exosite and complicate the determination of kinetic parameters. We also acknowledge that the failure of our activators to enhance cleavage of the FRET-based $A\beta_{1-28}$ reporter could be indicative of interference by the EDANS and/or DABCYL moieties leading to inappropriate folding of the peptide. It is unknown whether alternative fluorophores and quenchers will yield similar results.

There are many examples of enzymes that are activated by biological small molecules (e.g. PKA by cAMP). There are, however, relatively few examples of enzymes that can be activated through synthetic small molecules. This list of enzymes is growing and includes notable targets such as glucokinase, AMP-activated protein kinase (AMPK), and the sirtuins [41]. IDE activators can now be added to the limited set of small molecule enzyme activators, and it is expected that our development of a FRET-based $A\beta_{1-28}$ reporter will help drive the identification of species and Aβ-specific activators of IDE.

ACKNOWLEDGEMENTS

We thank the Developmental Therapeutics Program (National Institutes of Health) for providing the Diversity Set compound library and the following (all at the University of Georgia) - Dr. Z. A. Wood for help with IDE purification and design of the $A\beta_{1-28}$ reporter, Dr. J. P. Rose for assistance with thermal shift studies, the Bioexpression and Fermentation Facility for help with HPLC analyses, Dr. T. M. Dore, and members of the Schmidt laboratory for critical discussions and technical assistance. This work was supported by grants from the Alzheimer's Drug Discovery Foundation / Institute for the Study of Aging (grant #271223 to WKS) and the National Institutes of Health (5R01GM067092 to WKS).

REFERENCES

1. Haass, C. and D.J. Selkoe, *Soluble protein oligomers in neurodegeneration: lessons from the Alzheimer's amyloid beta-peptide.* Nat Rev Mol Cell Biol, 2007. 8(2): p. 101-12.
2. Nalivaeva, N.N., et al., *Are amyloid-degrading enzymes viable therapeutic targets in Alzheimer's disease?* J Neurochem, 2012. 120(Suppl. 1): p. 167-185.
3. Farris, W., et al., *Insulin-degrading enzyme regulates the levels of insulin, amyloid beta-protein, and the beta-amyloid precursor protein intracellular domain in vivo.* Proc Natl Acad Sci U S A, 2003. 100(7): p. 4162-7.
4. Leissring, M.A., et al., *Enhanced proteolysis of beta-amyloid in APP transgenic mice prevents plaque formation, secondary pathology, and premature death.* Neuron, 2003. 40(6): p. 1087-93.
5. Kim, M., et al., *Decreased catalytic activity of the insulin degrading enzyme in chromosome 10-linked Alzheimer's disease families.* J Biol Chem, 2007. 282(11): p. 7825-32.
6. Miller, B.C., et al., *Amyloid-beta peptide levels in brain are inversely correlated with insulysin activity levels in vivo.* Proc Natl Acad Sci U S A, 2003. 100(10): p. 6221-6.
7. Becker, A.B. and R.A. Roth, *Insulysin and pitrilysin: insulin-degrading enzymes of mammals and bacteria.* Methods in Enzymology, 1995. 248: p. 693-703.
8. Johnson, K.A., et al., *The closed structure of presequence protease PreP forms a unique 10,000 Angstroms3 chamber for proteolysis.* Embo J, 2006. 25(9): p. 1977-86.
9. Shen, Y., et al., *Structures of human insulin-degrading enzyme reveal a new substrate recognition mechanism.* Nature, 2006. 443(7113): p. 870-4.

10. Kim, S., et al., *Yeast as a tractable genetic system for functional studies of the insulin-degrading enzyme.* J Biol Chem., 2005. 280(30): p. 27481-27490.

11. Alper, B.J., T.E. Nienow, and W.K. Schmidt, *A common genetic system for functional studies of pitrilysin and related M16A proteases.* Biochem J, 2006. 398(1): p. 145-52.

12. Cornista, J., et al., *Cleavage of various peptides with pitrilysin from Escherichia coli: kinetic analyses using beta-endorphin and its derivatives.* Biosci Biotechnol Biochem, 2004. 68(10): p. 2128-37.

13. Alper, B., J. Rowse, and W. Schmidt, *Yeast Ste23p shares functional similarities with mammalian insulin-degrading enzymes.* Yeast, 2009. 26(11): p. 595-610.

14. Song, E.S., et al., *ATP effects on insulin-degrading enzyme are mediated primarily through its triphosphate moiety.* J Biol Chem, 2004. 279(52): p. 54216-20.

15. Cabrol, C., et al., *Small-molecule activators of insulin-degrading enzyme discovered through high-throughput compound screening.* PLoS ONE, 2009. 4(4): p. e5274.

16. Farias, M., 3rd, et al., *Plasma ATP during exercise: possible role in regulation of coronary blood flow.* Am J Physiol Heart Circ Physiol, 2005. 288(4): p. H1586-90.

17. Kwak, J., et al., *Intracellular ATP increases capsaicin-activated channel activity by interacting with nucleotide-binding domains.* The Journal of Neuroscience, 2000. 20(22): p. 8298-8304.

18. Adessi, C., et al., *Activator for Insulin Degrading Enzyme*, W.I.P. Organization, Editor. 2006.

19. Hollander, I., E. Frommer, and R. Mallon, *Human ras-converting enzyme (hRCE1) endoproteolytic activity on K-ras-derived peptides.* Anal Biochem, 2000. 286(1): p. 129-37.

20. Porter, S.B., et al., *Inhibition of the CaaX proteases Rce1p and Ste24p by peptidyl (acyloxy)methyl ketones.* Biochim Biophys Acta, 2007. 1773(6): p. 853-62.

21. Alper, B. and W. Schmidt, *A capillary electrophoresis method for evaluation of Aβ proteolysis in vitro.* Journal of Neuroscience Methods, 2009. 178(.): p. 40-5.

22. Affholter, J.A., et al., *Insulin-degrading enzyme: stable expression of the human complementary DNA, characterization of its protein product, and chromosomal mapping of the human and mouse genes.* Mol Endocrinol, 1990. 4(8): p. 1125-35.

23. Barstead, R.J. and R.H. Waterston, *The basal component of the nematode dense-body is Vinculin.* J Biol Chem, 1989. 264(17): p. 10177-10185.

24. Holbeck, S.L., *Update on NCI in vitro drug screen utilities.* Eur J Cancer, 2004. 40(6): p. 785-93.

25. Goode, D.R., et al., *Identification of promiscuous small molecule activators in high-throughput enzyme activation screens.* J Med Chem, 2008. 51(8): p. 2346-9.

26. Chan, R.K. and C.A. Otte, *Isolation and genetic analysis of Saccharomyces cerevisiae mutants supersensitive to G1 arrest by a factor and alpha factor pheromones.* Mol. Cell. Biol., 1982. 2(1): p. 11-20.

27. Michaelis, S. and I. Herskowitz, *The a-factor pheromone of Saccharomyces cerevisiae is essential for mating.* Mol. Cell. Biol., 1988. 8(3): p. 1309-18.

28. Adames, N., et al., *Role of yeast insulin-degrading enzyme homologs in propheromone processing and bud site selection.* Science, 1995. 270: p. 464-67.

29. Elble, R., *A simple and efficient procedure for transformation of yeasts.* BioTechniques, 1992. 13: p. 18-20.

30. Sikorski, R.S. and P. Hieter, *A system of shuttle vectors and yeast host strains designed for efficient manipulation of DNA in Saccharomyces cerevisiae.* Genetics, 1989. 122(1): p. 19-27.

31. Chen, P., et al., *Biogenesis of the Saccharomyces cerevisiae mating pheromone a-factor.* J Cell Biol, 1997. 136(2): p. 251-69.

32. Lipinski, C., et al., *Experimental and computational approaches to estimate solubility and permeability in drug discovery and development settings.* Adv Drug Del Rev, 1997. 23: p. 3–25.

33. Tam, A., W.K. Schmidt, and S. Michaelis, *The multispanning membrane protein Ste24p catalyzes CAAX proteolysis and NH2-terminal processing of the yeast a-factor precursor.* J Biol Chem, 2001. 276(50): p. 46798-806.

34. Im, H., et al., *Structure of substrate-free human insulin-degrading enzyme (IDE) and biophysical analysis of ATP-induced conformational switch of IDE.* J Biol Chem, 2007. 282(35): p. 25453-63.

35. Kurochkin, I.V., *Amyloidogenic determinant as a substrate recognition motif of insulin-degrading enzyme.* FEBS Lett, 1998. 427(2): p. 153-6.

36. Selkoe, D.J., *Clearing the brain's amyloid cobwebs.* Neuron, 2001. 32(2): p. 177-80.

37. Kaur, M., et al., *Suramin's development: what did we learn?* Invest New Drugs, 2002. 20(2): p. 209-19.

38. McCain, D.F., et al., *Suramin derivatives as inhibitors and activators of protein-tyrosine phosphatases.* J Biol Chem, 2004. 279(15): p. 14713-25.

39. Zagorski, M., et al., *Methodological and Chemical Factors Affecting Amyloid Beta Peptide Amyloidogenicity*. Methods in Enzymology, 1999. 309(Amyloid, Prions, and Other Protein Aggregates): p. 189-204.

40. Leissring, M.A., et al., *Kinetics of amyloid beta -protein degradation determined by novel fluorescence- and fluorescence polarization-based assays.* J Biol Chem, 2003. 278(39): p. 37314-20.

41. Zorn, J.A. and J.A. Wells, *Turning enzymes ON with small molecules*. Nature chemical biology, 2010. 6(3): p. 179-187.

Table 2.1. *Activities of various proteases in the presence of rat IDE activators.*

Compounds (100 μM final concentration, unless otherwise indicated) were evaluated using fluorescence-based *in vitro* assays. Activities were normalized to that of the appropriate DMSO-treated control, which was set at 100%. Specific reaction conditions are described in the methods section. NSC – Cancer Chemotherapy National Service Center. ND – Not Determined, dash – no identifier.

		% Activity					
Compound	**NSC #**	**IDE**	**Ste23p**	**Trypsin**	**Pronase**	**Rce1p**	**Ste24p**
DMSO	-	100.0± 6.0	100.0±2.8	100.0 ±10.6	100.0±0.8	100.8± 0.8	100.0±16.0
1	2737	195.4±12.2	112.0±5.4	94.2± 0.3	100.9±0.1	89.7± 3.8	97.2±12.7
2	19139	170.3±16.0	117.2±2.8	115.1± 3.9	89.2±0.6	83.2± 3.4	93.0± 6.8
3	45208	356.0±16.0	90.4±0.6	99.3± 2.2	103.8±0.1	55.3± 1.0	74.7± 8.6
5	49713	263.5± 1.0	103.4±1.6	94.3± 5.4	65.3±3.6	101.2±11.0	131.4±18.8
6	95570	230.7±13.5	82±0.3	111.5± 2.8	104.4±0.0	90.1± 1.0	98.6± 9.9
7	122335	186.6± 7.4	102.1±1.7	111.0± 1.2	104.3±0.9	89.6± 2.4	92.8±13.1
8	150982	195.0±14.0	80.1±6.0	101.8± 1.8	93.3±1.8	60.6± 2.6	89.2±10.7
Ia1 (50 μM)	-	144.0± 5.0	ND	ND	ND	ND	ND
Ia2 (10 μM)	-	157.0± 8.0	ND	ND	ND	ND	ND

Table 2.2. *Kinetic assessment of activators.*

Compounds (100 μM final) were evaluated using the fluorescence-based *in vitro* assay in 0.1 M KPi buffer, pH 7.6. Kinetic parameters were derived using non-linear regression analysis in GraphPad Prism 4.0.

Compound	Km (μM)	Vmax (nmol/min/mg)
DMSO	183.7±25.94	154.8±12.26
1	107.7±6.42	194.1±5.85
2	117.9±9.04	164.2±6.4
3	122.1±6.08	267.9±6.7
5	148.8±23.67	127.8±10.41
6	92.2±7.7	176.3±7.35
7	148.3±20.07	194.1±13.81
8	123.8±13.14	185.0±9.73

Figure 2.1. *Reporters of M16A enzyme activity.*

A) Production of the yeast **a**-factor mating pheromone is dependent on the action of several proteases, including the M16A enzymes Axl1p and Ste23p.

B) Rat IDE can substitute for the yeast M16A enzymes in **a**-factor production *in vivo*. Yeast strain y272 (*MAT***a** *axl1*Δ *ste23*Δ) was transformed with an IDE-encoding plasmid (pWS491) or an empty vector (pRS316), and resultant strains were evaluated for their ability to produce **a**-factor. A wild type *MAT***a** strain (IH1783) transformed with an empty vector (pRS316) was evaluated in parallel. The appearance of a clear spot (i.e. zone of reduced growth) within the lawn of *MAT*α cells indicates the presence of **a**-factor.

C) An internally quenched fluorogenic dodecapeptide modeled on the M16A cleavage site in the yeast **a**-factor precursor. The NH_2-terminal fluorophore is aminobenzoic acid (Abz) and the COOH-terminal quenching group is 3-nitro-tyrosine (3NY).

D) Progress curves demonstrating time-dependent fluorescent output in the presence or absence of purified recombinant rat IDE. The reactions contained rat IDE (10 μg/ml; 87.7 nM) or enzyme Storage Buffer (mock). RFU – relative fluorescence units.

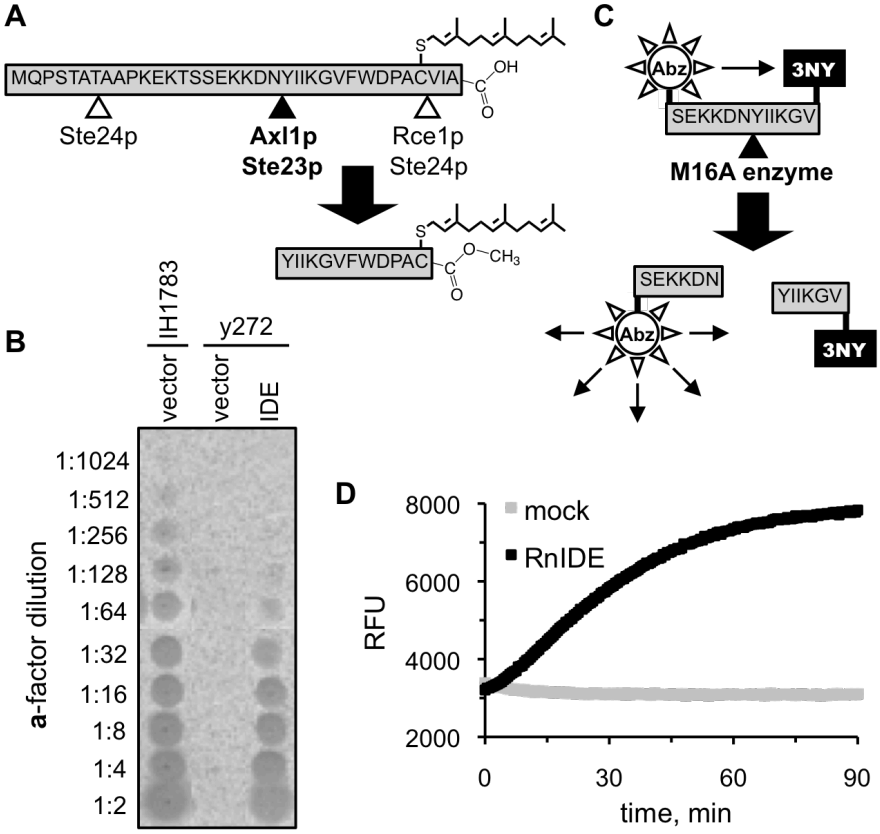
A
MQPSTATAAPKEKTSSEKKDNYIIKGVFWDPACVIA
Ste24p
Axl1p
Ste23p
Rce1p
Ste24p
YIIKGVFWDPAC
B
IH1783
y272
vector
vector
IDE
1:1024
1:512
1:256
1:128
1:64
1:32
1:16
1:8
1:4
1:2
a-factor dilution
C
Abz
3NY
SEKKDNYIIKGV
M16A enzyme
SEKKDN
YIIKGV
3NY
D
8000
6000
4000
2000
RFU
mock
RnIDE
0
30
60
90
time, min

Figure 2.2. *Chemical structures and dose-response profiles of IDE activators.*

Compounds were identified by their ability to enhance rat IDE-mediated *in vitro* cleavage of the peptide reporter depicted in Figure 2.1C. Structures were downloaded from the DTP structure database (http://dtp.nci.nih.gov/branches/dscb/diversity_explanation.html) and converted to ChemDraw images. Compound **4** is not reported due to a lack of effect on the kinetic parameters of rat IDE and inconsistent behavior observed between experiments. Compounds were evaluated for their effectiveness at stimulating rat IDE activity over the indicated dose range using the fluorescence-based IDE activity assay described in Figure 2.1. Data points were plotted using GraphPad Prism 4.0. A best-fit non-linear dose response curve was determined for data points associated with all compounds using Prism and a 4-parameter logistic equation (solid line). Where sigmoidal dose-response curves were observed, AC_{50} values were determined. Where hormetic response curves were observed (i.e. **3**, **5**, **8**), the fitted curves could not be used to determine accurate AC_{50} values, so the lowest half maximal activating concentration is reported ($[Max]_{50}$).

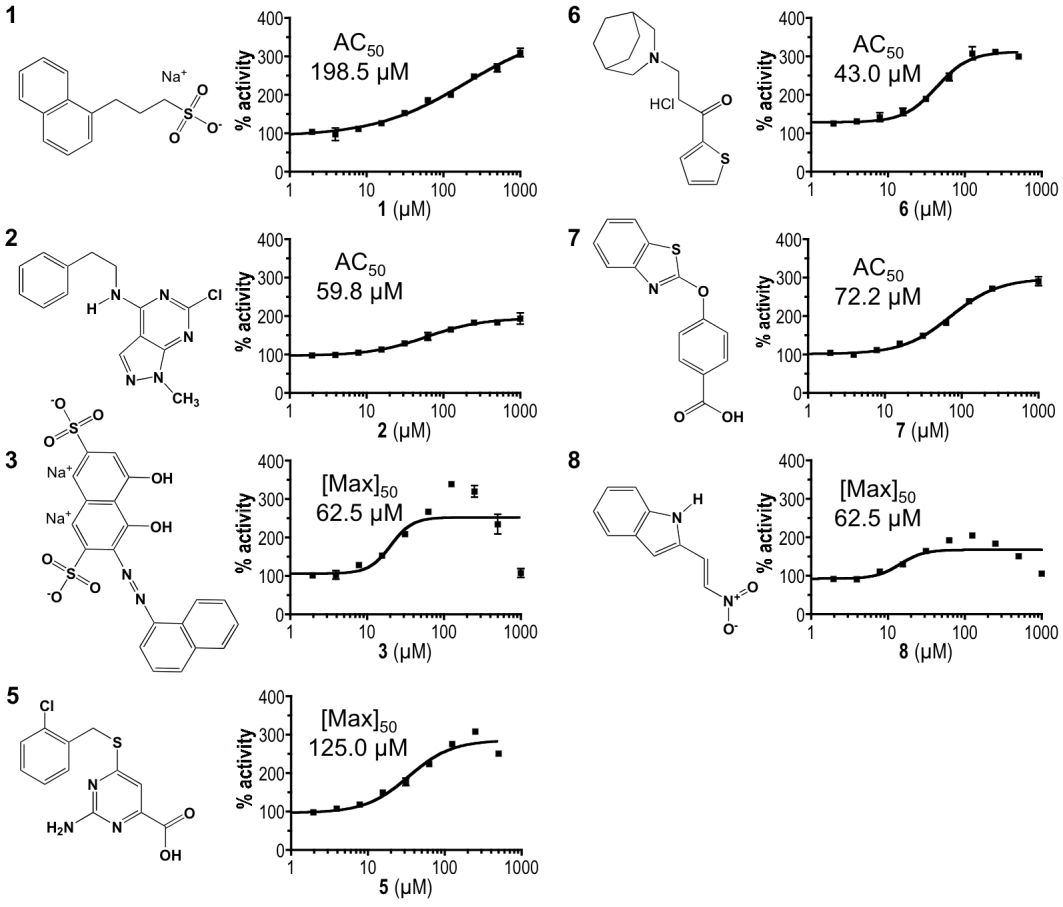
1
Na+
O
S
O
O-
AC50
198.5 μM
% activity
400
300
200
100
0
1
10
100
1000
1 (μM)
2
H
N
N
Cl
N
N
N
CH3
AC50
59.8 μM
% activity
2 (μM)
3
-O
S
O
Na+
OH
Na+
OH
O
S
-O
O
N
N
[Max]50
62.5 μM
% activity
3 (μM)
5
Cl
S
N
H2N
N
O
OH
[Max]50
125.0 μM
% activity
5 (μM)
6
N
HCl
O
S
AC50
43.0 μM
% activity
6 (μM)
7
S
N
O
O
OH
AC50
72.2 μM
% activity
7 (μM)
8
H
N
N+
O
O-
[Max]50
62.5 μM
% activity
8 (μM)

Figure 2.3. *Effect of compounds on the biophysical properties of rat IDE.*

A) Thermal melt midpoints (T_m) observed in the presence of IDE activators were determined using a thermal shift assay. Compounds identified in Figure 2.2 were evaluated at 100 μM with rat IDE (0.5 μM) within the temperature range 28-70 °C.

B) Mobility shifts observed in the presence of IDE activators. The indicated compounds were incubated with 1 mg/ml of IDE for 60 min at 37 °C prior to analysis by native PAGE (10%). ATP (A) was used at 3 mM; compounds **1**-**8** were used at 100 μM. D – DMSO. A dashed horizontal line has been drawn across the image at the expected mobility of IDE.

A

Compound	T_m (°C)
DMSO	45.37±0.27
1	44.77±0.28
2	44.33±0.23
3	84.78±14.09
5	45.11±0.06
6	45.04±0.09
7	44.69±0.04
8	44.00±0.34

B

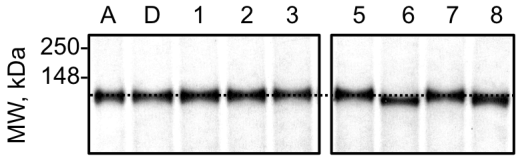

Figure 2.4. *Effect of assay conditions on the properties of rat IDE activators.*

The effects of BSA, insulin, and ATP on the activity of IDE were determined, which was followed by an examination of the impact of these components on the properties of activators. In all cases, rat IDE was used (87.7 nM), the assay is as described in Figure 2.1. Values are reported as percentages relative to a water or DMSO-treated control as appropriate (n=4); *p<0.05, **p<0.01 and ***p<0.001 relative to the mock-treated control.

A) Observed activity of IDE in 0.1 M KPi over a range of BSA concentrations (0-0.5% final). Data points were plotted, and a best-fit non-linear dose response curve determined using GraphPad Prism 4.0 as described in Figure 2.2.

B) Observed activity in presence of compounds (100 μM) in 0.1 M KPi / 0.01% BSA. The dashed line is provided as a visual reference for 100% activity (also present in panels D and F).

C) Observed activity of IDE in 0.1 M KPi over a range of concentrations of human insulin (0-17.2 μM). Data points were plotted and a best-fit non-linear dose response curve determined using GraphPad Prism 4.0 as described in Figure 2.2.

D) Observed activity in presence of compounds (100 μM) in 0.1 M KPi containing 0.92 μM (IC_{50}) insulin.

E) The effect of ATP (0-10 mM) on IDE activity was evaluated in 0.1 M KPi or 50 mM Tris, pH 7.5 containing 0.01% BSA (Tris/BSA). Curve fitting of data was performed as described for panel C. The maximum activating effect of ATP observed was 1 mM in Tris/BSA.

F) Observed activity of IDE in presence of compounds in Tris/BSA containing 1 mM ATP. Compounds were used at optimal concentrations from dose response curves in Tris/BSA buffer (Manandhar and Schmidt, unpublished observations). Compound **1** was used at 1000 μM, compounds **5, 6** and **7** at 500 μM, compound **2** at 250 μM, and compounds **3** and **8** at 125 μM.

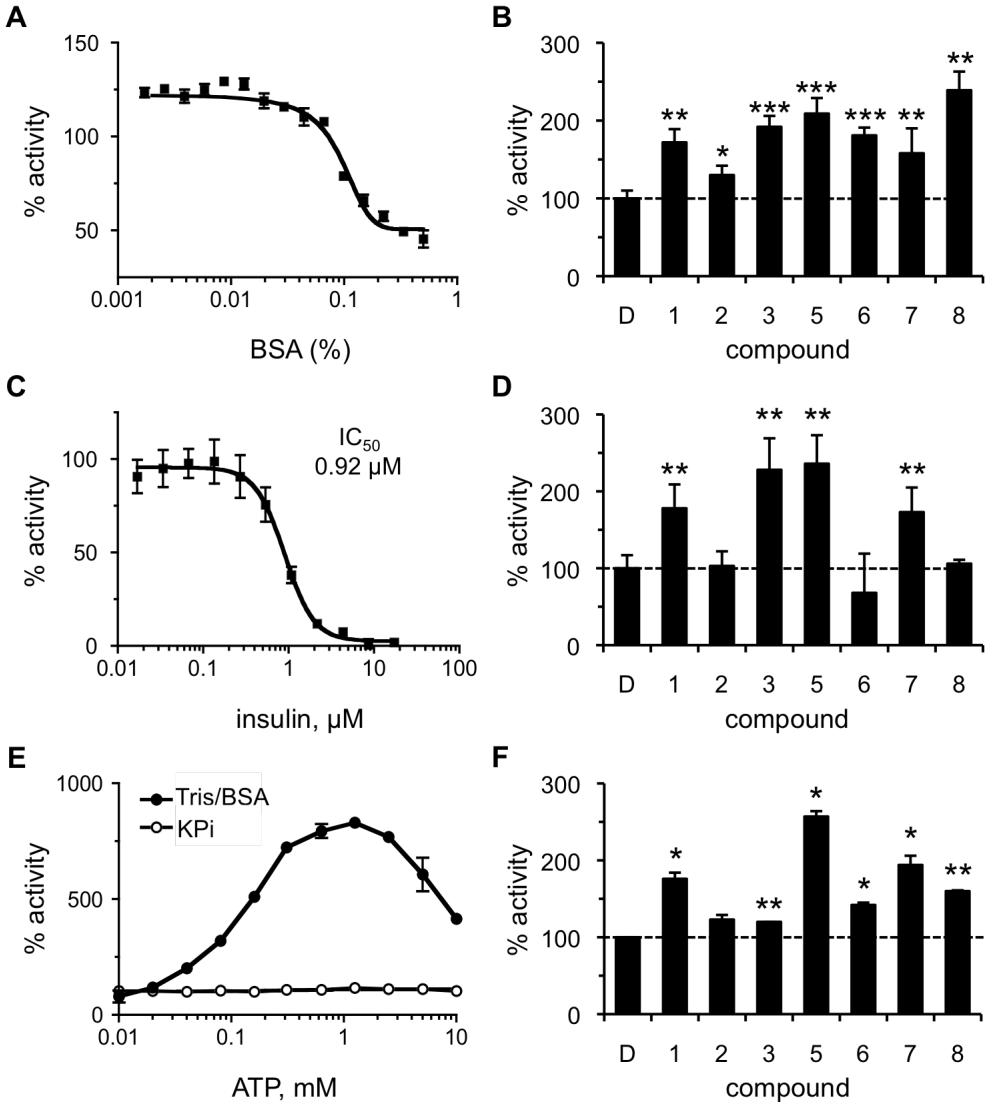
A
150
100
50
% activity
0.001
0.01
0.1
1
BSA (%)
B
300
200
100
0
% activity
**
*
***
***
***
**
**
D 1 2 3 5 6 7 8
compound
C
100
50
0
% activity
IC50
0.92 µM
0.01
0.1
1
10
100
insulin, µM
D
300
200
100
0
% activity
**
**
**
**
D 1 2 3 5 6 7 8
compound
E
1000
500
0
% activity
Tris/BSA
KPi
0.01
0.1
1
10
ATP, mM
F
300
200
100
0
% activity
*
*
**
*
*
*
**
D 1 2 3 5 6 7 8
compound

Figure 2.5. *Select compounds enhance the in vivo IDE-dependent production of yeast* ***a****-factor.* Diluted yeast cultures (1:2000; y272 co-transformed with pWS192 and pWS496) were grown to saturation density (72 hrs) in the presence of activators, and the **a**-factor produced was recovered and analyzed. Compounds were used at 100 μM, with the exception of compounds **5**, **6** and **8,** which were used at 12.5 μM, 50 μM and 25 μM, respectively. The raw data (**A**) was quantified, and mean values graphed relative to a DMSO-treated control (**B**). Each value is normalized to the density of the culture at the time **a**-factor was collected (n=4 for all compounds except **6** for which n=2); *$p<0.05$ and **$p<0.01$ relative to the DMSO-treated control. A nearly identical graph is observed in the absence of normalization.

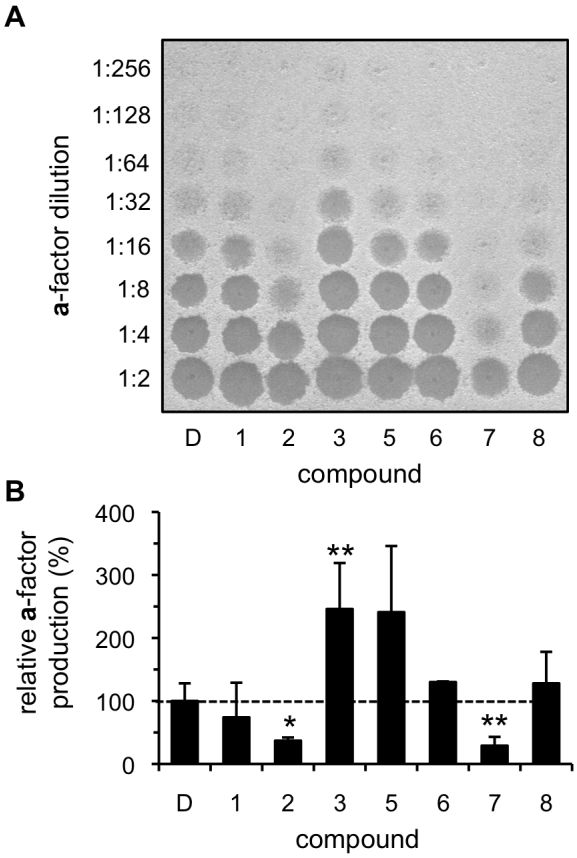
A
1:256
1:128
1:64
1:32
1:16
1:8
1:4
1:2
a-factor dilution
D 1 2 3 5 6 7 8
compound
B
relative a-factor production (%)
400
300
200
100
0
**
*
**
D 1 2 3 5 6 7 8
compound

Figure 6. *Rat IDE activators are substrate and species-specific.*

A) An internally quenched fluorogenic peptide was modeled on $A\beta_{1\text{-}28}$. The quencher DABCYL is conjugated to Lys16 and the fluorophore EDANS (EDS) to Glu22. The peptide has unmodified N- and C-termini.

B) Effect of compounds (100 μM) on rat (*Rn*IDE; 10 μg/ml), human (*Hs*IDE; 100 μg/ml), and worm (*Ce*IDE; 10 μg/ml) mediated cleavage of the $A\beta_{1\text{-}28}$ reporter (50 μM) was evaluated in 0.1 M KPi, pH 7.6. Mean activity values are reported as percentages relative to a DMSO-treated control (n=3). **C**) Effect of compounds (100 μM) on the ability of *Rn*IDE and *Ce*IDE (each at 10 μg/ml) to cleave the **a**-factor reporter was evaluated as in Figure 2.1. *Hs*IDE does not recognize the **a**-factor-based reporter and was thus not evaluated. Mean activity values are reported as percentages relative to the DMSO-treated control (n=3).

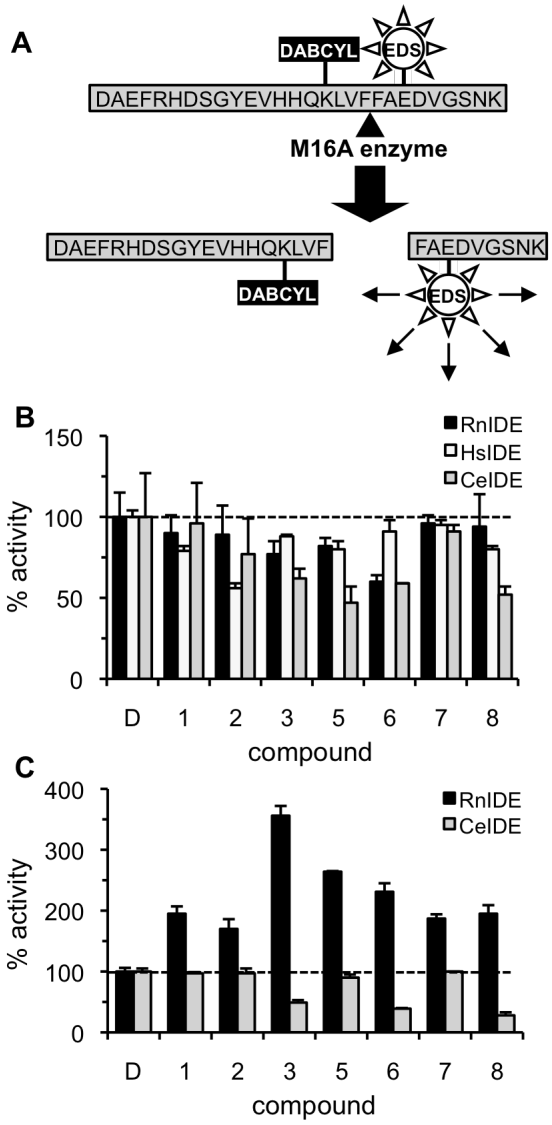
A
DABCYL
EDS
DAEFRHDSGYEVHHQKLVFFAEDVGSNK
M16A enzyme
DAEFRHDSGYEVHHQKLVF
FAEDVGSNK
DABCYL
EDS
B
RnIDE
HsIDE
CeIDE
% activity
150
100
50
0
D 1 2 3 5 6 7 8
compound
C
RnIDE
CeIDE
% activity
400
300
200
100
0
D 1 2 3 5 6 7 8
compound

Table 2.S1. *Chemical properties of IDE activators.*

ClogP, calculated molar refractivity index (CMR) and topological polar surface area (tPSA) values of rat IDE activators were assessed using ChemBioDraw Software (CambrigeSoft, Cambridge, MA). Compounds are identified as in Figure 2.2. Values for compounds **1, 3** and **6** were obtained by excluding the associated counter ions.

Compound	Molecular weight	CLogP	CMR	tPSA
1	249	-2.474	6.70	57.20
2	288	1.776	7.94	52.35
3	472	-6.042	11.77	179.58
5	296	3.380	7.56	88.04
6	263	3.674	7.65	20.31
7	271	3.921	7.29	58.89
8	188	1.573	5.47	63.84

Figure 2.S1. *Correlation between Abz fluorescence and NitroY concentration*.

Fluorescence output was independently measured for free Abz and a 1:1 mixture of Abz and NitroY over a range of concentrations (0-250 μM) in 0.1 M KPi buffer, pH 7.6. The observed fluorescence for free Abz was plotted (GraphPad Prism 4.0) and data points fit to a polynomial function ($y = -0.0628x^2 + 107.09x + 1E\text{-}12$; $R^2 = 1.0000$). The data for the Abz-NitroY mixture was fit to a non-linear, 4-parameter logistic equation ($y = -0.1853x^2 + 98.631x + 232.93$; $R^2 = 0.9989$). These curves were used to determine correction factors that were applied under conditions where different substrate concentrations were employed (e.g. kinetic and dose response experiments; Table 2.2 and Figure 2.2, respectively). At each particular substrate concentration evaluated, the fluorescence data obtained was corrected by multiplying against the observed ratio of Abz/Abz-NitroY at that same concentration. The corrected data was then used for calculations of IDE activity.

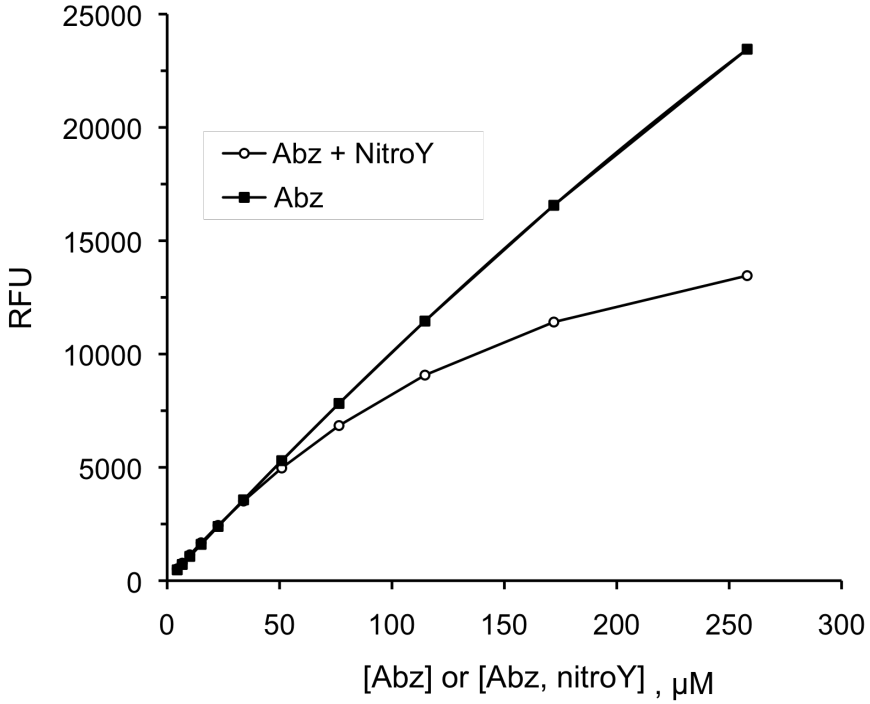
25000
20000
15000
10000
5000
0
RFU
Abz + NitroY
Abz
0
50
100
150
200
250
300
[Abz] or [Abz, nitroY] , μM

Figure 2.S2. *Purity assessment of activators using HPLC.*

Activators were analyzed using C-4 or C-18 columns (Thermo Electron Corp, MA, USA) and absorbance measured at 214 nm (compounds **1, 2,** and **3**), 319 nm (compound **5**), 310 nm (compound **6** and **7**), and 220 nm (compound **8**). The initial peak in each chromatogram represents the solvent front.

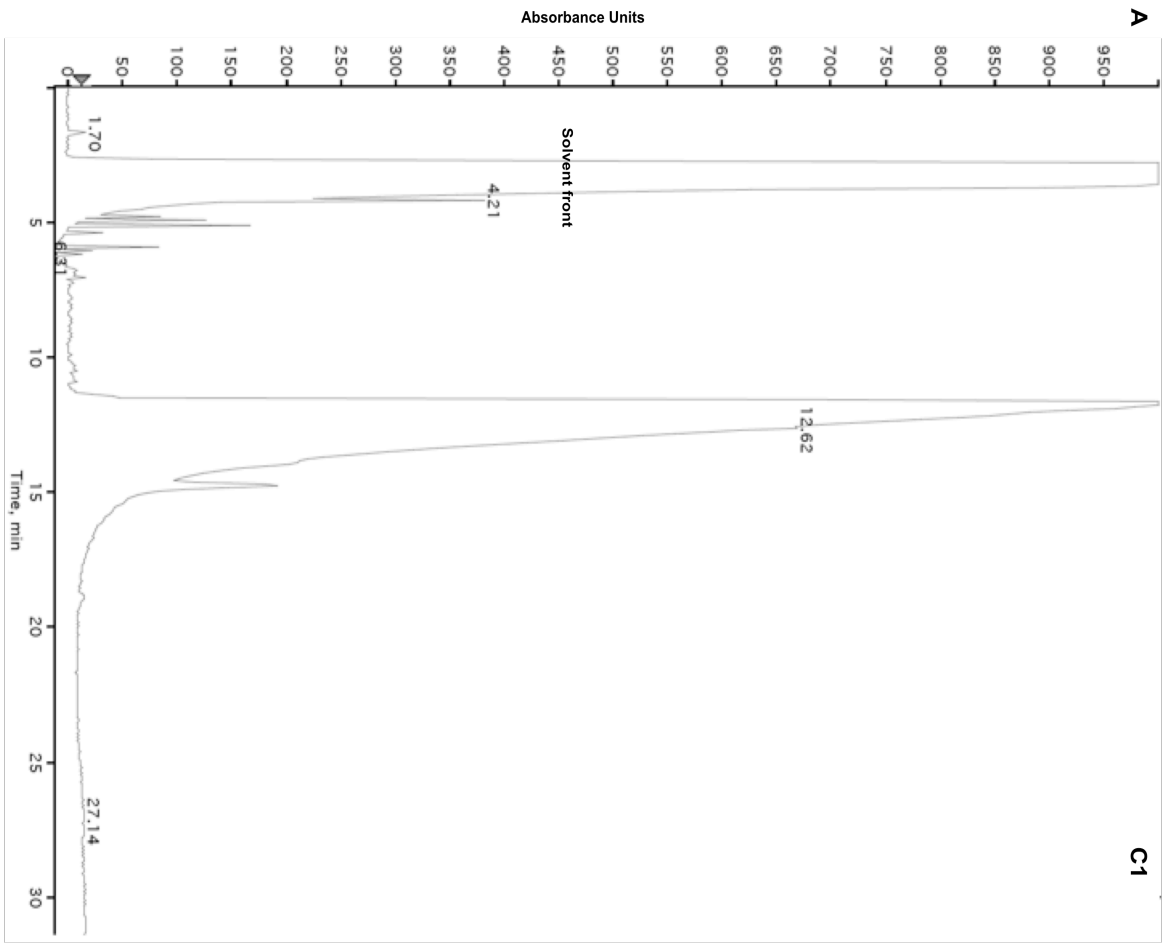
A
Absorbance Units
Solvent front
1.70
4.21
6.31
12.62
27.14
Time, min
C1

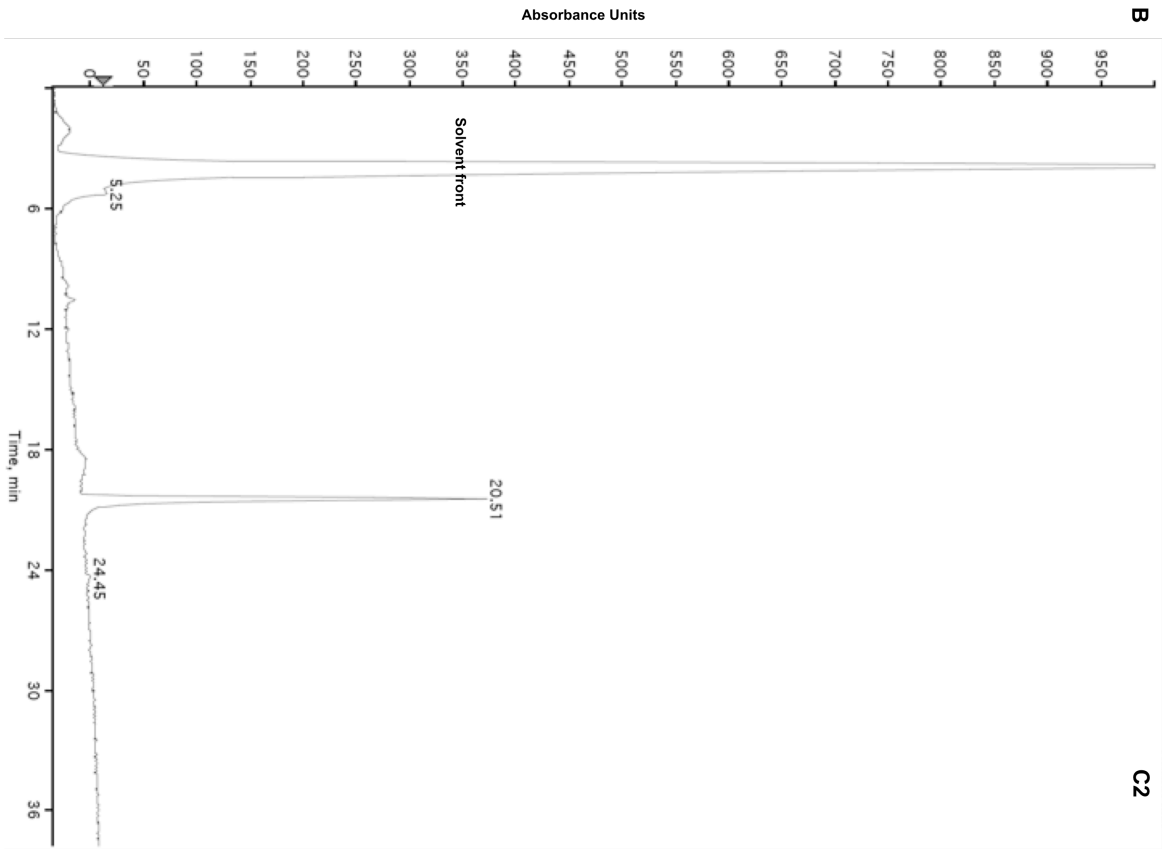
B
Absorbance Units
Solvent front
5.25
20.51
24.45
Time, min
C2

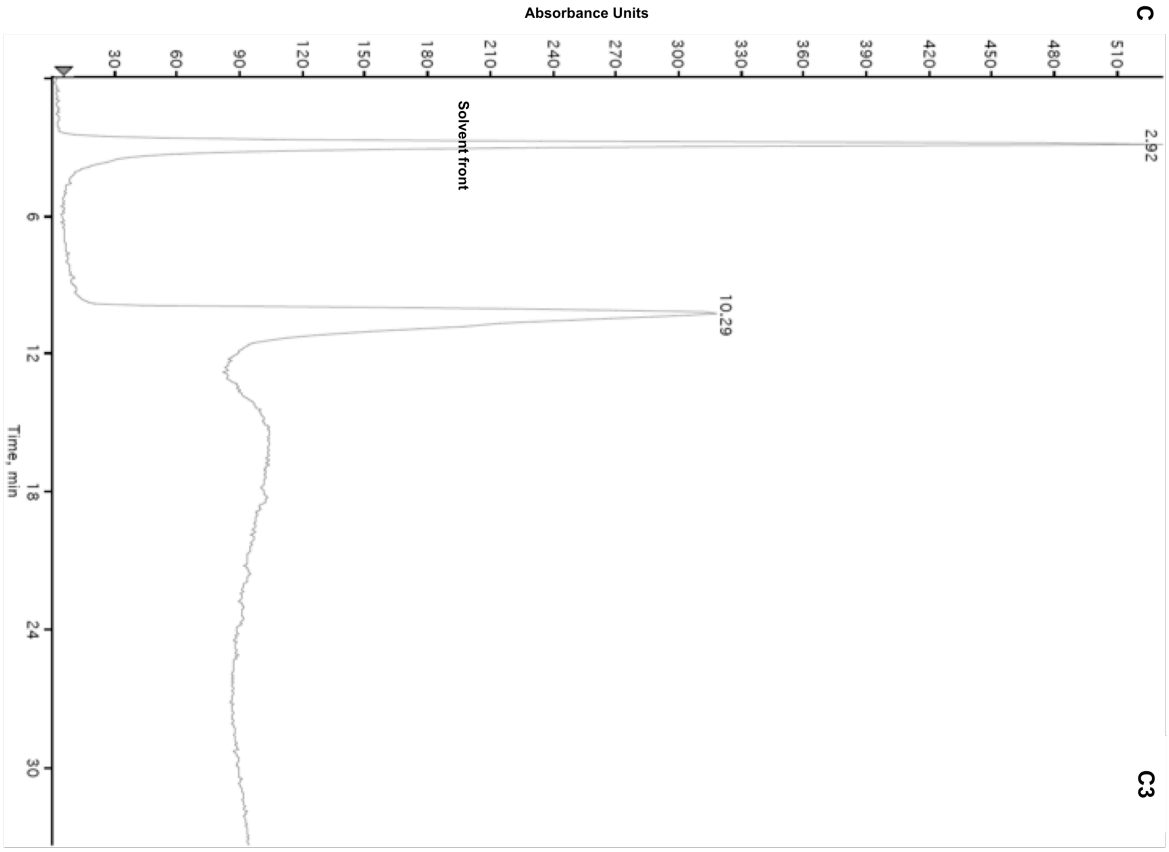
C
Absorbance Units
Solvent front
2.92
10.29
Time, min
C3

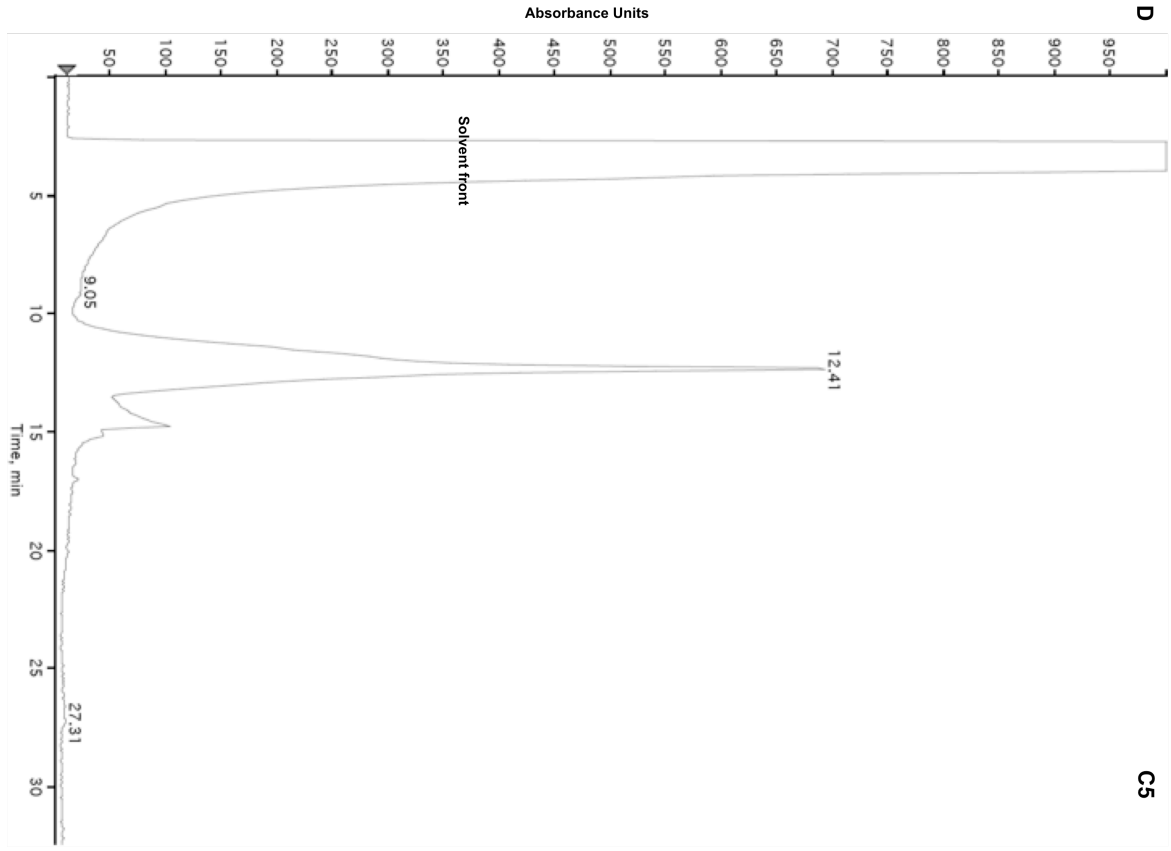
D
Absorbance Units
Solvent front
9.05
12.41
27.31
Time, min
C5

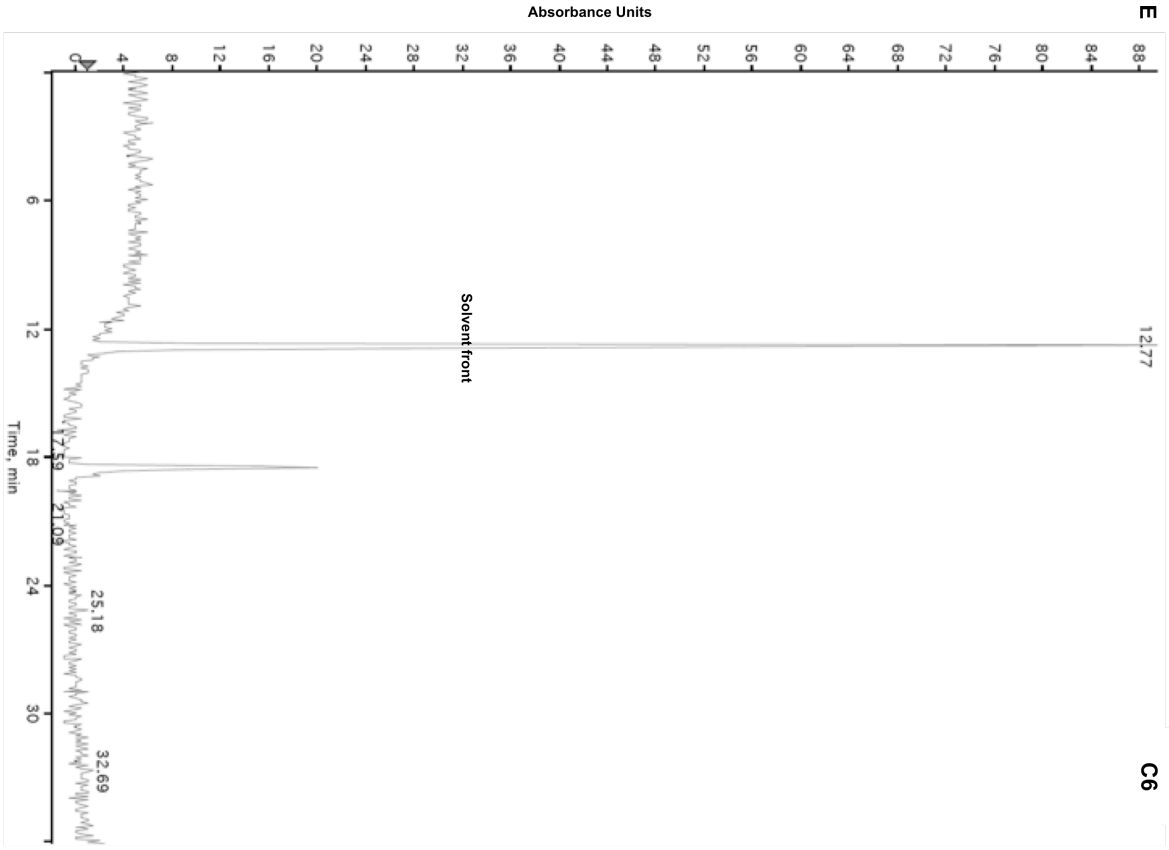
E
Absorbance Units
Solvent front
12.77
17.59
21.09
25.18
32.69
Time, min
C6

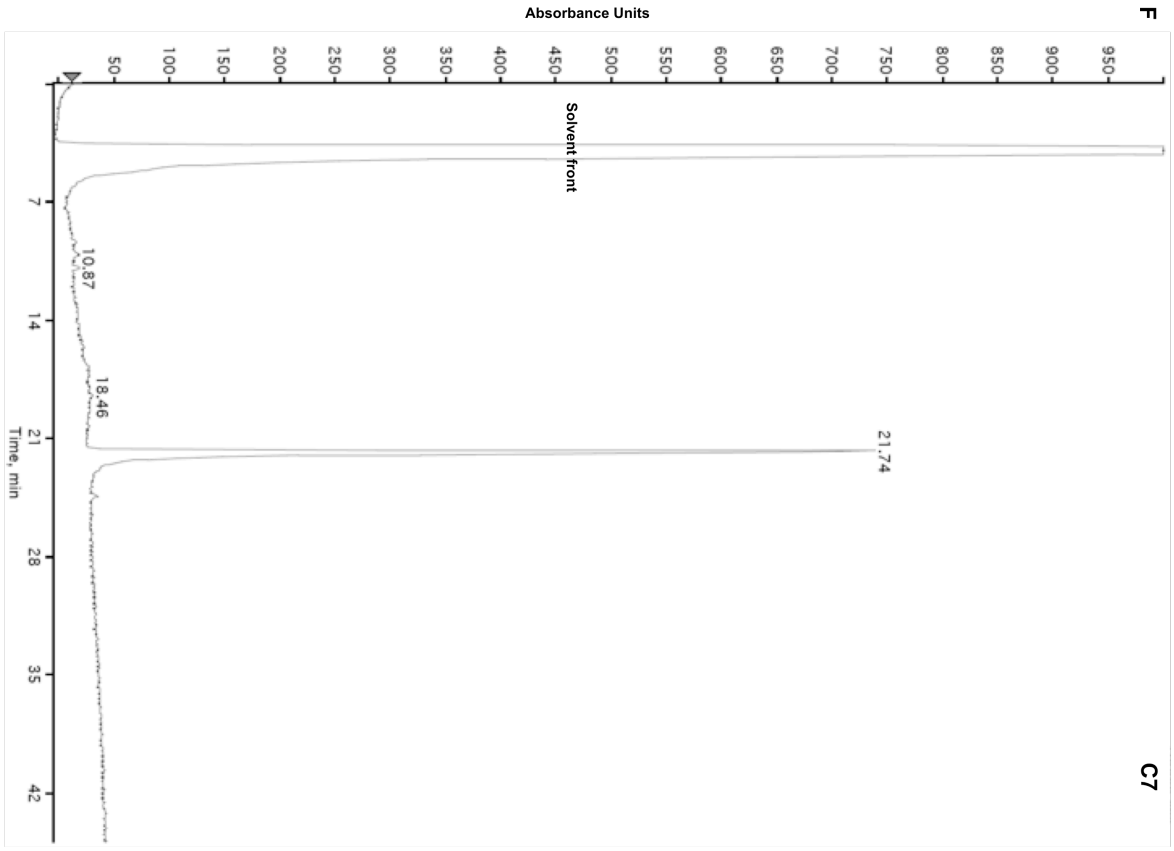
F
Absorbance Units
Solvent front
10.87
18.46
21.74
Time, min
C7

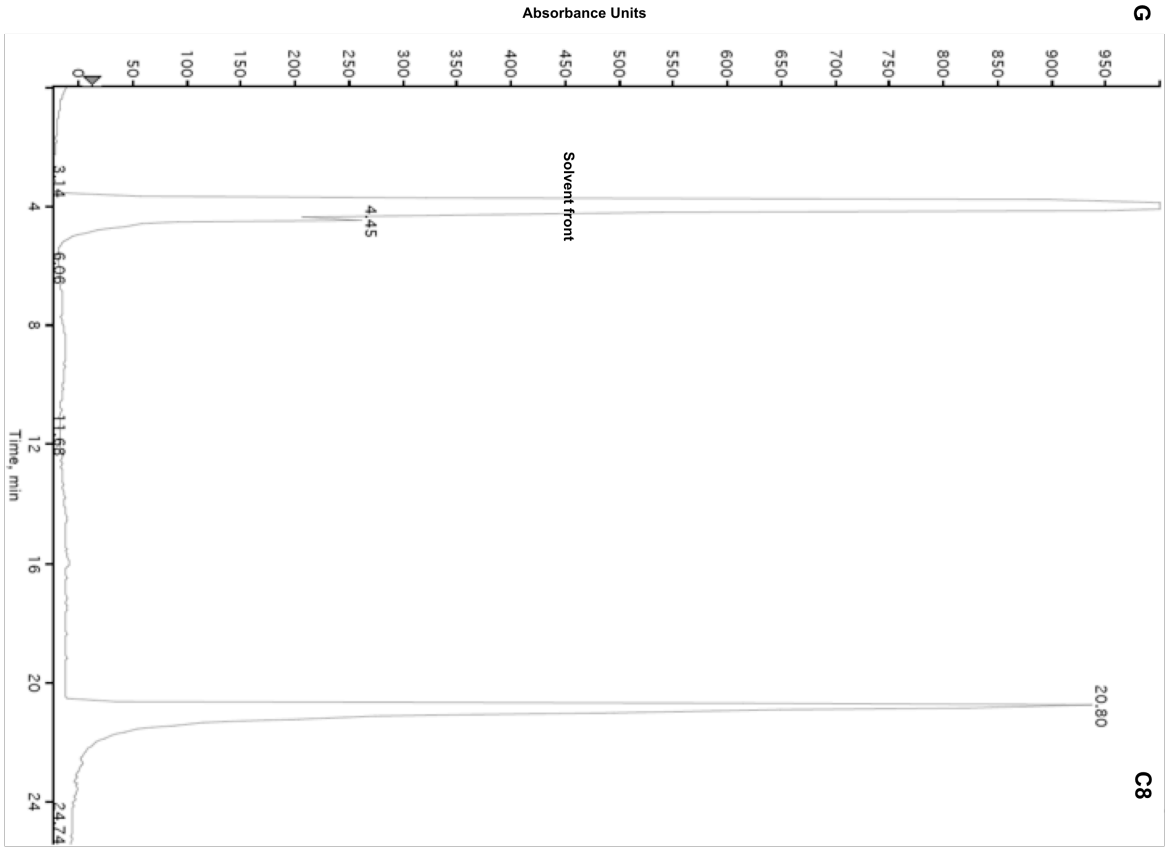
G
Absorbance Units
0
50
100
150
200
250
300
350
400
450
500
550
600
650
700
750
800
850
900
950
Solvent front
3.14
4.45
6.06
11.68
20.80
24.74
4
8
12
16
20
24
Time, min
C8

Figure 2.S3. *Purity assessment of activators using MS.*

The mass of sample components in peak fractions identified by HPLC (see Figure 2.S2) were determined using mass spectrometry (Perkin Elmer-Sciex API I plus) in negative ion mode for all compounds except **2**, **6** and **7**, which were analyzed in positive ion mode.

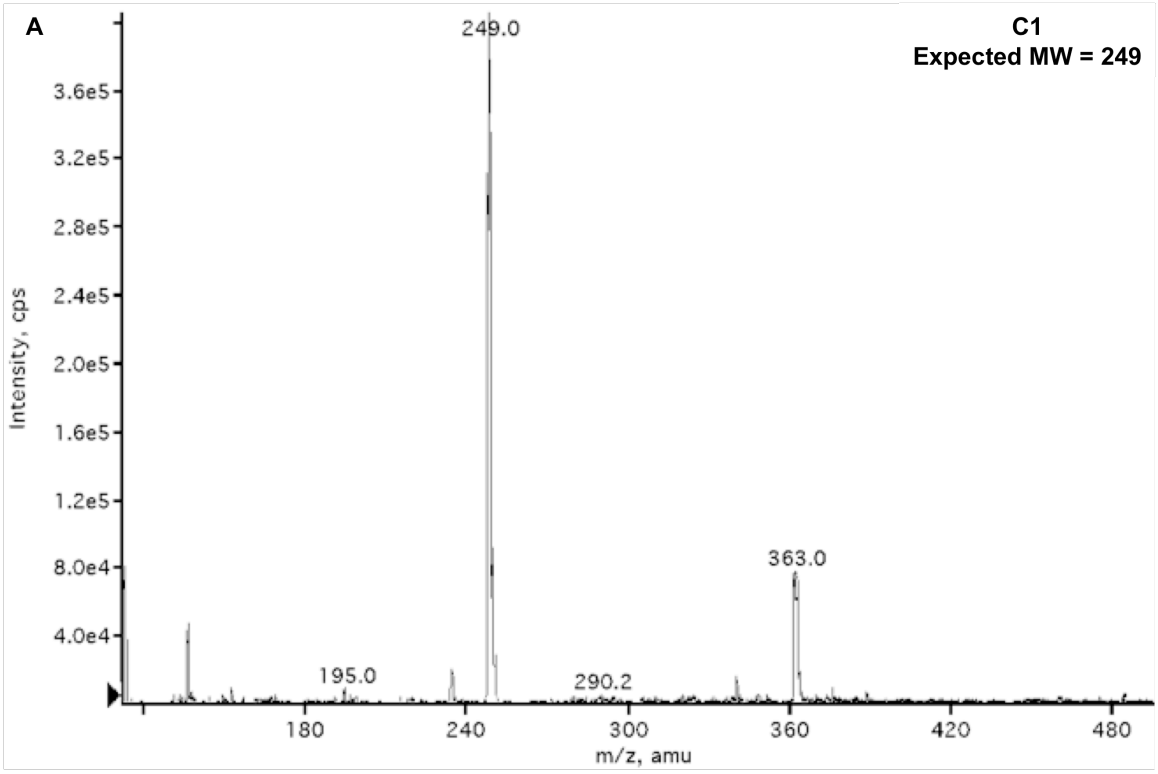
A
C1
Expected MW = 249
249.0
363.0
195.0
290.2
Intensity, cps
3.6e5
3.2e5
2.8e5
2.4e5
2.0e5
1.6e5
1.2e5
8.0e4
4.0e4
180
240
300
360
420
480
m/z, amu

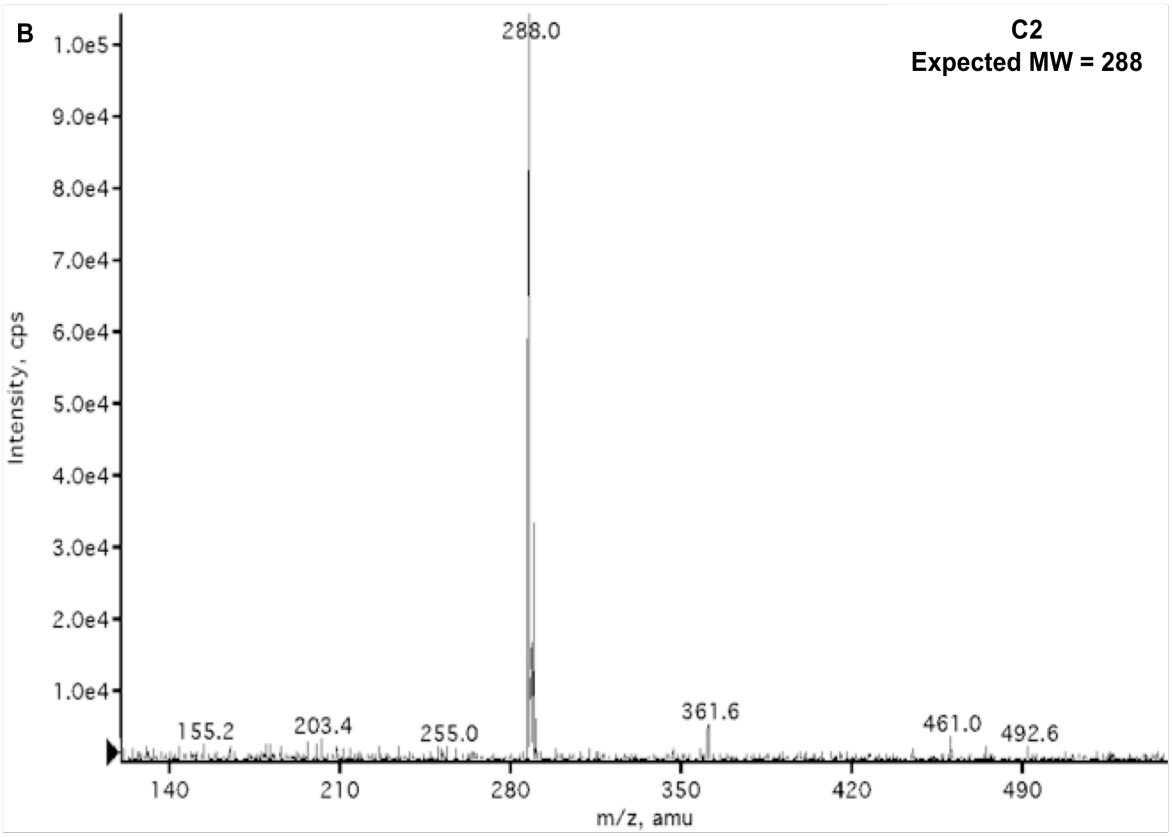
B
C2
Expected MW = 288
288.0
361.6
155.2
203.4
255.0
461.0
492.6
Intensity, cps
1.0e5
9.0e4
8.0e4
7.0e4
6.0e4
5.0e4
4.0e4
3.0e4
2.0e4
1.0e4
140
210
280
350
420
490
m/z, amu

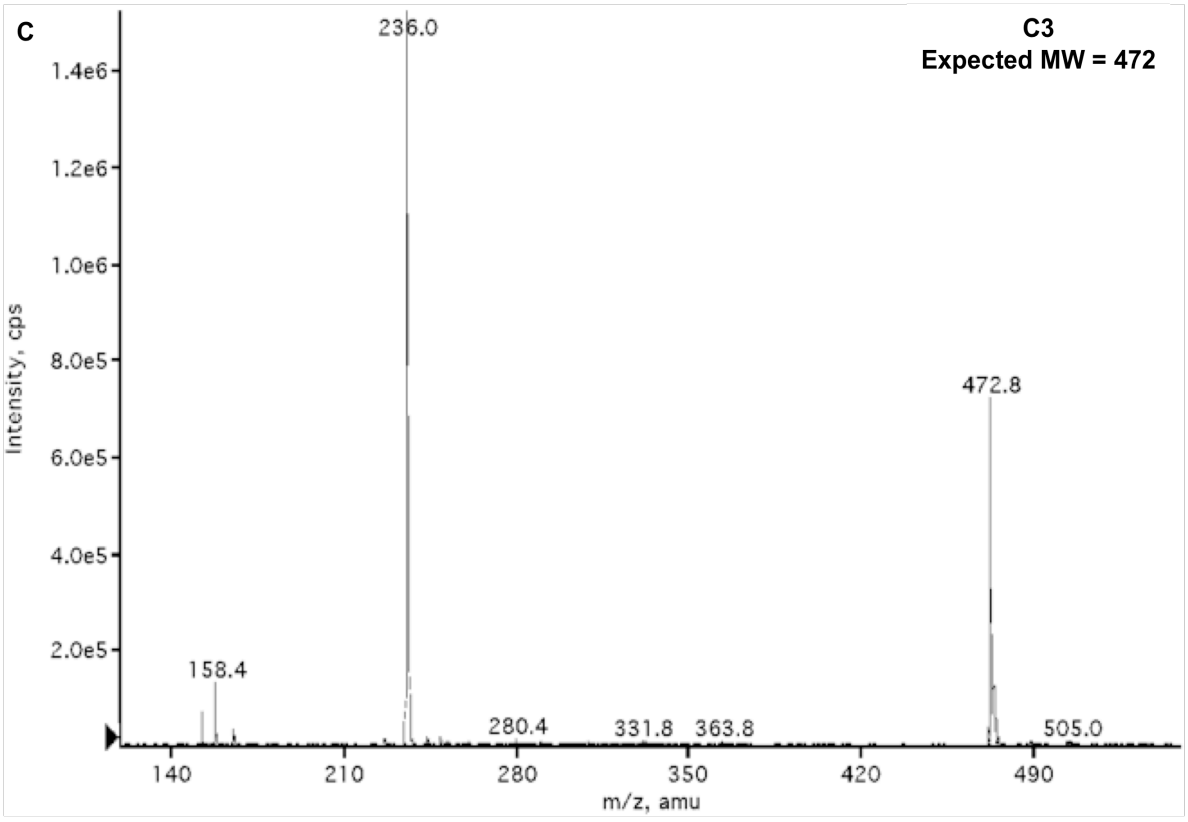
C
C3
Expected MW = 472
236.0
472.8
158.4
280.4
331.8
363.8
505.0
Intensity, cps
1.4e6
1.2e6
1.0e6
8.0e5
6.0e5
4.0e5
2.0e5
140
210
280
350
420
490
m/z, amu

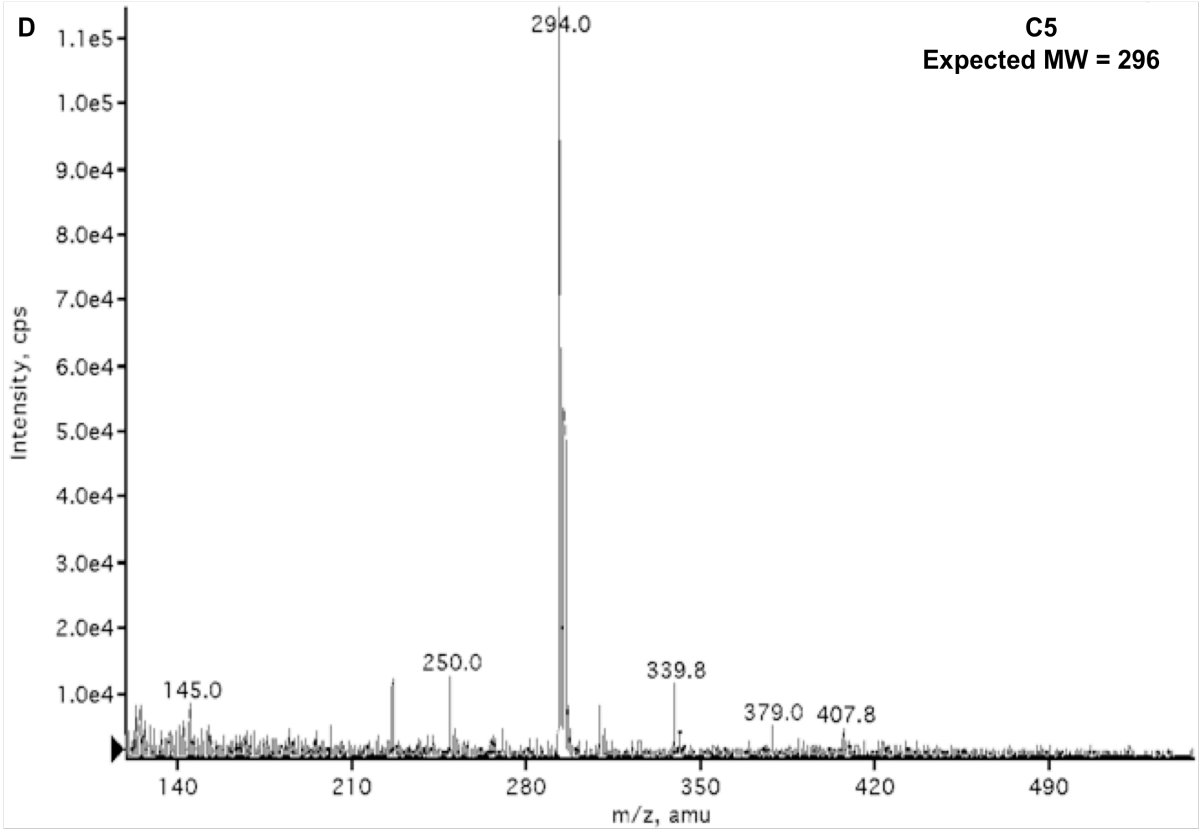
D
C5
Expected MW = 296
294.0
250.0
145.0
339.8
379.0
407.8
Intensity, cps
1.1e5
1.0e5
9.0e4
8.0e4
7.0e4
6.0e4
5.0e4
4.0e4
3.0e4
2.0e4
1.0e4
140
210
280
350
420
490
m/z, amu

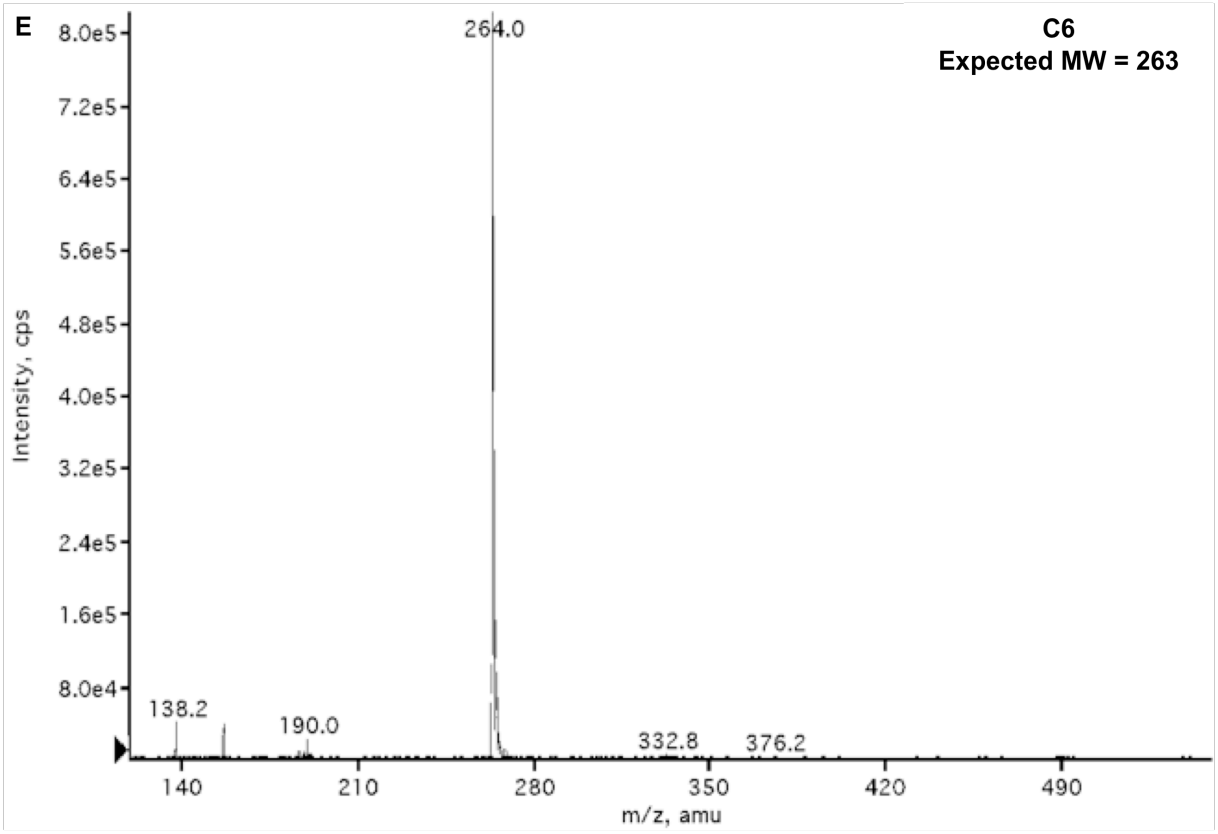
E
C6
Expected MW = 263
264.0
8.0e5
7.2e5
6.4e5
5.6e5
4.8e5
4.0e5
3.2e5
2.4e5
1.6e5
8.0e4
Intensity, cps
138.2
190.0
332.8
376.2
140
210
280
350
420
490
m/z, amu

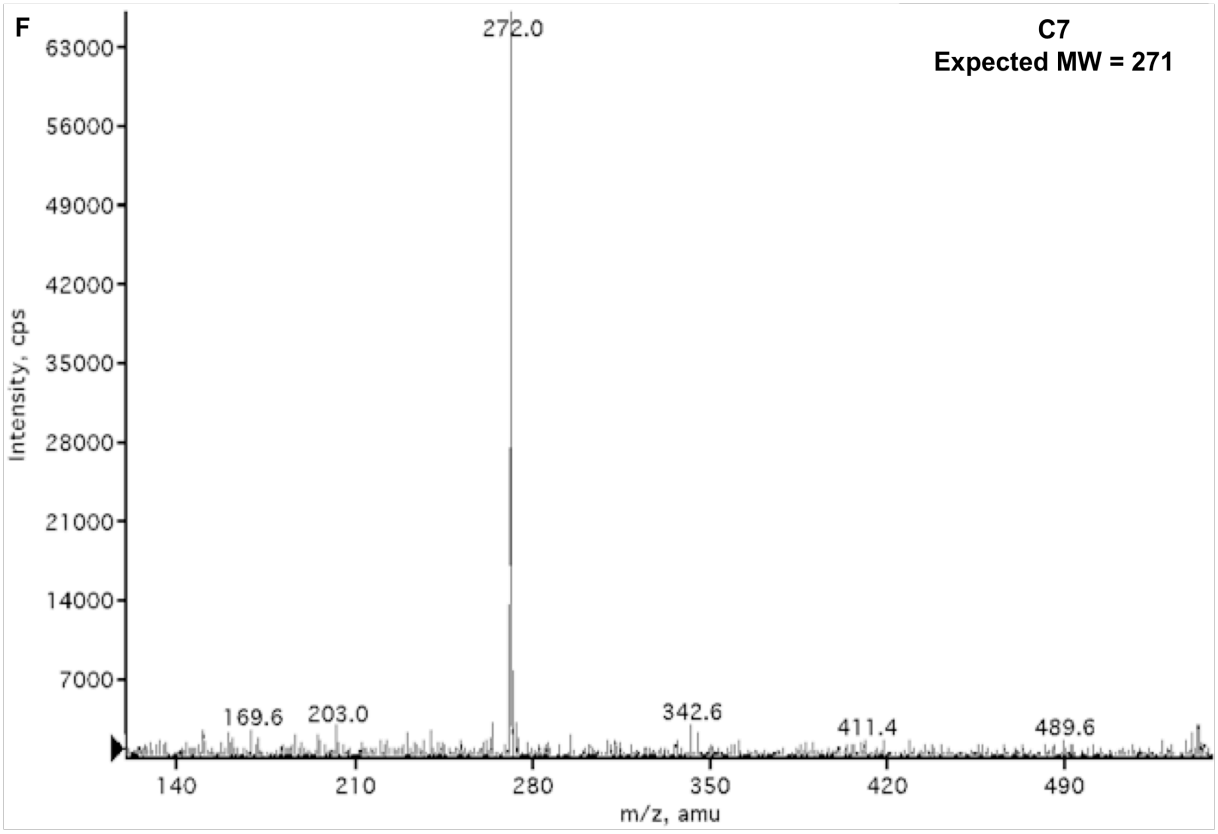
F
C7
Expected MW = 271
272.0
63000
56000
49000
42000
35000
28000
21000
14000
7000
Intensity, cps
169.6
203.0
342.6
411.4
489.6
140
210
280
350
420
490
m/z, amu

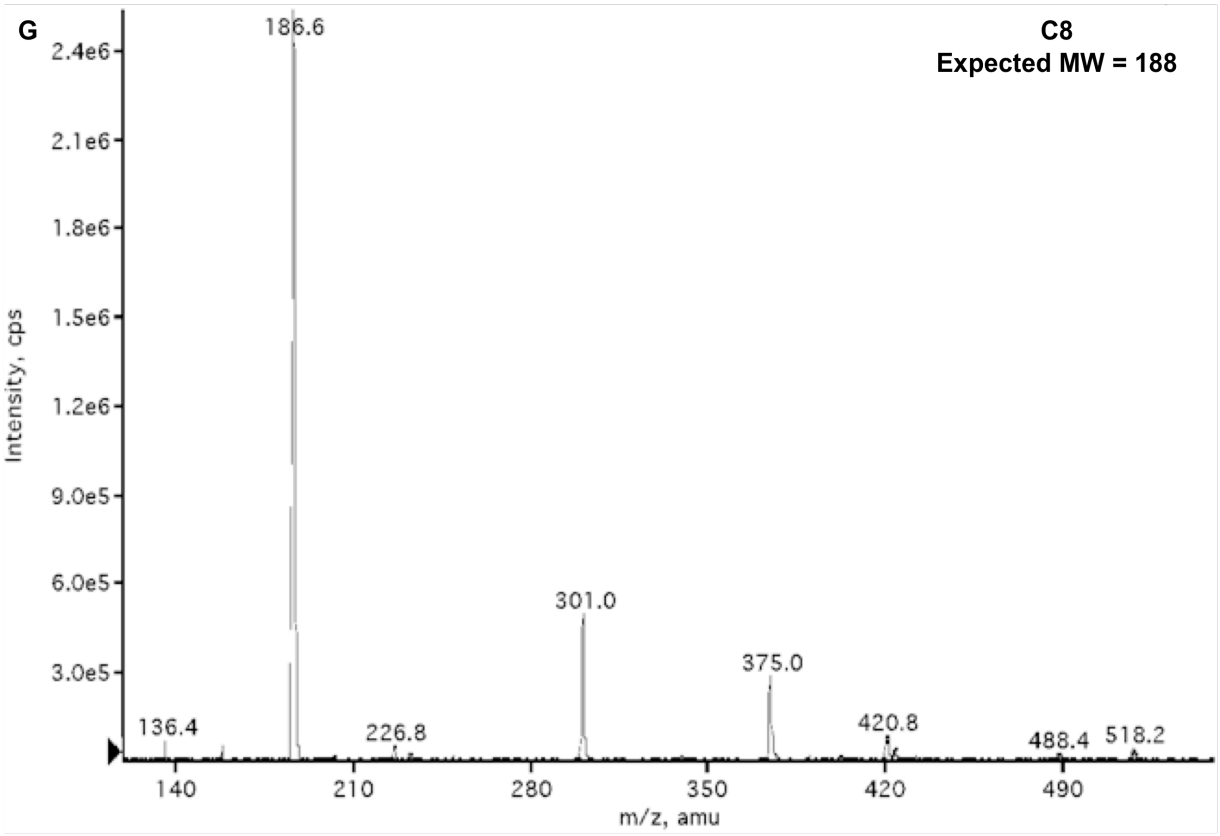
G
C8
Expected MW = 188
186.6
301.0
375.0
136.4
226.8
420.8
488.4
518.2
2.4e6
2.1e6
1.8e6
1.5e6
1.2e6
9.0e5
6.0e5
3.0e5
Intensity, cps
140
210
280
350
420
490
m/z, amu

CHAPTER 3

HIGH-THROUGHPUT SCREEN TO IDENTIFY SMALL-MOLECULE ACTIVATORS OF *Hs*IDE[2]

[2] Kukday, S.S. and W.K. Schmidt. To be submitted to *Journal of Biomolecular Screening*.

ABSTRACT

In the previous study, we described seven small-molecule activators of rat IDE (*Rn*IDE) identified through a high-throughput screen using a synthetic fluorogenic reporter based on the precursor of the yeast mating pheromone **a**-factor. Our previous studies indicated that these activators function in the context of a specific IDE ortholog and the corresponding substrate. In this study, we describe a high-throughput screen to identify *Hs*IDE activators. This screen failed to yield compounds that increased *Hs*IDE activity, reasons for which are discussed and some recommendations made for future screens that would involve identification of IDE activators. This study provides a better understanding of the challenges faced in trying to modulate the activity of this complex metalloprotease.

INTRODUCTION

Alzheimer's disease (AD) is a neurological disorder that typically affects individuals past the age of 65 years. One of the hallmarks of this disease is the progressive accumulation of the amyloid β (Aβ) peptide in the cerebral cortex and hippocampus of AD patients leading to neurodegeneration, cognitive decline, and memory loss [1]. Aβ is derived from the Amyloid Precursor Protein (APP) through successive processing steps mediated by the β- and γ-secretases [2] (Figure 1.1). There are several pathways that lead to the removal of Aβ from the brain. These include receptor-mediated transport across the blood-brain barrier, deposition to form plaques and fibrils, and cleavage by proteases (Figure 1.1). It has been proposed that an imbalance between production and clearance of Aβ results in loss of Aβ homeostasis and subsequent toxicity [3].

The insulin-degrading enzyme (IDE) is a Zn^{2+} metalloprotease belonging to the M16A subfamily of which the yeast enzymes Axl1p and Ste23p are also members. IDE has an inverted HXXEH motif that coordinates the Zn^{2+} ion and an exosite that binds and stabilizes the substrate in a position that is suitable for cleavage [4]. Previous studies have demonstrated the important role of IDE in regulating Aβ levels. These studies have established that modest IDE deficiency results in increased amounts of Aβ in the brains of IDE knockout mice [5]. In addition to these findings, other studies have shown that IDE overexpression leads to ≥50% reduction in Aβ levels in transgenic mice [6]. Thus, the ability of IDE to cleave and neutralize monomeric Aβ makes the enzyme an attractive therapeutic target.

The yeast **a**-factor mating pheromone precursor is recognized as a substrate by several orthologs of Axl1p and Ste23p on their heterologous expression in these cells (e.g., pitrilysin,

*Rn*IDE, *Ce*IDE) [7, 8] (Burriss and Schmidt, unpublished observation). We previously conducted a high-throughput screen to identify small-molecules that can facilitate *Rn*IDE-mediated degradation of a synthetic reporter based on the **a**-factor precursor and identified seven small molecules that significantly enhanced *Rn*IDE activity *in vitro*, some of which also stimulated IDE activity *in vivo* [9]. In order to evaluate the physiological relevance of the hits, we subsequently designed a novel synthetic fluorogenic Aβ-based reporter. Aβ degradation assays that have been reported in the literature were not suitable for our purposes for several reasons. An FAβB reporter has been described for its utility in *in vitro* assays to measure Aβ degradation [10]. This reporter has modifications on the N-terminus (fluorescein) that could interfere with substrate-exosite interactions. Other assays including trichloroacetic acid precipitation of radiolabeled Aβ and HPLC are not suitable for high-throughput screening because they are tedious and time-consuming. Aβ ELISA assays have also been used to measure amount of Aβ in brain homogenates, although they cannot be used to monitor Aβ cleavage since they are unable to distinguish between cleaved and uncleaved Aβ [11]. Using the fluorogenic Aβ-based reporter, designed with help from Dr. Zachary Wood (University of Georgia) in our *in vitro* fluorescence assay, we discovered that the activators we had previously identified were unable to facilitate degradation of this reporter. Moreover, these activators also failed to enhance the activity of IDE isolated from other species (*H. sapiens* and *C. elegans*) [9].

In this study, we report on a high-throughput screen using our Aβ-based reporter as the substrate and *Hs*IDE as the target enzyme. This screen failed to generate activators of *Hs*IDE, possible reasons for which are discussed. In addition, we provide recommendations for future screens aimed at identifying IDE activators. This study provides a glimpse into the complexity of IDE and illuminates the challenges in modulating its activity.

EXPERIMENTAL

Plasmid cloning

A pET30b(+) bacterial expression vector (Novagen®, EMD Millipore, Billerica, MA) expressing an N-terminally tagged 6XHis-*Hs*IDE was constructed according to the following method. The *Hs*IDE open reading frame (ORF) was amplified from IDE-pSRα (kind gift from Dr. R.A. Roth, Stanford University) such that a *Not*I site (5′-end) preceded the M42 start codon which was followed by a 6X-His tag, *Hs*IDE ORF, and an *Xba*I site (3′-end). This PCR product was then subcloned into the corresponding sites in the digested pET30b(+) vector. The resulting plasmid DNA was sequenced, and the *Hs*IDE gene was found to be free of mutations.

Expression and purification of recombinant HsIDE

BL21(DE3) cells transformed with [pET30b(+)-T7-6XHis-*Hs*IDE] were cultured in the presence of kanamycin (50 μg/ml). Protein expression was induced with 210 μM isopropyl β-D-1-thiogalactopyranoside (IPTG) overnight at 20 °C with shaking at 80 rpm. Cells were harvested by centrifuging the bacterial cultures at 6000 rpm for 10 min. The resulting pellet was resuspended in lysis buffer (50 mM Na-K phosphate, 300 mM NaCl, pH 8.0) and sonicated to lyse the cells. The lysate containing 6XHis-tagged *Hs*IDE was applied to a column packed with BD Talon^{TM} cobalt affinity resin (BD Biosciences, Sparks, MD) (4 ml bed volume). After several washes to remove unbound cell components, protein bound to the column was eluted using 300 mM imidazole and dialyzed several times to reduce the imidazole concentration before resuspending in storage buffer (25 mM KPi, 200 mM NaCl, 20% glycerol, pH 7.6). Aliquots of 1 mg/ml enzyme were stored at -80 °C until needed. This procedure was performed in the laboratory of Dr. Zachary Wood (University of Georgia).

Two-fold serial dilutions of the enzyme preparation were analyzed by 10% SDS-PAGE and stained using Coomassie^{TM} Brilliant Blue R-250 solution. Western blot was carried out using an anti-IDE primary antibody (kind gift of Dr. L.B. Hersh, University of Kentucky).

Peptides and other reagents

The synthetic fluorogenic substrate used in the high-throughput screen to identify *Hs*IDE activators was based on the $A\beta_{1-28}$ sequence DAEFRHDSGYEVHHQK^{DABCYL}LVFFAE^{EDANS}DVGSNK-OH (CHI Scientific, Maynard, MA), where K16 was conjugated to DABCYL [4-(4-(Dimethylamino)phenylazo)benzoic acid] and E22 was conjugated to EDANS [5-(2-Aminoethylamino)-1-naphthalenesulfonic acid]. The peptide, received in powder form, was resuspended in DMSO and stored as 10 mM stocks at -80 °C until needed. Proteinase K was purchased from Sigma-Aldrich (St. Louis, MO).

Assay optimization and kinetic analyses

A range of *Hs*IDE concentrations (10-100 μg/ml) was incubated with 50 μM substrate to determine optimum enzyme concentration in the assay. Reactions were performed in 100 mM KPi, pH 7.6. To determine whether the addition of zinc enhanced enzyme activity, either 12.5 or 25 μM $ZnCl_2$ was added to reactions containing 10 μg/ml HsIDE, 50 μM substrate, and 0.1% BSA (to increase protein stability).

To determine the optimum buffer conditions, the *Hs*IDE-$A\beta_{1-28}$ reaction was conducted in either 100 mM KPi, pH 7.6, 100 mM HEPES or 50 mM Tris-HCl, pH 7.4. In a separate experiment, a range of substrate concentrations (6.25-100 μM) was used to determine optimum concentration for the HTS assay. These reactions were carried out in 0.1 mM KPi, pH 7.6.

Increase in fluorescence output was measured over a 60 min period using a Biotek Synergy microtiter plate reader with a 320/485 nm excitation/emission filter set.

Kinetic analyses were carried out using *Hs*IDE (100 μg/ml) and increasing substrate concentrations (0-250 μM). Kinetic parameters were derived from non-linear regression curves obtained by fitting the data to the equation $Y=Vmax*X/[K_M+X]$ in Prism 4.0.

Compound library

The Developmental Therapeutics Program (DTP) Diversity Set compound library was obtained through the National Cancer Institute at the National Institutes of Health (NIH). The library consists of 1981 compounds that were selected from over 70,000 compounds based on unique pharmacophores that they possessed. Selection was performed using the Chem-X software (Chemical Design Ltd., Mahwah, NJ) through virtual screening of the compounds based on the criteria of bond flexibility, number of pharmacophores and overlap of pharmacophores.

High-throughput screen (HTS)

Reactions were set up in clear-bottomed 96-well microtiter plates (Costar, Corning Inc., NY). Each 100 μl reaction contained *Hs*IDE (100 μg/ml) and fluorogenic $A\beta_{1-28}$ (50 μM) and a unique compound (100 μM) from the Diversity Set library. Rates were calculated from the first six minutes of the reaction and normalized by the maximum fluorescence generated on digestion of the substrate with Proteinase K. To eliminate background fluorescence contributed by the substrate, fluorescence generated by the substrate alone was measured and subtracted from that generated by degradation products. Compounds that enhanced IDE activity to >125% of the

control activity (set at 100%) were designated as hits (n=29) and were selected for further analysis.

Competition assays

Competition assays were performed in 100 mM KPi, pH 7.6 at a fixed substrate (fluorogenic $A\beta_{1-28}$) concentration of 50 μM. Increasing concentrations (0-60 μM) of unmodified $A\beta_{1-28}$ were added either with or without sonication, to reactions containing the fluorogenic substrate and *Rn*IDE (100 μg/ml).

RESULTS

Purification of HsIDE

6X-His-tagged *Hs*$IDE_{M42-L1019}$ was successfully purified using Co^{2+}-affinity chromatography. The protein migrated at the expected size of ~114 kDa on an SDS-PAGE gel (Figure 3.1A). Some additional bands are degradation products of IDE as revealed by Western blot analysis of the same preparation (Figure 3.1B). Similar truncated species were observed after the purification of *Rn*IDE [12], albeit the intensity of the additional bands was lower. The expressed protein lacks the first 41 amino acids since the true initiator methionine for IDE is M42 as has been established previously [12]. A lack of these residues does not affect protein expression or activity.

Fluorogenic $A\beta_{1-28}$ is cleaved by HsIDE

Previously identified *Rn*IDE activators were discovered in a high-throughput screen based on IDE-mediated cleavage of an internally quenched **a**-factor based reporter [9]. To make

the substrate more physiologically relevant, we designed an Aβ-based reporter for use in our *in vitro* fluorescence assay. This reporter was indeed cleaved by *Hs*IDE with a K_M of 48.79 μM and Vmax of 8.89 nmol/min/mg. To determine the optimum conditions for the reaction, a range of concentrations of substrate and enzyme were evaluated separately. Optimum assay concentrations for the substrate and *Hs*IDE were found to be 50 μM and 100 μg/ml, respectively in 100 mM KPi, pH 7.6. Using HEPES and Tris-HCl as buffers also enhanced IDE activity at 100 μg/ml although to a lesser extent than KPi. Assay optimization and kinetic data is depicted in Figure 3.2.

Identification of HsIDE activator hits from the HTS

To identify activators of *Hs*IDE, compounds from the DTP library were screened in a 96-well plate format. Compounds that increased *Hs*IDE activity by >25% were identified as hits (n=29). The results of the HTS are summarized in Table 3.1. In order to verify their activation properties, the hits were re-ordered from NCI. All of the compounds identified as hits from the screen turned out to be false positives, except two compounds (**7** and **9**), which appeared to reproducibly activate IDE. On further investigation, we found that this increased activity was the result of a lower fluorescence yield obtained on addition of Proteinase K to the reactions. This fluorescence yield was lower for compound-containing reactions than that for the DMSO-treated controls resulting in a higher estimate of IDE activity in the presence of these compounds relative to the control. These results are depicted in Figure 3.3.

Unmodified $A\beta_{1-28}$ enhances cleavage of fluorogenic $A\beta_{1-28}$

We wanted to determine the effect of unmodified $A\beta_{1-28}$ on IDE-mediated degradation of the fluorogenic $A\beta_{1-28}$ substrate in order to gauge the ability of the fluorogenic peptide to mimic

the native peptide. The aim of this experiment was to determine the K_i of inhibition by unmodified $A\beta_{1-28}$, which would provide information about the ability or lack thereof of IDE to distinguish between the two substrates. Surprisingly, addition of increasing concentrations of unlabeled $A\beta_{1-28}$ facilitated IDE-mediated cleavage of fluorogenic $A\beta_{1-28}$. There was a 1.3-fold increase in the fluorescence generated by fluorogenic $A\beta_{1-28}$ in the presence of 60 μM unlabeled peptide. This effect was neutralized when the unlabeled $A\beta_{1-28}$ premixes were sonicated before adding them to the reaction. Progress curves of the reactions at each concentration of unlabeled $A\beta_{1-28}$ are presented in Figure 3.4.

DISCUSSION

The ability of IDE to clear toxic Aβ species from the brain has made the enzyme an attractive therapeutic target for the treatment of AD. Based on the finding that **a**-factor is recognized by IDE orthologs isolated from various species besides yeast (e.g., rat, bacteria) both *in vitro* and *in vivo* [7, 8], we designed a fluorogenic reporter based on the **a**-factor sequence. We previously identified small-molecules that could stimulate *Rn*IDE activity against this **a**-factor-based reporter, albeit these compounds failed to stimulate the activity of *Ce*IDE. Moreover, *Hs*IDE was unable to recognize the **a**-factor-based peptide as a substrate [9]. This result could be explained by the fact that **a**-factor is not a natural substrate for *Hs*IDE. Based on these observations, we designed a more Aβ-like fluorogenic substrate and sought to determine whether the activators would enhance IDE-mediated degradation of this peptide. Interestingly, these activators failed to enhance the activity of *Rn*IDE, *Hs*IDE, and *Ce*IDE. We therefore

concluded that, in addition to exhibiting species-specificity, the activators also appeared to be substrate-specific [9].

Predicting that the activators work in the context of a specific enzyme-substrate pair, we re-screened the DTP compound library in order to identify small-molecule activators that function in the context of *Hs*IDE and $A\beta_{1-28}$. This screen resulted in two reproducible hits, which were later found to be false positives as a result of an artifact introduced during the normalization of the reaction rates (Figure 3.3). There are several possible reasons for this result. One possibility is that the fluorophore and quencher attached to the substrate affect the folding of the peptide making it less susceptible to cleavage by IDE. It is also possible that the truncated IDE species seen in the purified enzyme preparation (Figure 3.1) interfere with the ability of the activators to bind and/or activate *Hs*IDE at the concentration used in the fluorescence assay. A third possibility is that these modifications structurally disrupt the interaction between the active site residues of IDE with the cleavage site on the peptide substrate.

To investigate the ability of the fluorogenic $A\beta_{1-28}$ reporter to mimic the unmodified $A\beta_{1-28}$, we performed a competition experiment including both substrates and *Rn*IDE. The aim of this experiment was to measure the Ki for inhibition of the unmodified peptide for the fluorogenic peptide. Surprisingly, unmodified $A\beta_{1-28}$ stimulated *Rn*IDE-mediated cleavage of the fluorogenic $A\beta_{1-28}$ reporter. Although this observation is consistent with allosteric activation exhibited by other IDE substrates, it has not been demonstrated before for Aβ-based substrates [13], although we have not yet analyzed the mechanism of this effect (e.g., dimerization status of the enzyme), which remains open for future investigation. We also observed that this effect is neutralized when sonicated preparations of unmodified $A\beta_{1-28}$ are added to the reaction. This observation suggests that subjecting $A\beta_{1-28}$ to sonication might cause aggregation of the peptide,

reducing the monomer concentration, thus preventing them from activating the enzyme. We predict that similar to what Song and colleagues observed, binding of the unmodified peptide to one subunit of the active dimer of the enzyme may increase the probability of binding of the fluorogenic peptide to the other subunit of the dimeric form. From our studies of the rat and human IDE orthologs, we observed that although the two proteins share 96% sequence identity, the K_M of *Hs*IDE (48.79 μM) is lower than that of *Rn*IDE (142.3 μM) for fluorogenic $A\beta_{1-28}$, indicative of a more favorable interaction between *Hs*IDE and the reporter [9]. Although speculative, the few amino acid differences between the two proteins could affect binding of the peptide substrate. For example, a change from glutamic acid (hydrophilic) at position 176 in *Hs*IDE to alanine (hydrophobic) in *Rn*IDE could stabilize the closed conformation of the enzyme since this residue lies in the region of contact between the N- and the C-terminal halves of IDE. This would prevent opening of the chamber, thus leading to a reduced reaction rate. The amino acid differences between *Hs*IDE and *Rn*IDE are depicted in Figure 3.5. Isoforms of proteins such as the human leukocyte antigen have been described in which similar differences are predicted to alter the peptide-binding properties of the protein [14].

Our attempts to identify activators of IDE have revealed the complexity of this Zn^{2+} metalloprotease. In their attempts to identify IDE activators, Cabrol and colleagues also encountered similar problems. They identified Ia1 and Ia2 after conducting a high-throughput screen using a synthetic fluorogenic peptide reporter. They later found that Ia1 and Ia2 enhanced IDE-mediated Aβ1-40 degradation only in the presence of the synthetic reporter [15]. Failure of activators identified through high-throughput screens to enhance enzyme activity against the native substrate is a common problem. In another study, Howitz et al., identified resveratrol as an activator of SIRT1, a histone deacetylase involved in ageing. They also used a synthetic reporter

conjugated to a fluorescent tag in their screen [16]. A few years later two distinct studies demonstrated that resveratrol enhanced SIRT1 activity only in the presence of the fluorescent tag and that the tag was responsible for tighter binding of the reporter to SIRT1 [17-19]. These studies emphasize the importance of choosing the right enzyme-substrate combination for high-throughput screens. It is very important that the synthetic reporter resemble the native substrate as closely as possible.

Future work should be directed toward the design of IDE activators that could interact with regions of the enzyme known to be involved in increased activity, including the exosite, the opening of the catalytic chamber, and the allosteric ATP-binding site. Also, obtaining structural information about the binding site for *Rn*IDE activators would be important for investigating how their binding induces conformational change in IDE with respect to a specific substrate (**a**-factor-based vs Aβ-based). This would inform better design strategies for future *Hs*IDE activator screens.

ACKNOWLEDGMENTS

We would like to thank Dr Zachary Wood (University of Georgia), for help and guidance with the purification of *Hs*IDE and members of the Schmidt laboratory for intellectual discussions related to the work presented here.

REFERENCES

1. Jakob-Roetne, R. and H. Jacobsen, *Alzheimer's disease: From pathology to therapeutic approaches.* Angew Chem Int Ed, 2009. **48**: p. 3030-3059.
2. Selkoe, D.J., *Deciphering the genesis and fate of amyloid-β protein yields novel therapies for Alzheimer's disease.* J Clin Invest, 2002. **110**: p. 1375-1381.
3. Tanzi, R.E., R.D. Moir, and S.L. Wagner, *Clearance of Alzheimer's Aβ peptide: The many roads to perdition.* Neuron, 2004. **43**: p. 605-608.
4. Shen, Y., et al., *Structures of human insulin-degrading enzyme reveal a new substrate recognition mechanism.* Nature, 2006. **443**: p. 870-874.
5. Farris, W., et al., *Insulin-degrading enzyme regulates the levels of insulin, amyloid β-protein, and the β-amyloid precursor protein intracellular domain in vivo.* Proc Natl Acad Sci USA, 2003. **100**(7): p. 4162-4167.
6. Leissring, M.A., et al., *Enhanced proteolysis of β-Amyloid in APP transgenic mice prevents plaque formation, secondary pathology, and premature death.* Neuron, 2003. **40**: p. 1087-1093.
7. Kim, S., et al., *Yeast as a tractable genetic system for functional studies of the insulin-degrading enzyme.* J Biol Chem., 2005. **280**(30): p. 27481-27490.
8. Alper, B.J., T.E. Nienow, and W.K. Schmidt, *A common genetic system for functional studies of pitrilysin and related M16A proteases.* Biochem J, 2006. **398**(1): p. 145-52.
9. Kukday, S.K., et al., *Cell-permeable, small molecule activators of the insuli-degrading enzyme.* J Biomol Screen, 2012.

10. Leissring, M.A., et al., *Kinetics of amyloid β-protein degradation determined by novel fluorescence - and fluorescence polarization-based assays.* J Biol Chem, 2003. **278**(39): p. 37314-37320.

11. Schmidt, S.D., et al., *Aβ measurement by enzyme-linked immunosorbent assay.* Methods Mol Biol, 2012. **849**: p. 507-527.

12. Alper, B.J., J.W. Rowse, and W.K. Schmidt, *Yeast Ste23p shares functional similarities with mammalian insulin-degrading enzymes.* Yeast, 2009. **26**(11): p. 595-610.

13. Song, E.S., et al., *Substrate activation of insuling-degrading enzyme (insulysin).* J Biol Chem, 2003. **278**(50): p. 49789-49794.

14. Becker, P.S., et al., *Two amino acid changes located in the alpha 1 domain specify the novel HLA-B*27:67 allele affecting the peptide-binding-site characteristics.* Tissue Antigens, 2011. **77**(6): p. 599-601.

15. Cabrol, C., et al., *Small-molecule activators of insulin-degrading enzyme discovered through high-throughput compound screening.* PLoS One, 2009. **4**(4): p. e5274.

16. Howitz, K.T., et al., *Small molecule activators of sirtuins extend Saccharomyces cerevisiae lifespan.* Nature, 2003. **425**: p. 191-196.

17. Borra, M.T., B.C. Smith, and J.M. Denu, *Mechanism of human SIRT1 activation by resveratrol.* J Biol Chem, 2005. **280**(17): p. 17187-17195.

18. Pacholec, M., et al., *SRT1720, SRT2183, SRT1460, and resveratrol are not direct activators of SIRT1.* J Biol Chem, 2010. **285**(11): p. 8340-8351.

19. Kaeberlein, M., et al., *Substrate-specific activation of sirtuins by resveratrol.* J Biol Chem, 2005. **280**(17): p. 17038-17045.

Table 3.1. *Results of the HTS to identify HsIDE activators.*

IDE activity in the presence of each compound from the library was expressed as a percentage relative to a DMSO-treated control, which was set at 100% activity.

Observed Activity	Number of compounds
< 100%	1388
100-125%	564
>125%	29

Figure 3.1. *Purification of recombinant HsIDE.*

Recombinant 6X-His-*Hs*IDE$_{M42\text{-}L1019}$ was expressed and purified from *E. coli* using metal affinity chromatography as described in the Experimental section. Bands marked with an arrow indicate *Hs*IDE and those marked with an asterisk indicate degradation products.

A) The enzyme preparation was analyzed by SDS-PAGE and stained using Coomassie™ Brilliant Blue R-250 solution. Lane 1 contains 10 μg total protein followed by two-fold serial dilutions. *Hs*IDE migrated at its predicted molecular weight of 114 kDa.

B) Western blot of a series of two-fold dilutions of the purified enzyme preparation analyzed by SDS-PAGE. Lane 1 contains 10 μg total protein followed by two-fold serial dilutions.

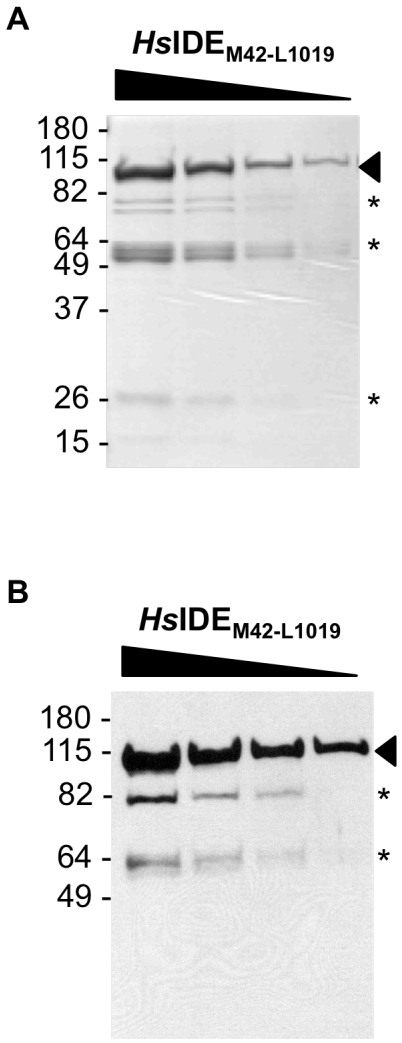
A
HsIDE M42-L1019
180
115
82
64
49
37
26
15
*
*
*
B
HsIDE M42-L1019
180
115
82
64
49
*
*

Figure 3.2. *Effect of varying assay conditions on HsIDE activity and kinetic analyses*.

A) Single point analysis of *Hs*IDE activity was performed at increasing concentrations (10-100 μg/ml), in the presence of 100 mM HEPES or 50 mM Tris-HCl, pH 7.4 and $ZnCl_2$ (12.5 or 25 μM) with 0.1% BSA. All reactions contained 50 μM substrate and were carried out in 100 mM KPi, pH 7.6 unless otherwise indicated. Activities are represented as percentages with respect to that of the reaction containing 10 μg/ml *Hs*IDE (set at 100%).

B) Analysis of a range of substrate concentrations (0-100 μM) was carried out keeping the enzyme concentration constant at 100 μg/ml. Reactions were carried out in 100 mM KPi, pH 7.6 (n=3).

C) Kinetic analysis of *Hs*IDE (100 μg/ml) was carried out in the presence of varying substrate concentrations (0-250 μM) in 100 mM KPi, pH 7.6 (n=2). Average values of specific activity were plotted in Prism 4.0 and kinetic parameters derived by fitting the data to the Hill equation [$Y=V_{max}*X\text{^}h/(K_M\text{^}h + X\text{^}h)$].

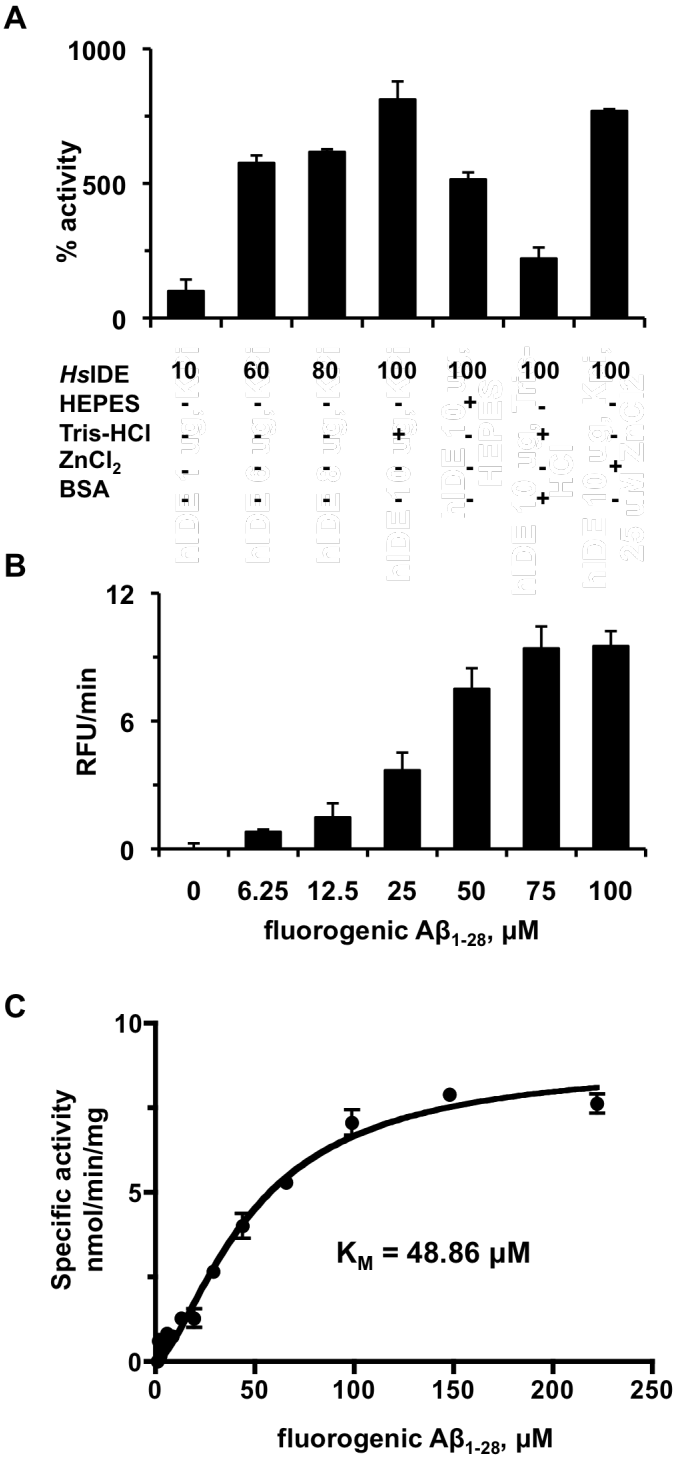
A
1000
500
0
% activity
HsIDE 10 60 80 100 100 100 100
HEPES - - - - + - -
Tris-HCl - - - + - + -
ZnCl2 - - - - - - +
BSA - - - - - + -
B
12
6
0
RFU/min
0 6.25 12.5 25 50 75 100
fluorogenic Aβ1-28, μM
C
10
5
0
Specific activity
nmol/min/mg
KM = 48.86 μM
0 50 100 150 200 250
fluorogenic Aβ1-28, μM

Figure 3.3. *Analysis of primary hits obtained from the HTS.*

A) Two compounds (**7** and **9**) identified as hits from the HTS reproducibly activate *Hs*IDE (100 μg/ml) at a concentration of 100 μM. Activities are represented as percentages relative to a DMSO-treated control, which was set at 100% (n=3). **: $p<0.01$; ***: $p<0.001$; D: DMSO.

B) Relative fluorescence unit (RFU) values obtained after complete digestion of fluorogenic $A\beta_{1-28}$ by Proteinase K (PK, 220 μg/ml) in the presence of DMSO (D), 100 μM compound **7**, or compound **9**.

A

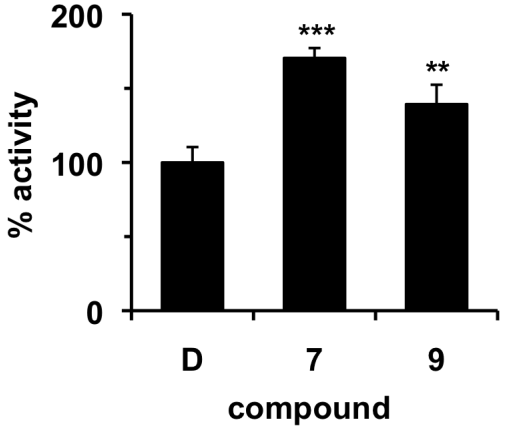

B

Compound	RFU (PK)
D	1342.04
7	794.22
9	922.52

Figure 3.4. *Unlabeled $A\beta_{1-28}$ stimulates IDE-mediated degradation of fluorogenic $A\beta_{1-28}$.*

A) and **B)** Progress curves of reactions containing *Rn*IDE (10 μg/ml), fluorogenic $A\beta_{1-28}$ (50 μM), and increasing concentrations of unlabeled $A\beta_{1-28}$ - 0 μM (open diamonds), 20 μM (closed triangles), 40 μM (open circles), 60 μM (closed squares), and no enzyme (black lines).

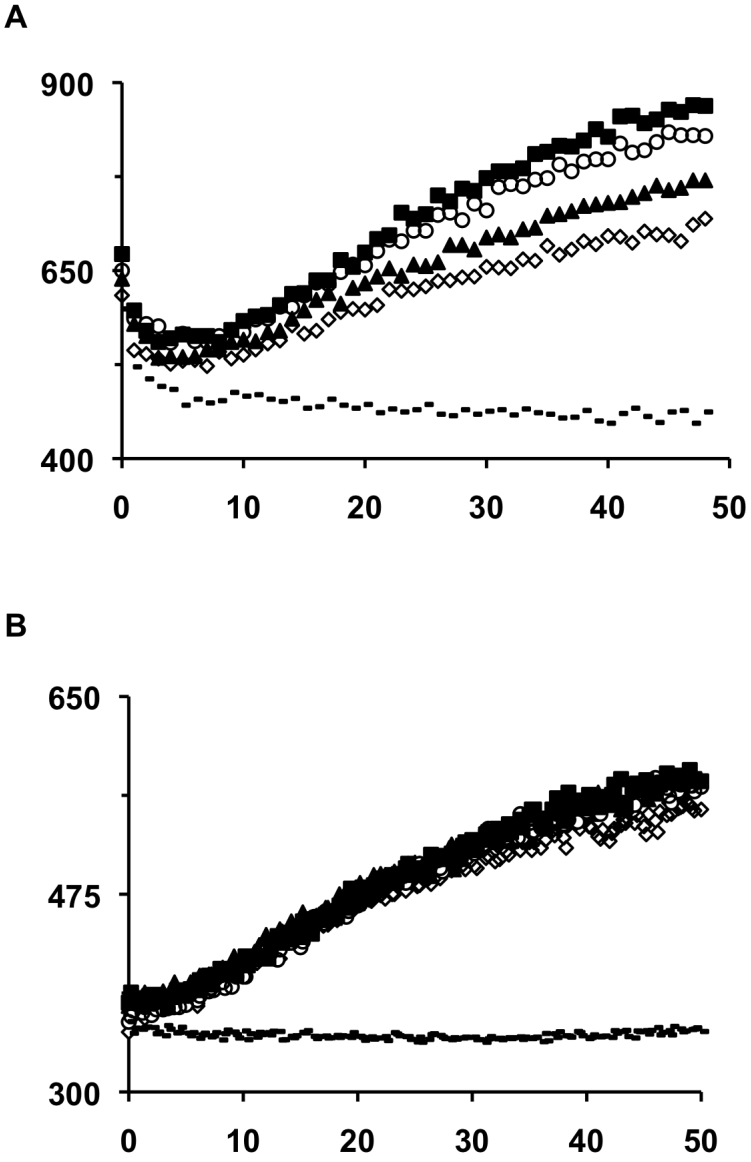
A
900
650
400
0
10
20
30
40
50
B
650
475
300
0
10
20
30
40
50

Figure 3.5. *Amino acid differences between HsIDE and RnIDE.*

Structures of the N- and C-terminal halves of *Hs*IDE and *Rn*IDE with the amino acid differences indicated as stick representations. Amino acid changes that do not result in a change in charge or polarity are colored orange whereas those that do are colored blue.

A) HsIDE

B) *Rn*IDE

A ***Hs*IDE**

N-term inner surface

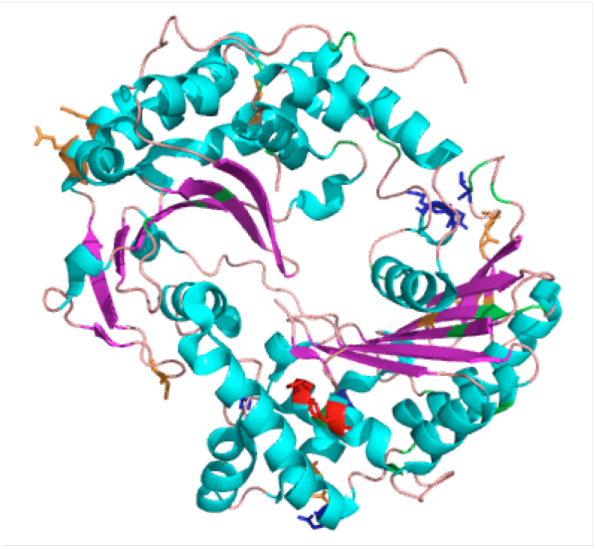

N-term outer surface

C-term inner surface

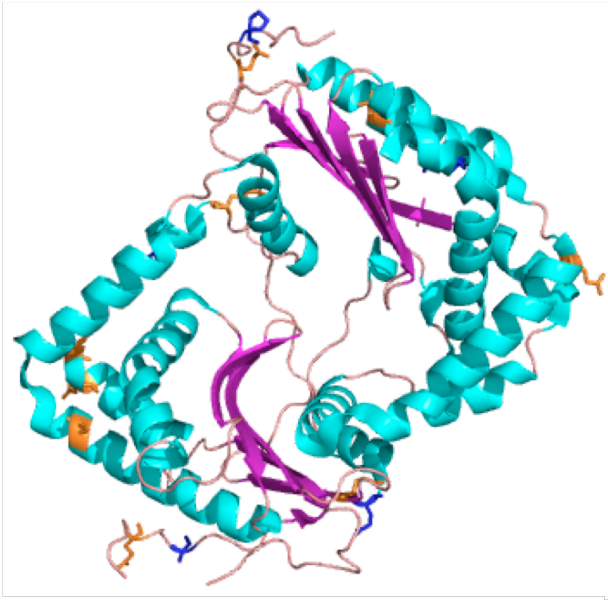

C-term outer surface

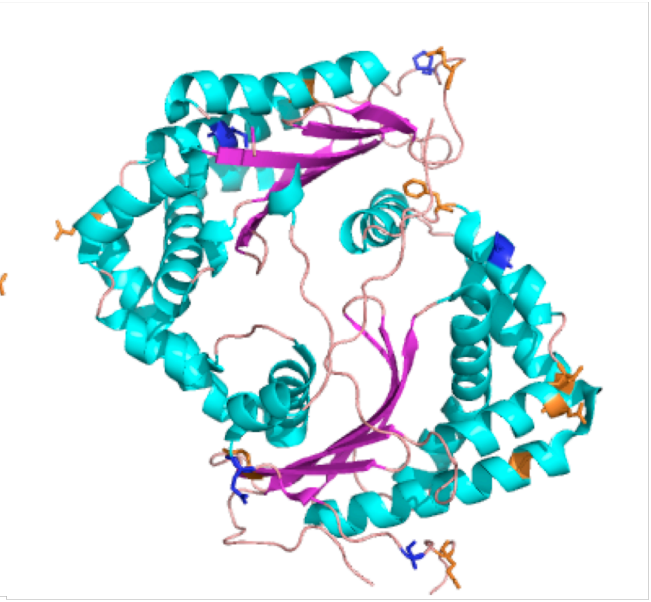

B ***Rn*IDE**

N-term inner surface

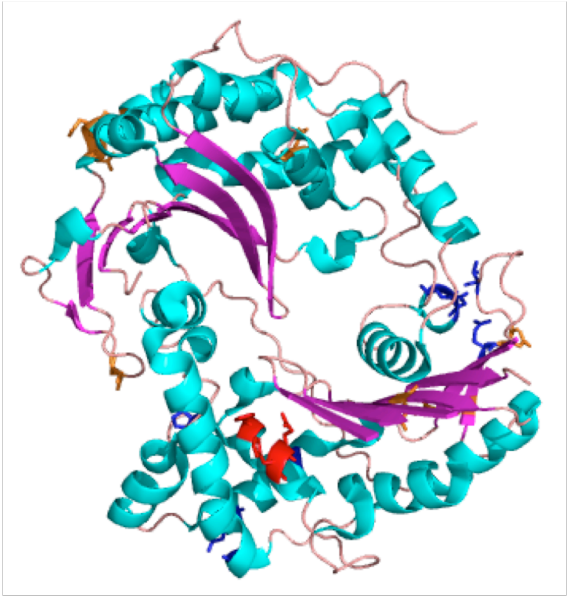

N-term outer surface

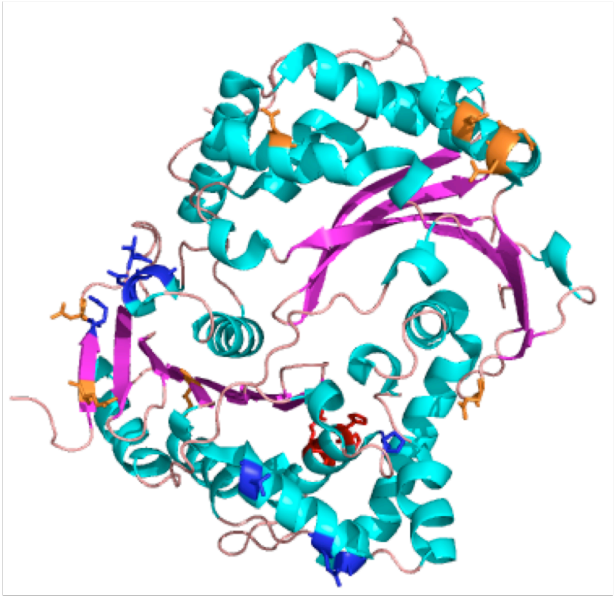

C-term inner surface

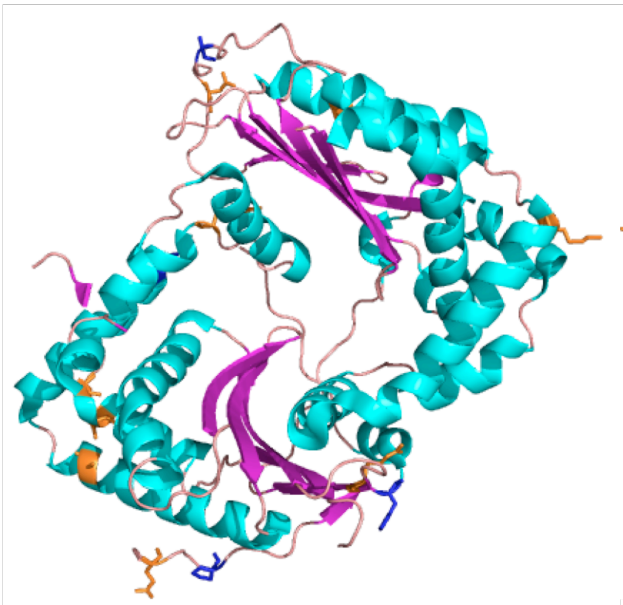

C-term outer surface

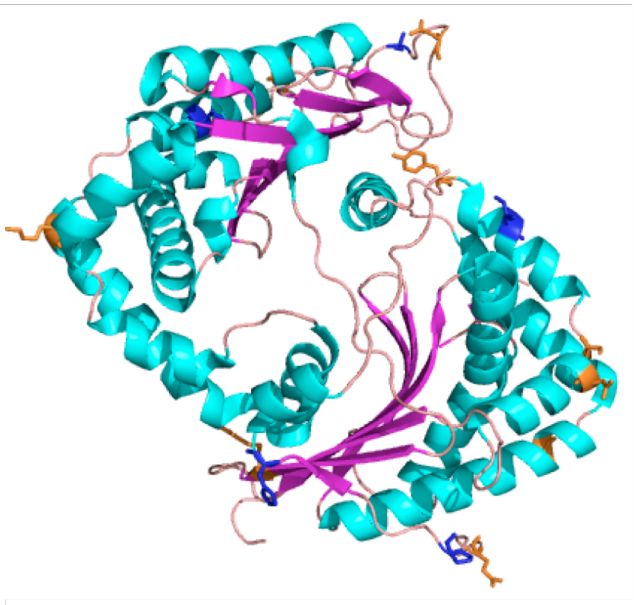

CHAPTER 4

DISCUSSION AND CONCLUSIONS

The work presented in Chapters 2 and 3 emphasizes the potential and feasibility of IDE as a drug target. In addition, we have described the identification of seven chemical agents that enhance the activity of *Rn*IDE both *in vitro* and in a cell-based assay. We have also demonstrated that these activators are species-specific, based on the observation that they are unable to activate other IDE orthologs (human and *C. elegans*). We describe the use of a novel synthetic $A\beta_{1\text{-}28}$ reporter to monitor the *in vitro* activity of IDE. The IDE activators also appear to work in the context of a specific substrate since the activators fail to stimulate *Rn*IDE activity against the synthetic $A\beta_{1\text{-}28}$ reporter (different from the one used in the first HTS screen), indicating that these activators are also substrate-specific. Lastly, we have also attempted to identify activators of *Hs*IDE using the synthetic $A\beta_{1\text{-}28}$ reporter as a substrate in the high-throughput screen.

Identification of IDE activators

Identification of enzyme activators as therapeutic agents is a field that is only about a decade old. To date, activators for only a few enzymes have been discovered that have therapeutic potential. Through our efforts, we have attempted to add IDE to this growing list. Using a high-throughput screening approach, we found that small-molecules that activate IDE from one species (e.g., rat) do not necessarily activate IDE from other species (e.g., human and

worm). Although, human and rat IDE share 94% sequence identity, changes in a few amino acid residues may alter the ability of the activators to exert their effects. For example, an amino acid change at position 176, which lies in a region where the N- and the C-terminal halves of IDE interact, from glutamic acid (hydrophilic) in *Hs*IDE to alanine (hydrophobic) in *Rn*IDE could stabilize the closed conformation preventing substrates from entering the catalytic chamber. Similar changes in isoforms of proteins such as the human leukocyte antigen have been described that affect the peptide-binding properties of the protein [1]. Possessing knowledge of the structure of human IDE [2] can help guide future drug design strategies thereby overcoming the issue of specificity. For example, compounds could be designed that bind residues at the opening of the catalytic chamber, and thus prevent the chamber from closing thereby significantly increasing enzyme activity. It has already been shown that mutations in this region of *Hs*IDE render the protease constitutively in the open state, increasing activity >30 fold [2]. Çakir et al. have recently described compounds that enhance *Hs*IDE activity by binding to the exosite [3]. They identified these activators through virtual screening of over a million small-molecules using a software program called Autodock 3.0.5. Three of the ten activators that had high-binding energies for the IDE exosite were able to reproducibly activate IDE both *in vitro* and *in vivo* in HeLa cells [3]. Virtual screening involves docking ligands (compounds from an existing library or novel chemical groups) onto the 3-D structure of a protein obtained through X-ray crystallography, NMR, or modeling methods. The technique has been successfully used to discover inhibitors of β-secretase that turned out to have EC50 values <10 μM in mammalian cell-based assays [4]. Thus, designing compounds from virtual libraries on the basis of their interactions with the IDE structure could accelerate the identification of leads, thereby reducing the time and resources that are typically invested in the traditional drug discovery process.

We also found that the activators we identified seemed to activate *Rn*IDE-mediated degradation of one synthetic substrate over another indicating that they were substrate-specific. This specificity might result from the length and/or folding differences between the two substrates. The **a**-factor based substrate was 12 residues long whereas the Aβ-based substrate was 28 residues long. One possibility is that these *Rn*IDE activators may exert their effect by binding to the exosite and thereby enhancing cleavage of the **a**-factor-based substrate. Presence of the longer Aβ-based reporter might prevent the activators from binding the exosite since it would then be occupied by the N-terminus of the reporter. It would be interesting to determine how these activators interact with IDE using methods such as X-ray crystallography (See Appendix A). Another possibility involves a difference in the folding of the two reporters that might explain the lack of activation observed against the Aβ-based substrate. Incorrect folding of the $A\beta_{1\text{-}28}$ reporter may restrict the enzyme's access to the cleavage site, making it a poor substrate. Also, we cannot exclude the possibility that the fluorophore-quencher (EDANS-DABCYL) pair conjugated to the $A\beta_{1\text{-}28}$ peptide may have interfered with the folding of the peptide, although we designed the reporter in a way that would prevent them from interfering with the enzyme-substrate interaction. Nevertheless, based on our observations, it would be possible to identify IDE activators that facilitate the clearance of Aβ, leaving levels of other IDE substrates like insulin unaffected.

Impact on IDE biology

IDE exhibits positive cooperativity, the active form of the enzyme being a dimer [5]. Previous studies have shown that smaller substrates of IDE like dynorphins or bradykinins increase the activity of the enzyme by inducing a conformational change and shifting the equilibrium toward the more active dimeric form [5]. This phenomenon has also been

previously observed when $A\beta_{1-40}$ and a synthetic fluorogenic reporter were present in the same reaction [6]. We report for the first time that Aβ also exerts an activating effect on IDE, the mechanism for which has not been assessed yet and thus remains opens for future studies. We observed that unmodified $A\beta_{1-28}$ facilitated IDE-mediated degradation of our fluorogenic $A\beta_{1-28}$ reporter. It would be interesting to determine whether $A\beta_{1-40}$ or $A\beta_{1-42}$, peptides that have a propensity to aggregate through β-sheet interactions in Alzheimer's disease, enhance IDE activity in a similar manner. Performing this type of analysis would reveal a novel aspect of IDE biology that has currently not been explored.

Implications for drug discovery

The *Rn*IDE activators we identified were unable to activate the enzyme when a fluorogenic reporter based on the $A\beta_{1-28}$ sequence was used in the *in vitro* assay. This finding suggests that reporters used to measure IDE activity should be designed to mimic the native Aβ peptide substrate in terms of length (28-42 residues), structure (ability to form β-sheet) and folding (ability of N-terminus and cleavage site to form stable interactions with the exosite and active site, respectively). Since IDE does not recognize substrates based on specific sequence motifs, this may not be an essential factor. Interference of substrate modifications such as conjugation of fluorophores could also interfere with the IDE-reporter interaction. There have been other instances reported in the literature, where enzyme activators identified through high-throughput screens using fluorogenic synthetic reporters have failed to activate the enzyme in the context of its native substrate. For example, resveratrol (a polyphenol found in red wine) was identified in a high-throughput screen conducted using a synthetic fluorogenic peptide substrate based on the tumor suppressor protein, p53 [7]. When later evaluated in an assay containing the native p53 protein, resveratrol failed to increase the deacetylase activity of SIRT1 [8]. In another

study, Cabrol *et al*. found that the IDE activators they had identified facilitated IDE-mediated degradation of Aβ only in the presence of the synthetic substrate that was used in their high-throughput screen [6]. These observations also support the recommendation that synthetic reporters of enzyme activity should resemble the native substrate as closely as possible.

FUTURE DIRECTIONS

The results of this study emphasize the importance of streamlining the high-throughput screening/drug discovery process to identify lead compounds that have therapeutic potential. IDE represents a complex molecular machine that contributes to Aβ homeostasis in the brain. There are several points that should be considered before designing a high-throughput screen to identify IDE activators. First, from our observations, it can be inferred that compounds that activate one enzyme (rat IDE) do not necessarily activate the human ortholog. Therefore, the HTS screen should be conducted with the human enzyme. Second, the type of reporter used to measure enzyme activity can influence the outcome of the screen (i.e., hits identified). It is important for the reporter to possess the same properties as the native substrate (Aβ). Third, competing substrates can also influence the properties of IDE activators. For example, the presence of insulin, a potent inhibitor of IDE-mediated Aβ degradation, can neutralize the activation properties of these compounds. Including insulin in the screen can avoid this problem and ensure that Aβ-specific activators are identified. Lastly, ATP has been known to enhance IDE activity. This effect is dependent on the triphosphate moiety rather than hydrolysis of the ATP molecule as established previously [9]. In our studies, this effect was observed under conditions in which phosphate buffers (KPi) were used. Addition of ATP did not enhance this

effect. Therefore, we contend that conducting the high-throughput screen in phosphate buffer can result in the identification of compounds that stimulate IDE activity in an ATP-independent manner.

Investigating the mechanism of *Rn*IDE activators identified in this study could aid in recognizing specific regions of IDE that interact with the activators (see Appendix A). This information can help guide structure-activity relationship studies. Extending the search for IDE activators to other commercial libraries represents another approach; examples of such libraries include Thermo Fisher Scientific's Maybridge HitFinder^{TM} and Ro3 fragment libraries, which are currently being used for Alzheimer's drug discovery by certain research groups (http://www.maybridge.com/portal/alias__Rainbow/lang__en/tabID__228/DesktopDefault.aspx). Ongoing efforts to identify IDE activators are currently underway at the Scripps Research Institute (Jupiter, FL) for Dr. Leissring's group at the Mayo Clinic (Jacksonville, FL). These efforts involve high-throughput screening of approximately 650,000 compounds using established FAβB and fluorescence polarization assays [10] and are currently active (Pubchem ID 493124). Although speculative, the observation that Aβ stimulates IDE activity can be used to design short peptide fragments that bind to the active site and increase IDE-mediated Aβ degradation through an allosteric mechanism. These fragments should mimic the cleavage sites on Aβ that are recognized by IDE.

IDE represents an attractive therapeutic target because it can degrade Aβ before the peptide can oligomerize and cause damage to neurons. Through our studies, we have demonstrated that IDE- and Aβ-specific activators can be identified. We have used novel fluorescence based *in vitro* assays optimized for high-throughput screening and cell-based assays to monitor IDE activity *in vivo*. The findings from our studies provide a significant contribution

to the field of Alzheimer's drug discovery. Although a cure for this devastating disease remains unavailable, the search for one continues, and we hope that our efforts have brought us one step closer to that goal.

REFERENCES

1. Becker, P.S., et al., *Two amino acid changes located in the alpha 1 domain specify the novel HLA-B*27:67 allele affecting the peptide-binding-site characteristics.* Tissue Antigens, 2011. **77**(6): p. 599-601.
2. Shen, Y., et al., *Structures of human insulin-degrading enzyme reveal a new substrate recognition mechanism.* Nature, 2006. **443**: p. 870-874.
3. Çakir, B., et al., *Structure based discovery of small molecules to regulate the activity of human insulin degrading enzyme.* PLoS One, 2012. **7**(2): p. e31787.
4. Huang, D., et al., *Discovery of cell-permeable non-peptide inhibitors of β-secretase by high-throughput docking and continuum electrostatics calculations.* J Med Chem, 2005. **48**(16): p. 5108-5111.
5. Song, E.S., et al., *Substrate activation of insuling-degrading enzyme (insulysin).* J Biol Chem, 2003. **278**(50): p. 49789-49794.
6. Cabrol, C., et al., *Small-molecule activators of insulin-degrading enzyme discovered through high-throughput compound screening.* PLoS One, 2009. **4**(4): p. e5274.
7. Howitz, K.T., et al., *Small molecule activators of sirtuins extend Saccharomyces cerevisiae lifespan.* Nature, 2003. **425**: p. 191-196.
8. Pacholec, M., et al., *SRT1720, SRT2183, SRT1460, and resveratrol are not direct activators of SIRT1.* J Biol Chem, 2010. **285**(11): p. 8340-8351.
9. Song, E.S., et al., *ATP effects on insulin-degrading enzyme are mediated primarily through its triphosphate moiety.* J Biol Chem, 2004. **279**(52): p. 54216-54220.

10. Leissring, M.A., et al., *Kinetics of amyloid β-protein degradation determined by novel fluorescence - and fluorescence polarization-based assays.* J Biol Chem, 2003. **278**(39): p. 37314-37320.

APPENDIX A

FOUNDATIONS FOR CONTINUING INVESTIGATION

Studies that are pertinent to this thesis and not presented elsewhere within this document are described below. The basis for each of the studies is also described.

Effect of RnIDE activators on $A\beta_{1-40}$ degradation

The study described in Chapter 2 involved the identification and characterization of *Rn*IDE activators and their effect on the degradation of synthetic and *in vivo* reporters of IDE activity. We wanted to determine whether these activators enhanced clearance of $A\beta_{1-40}$, the physiologically relevant substrate for IDE. To this end, we used high performance liquid chromatography (HPLC) to analyze the products of the reactions under conditions similar to those of the *in vitro* fluorescence assay. Peptide cleavage was expressed as percentage of total $A\beta_{1-40}$ remaining in the reaction, which was calculated from a standard curve created using increasing concentrations of $A\beta_{1-40}$ as depicted in Figure A.5A. The activators were unable to facilitate *Rn*IDE-mediated $A\beta_{1-40}$ degradation as shown in Figure A.5B. The data lends support to the idea that these activators indeed have preferences for specific substrates. Further investigation of the mechanism by which these activators stimulate *Rn*IDE could explain the differences in their substrate preferences. Techniques such as X-ray crystallography, circular dichroism, and analytical ultracentrifugation could be used to determine whether the activators

bind IDE and bring about a change in its conformation or oligomerization state (increased dimer: monomer ratio). Some of these studies have already been initiated as described below.

Crystallization studies of RnIDE

In order to determine whether the *Rn*IDE activators identified in our studies (see Chapter 2) interact with the enzyme, we have initiated crystallization studies of the enzyme with the intention of soaking crystals obtained in solutions containing the activators followed by X-ray diffraction and structure determination. For this purpose, we have purified *Rn*IDE to near homogeneity as depicted in Figure A.2. To find conditions suitable for crystal formation prior to soaking them in solutions containing the activators, we performed hanging drop crystallization screens provided by Hampton Research (Hampton Research Inc.; Aliso Viejo, CA). These screens yielded two conditions that were conducive to the growth of crystals as listed in Table A.1. Further optimization of these conditions was carried out in order to obtain diffraction quality crystals. Several conditions, listed in Table A.1, resulted in the formation of crystalline precipitates (data not shown). Future studies should utilize these conditions as starting points to obtain crystals for diffraction and structure determination. Once diffraction data from crystals of activator-bound *Rn*IDE is obtained, the structure of the complex can be determined using molecular replacement since the structure of *Rn*IDE is known (PDB ID 3P7L) [1]. This work was conducted in the laboratory of Dr. Zachary Wood (University of Georgia).

Studies with commercially purchased RnIDE activator NSC 45208 (compound 3)

In order to verify the function of *Rn*IDE activator NSC 45208 (compound **3**, see Chapter 2), the compounds was commercially purchased from two different companies (TCI America, Portland, OR and Calbiochem, Philadelphia, PA). The other activators were not available

commercially, and we did not possess the resources to synthesize them, and were therefore not analyzed. When these commercially purchased compounds were evaluated using our *in vitro* fluorescence assay, they were unable to activate *Rn*IDE as illustrated in Figure A.3. This result was surprising because the compounds from all three sources are chemically identical (structure, molecular weight). We formed two hypotheses to explain this observation. First, the difference in the activating property between the three samples could be explained by a difference in storage conditions of the sample obtained from National Cancer Institute (NCI) that could lead to changes in the sample (e.g., causing the compound to aggregate). Second, it is possible that a contaminant present in the NCI sample is responsible for IDE activation or a contaminant present in the other two samples might hinder the ability of compound **3** to stimulate IDE activity.

To address the first possibility, we examined the particle size of the three samples by performing dynamic light scattering (DLS) analysis. The results of this analysis, presented in Table A.2 revealed that the particle size of the sample obtained from NCI was ~20X larger than the samples obtained from TCI and Calbiochem indicating that the molecules in the NCI sample may have aggregated. 1-anilinonaphthalene-8-sulfonic acid (ANS) served as a negative control whereas Congo red and Triton X-100 served as positive controls.

To address the second possibility of the presence of a contaminant in the NCI sample, we performed thermal melt and NMR analyses on all three samples. Thermofluor analysis showed no significant difference between the melting temperatures (T_m) of the three samples, indicating a lack of contaminating material that could contribute to an increase in the T_m of the samples. In addition, there was no significant difference in the NMR spectra of proton peaks of each sample indicating that all of them contain identical components. The NMR spectra are illustrated in Figure A.4. The spectra for NCI sample has a higher background due to the limited availability

of thus compound for analysis. Future studies should be performed in order to explain the lack of reproducibility between the NCI sample and the samples obtained from TCI America and Calbiochem. These studies should include fractionation of the three samples using HPLC to determine whether the NCI sample contains aggregated species. Individual fractions collected should be evaluated for their ability to activate IDE.

Preliminary identification of HsIDE inhibitor hits through HTS

Diabetes mellitus is a condition caused by impaired insulin signaling, which leads to high blood glucose levels [2]. IDE plays a very important role in the regulation of insulin levels. IDE -/- mice are hyperinsulinemic and glucose-intolerant due to reduced insulin degradation [3]. Therefore, inhibition of IDE-mediated insulin catabolism could lead to an increase in insulin signaling and can thus serve as anti-diabetic therapy. Inhibitors of IDE that are active both *in vitro* and *in vivo* as judged by inhibited degradation of radioactive and fluorescently labeled insulin have been previously identified [4]. The high-throughput screen to identify activators of *Hs*IDE described in Chapter 3, also generated several inhibitor hits. A summary of these hits is shown in Table A.4, albeit inhibition was observed against an Aβ-based reporter. Only compounds that inhibited *Hs*IDE to <40% are included. Structures of six compounds that inhibited *Hs*IDE activity to ≤ 5% are depicted in Figure A.5. Future studies can pursue these primary hits to determine whether they inhibit *Hs*IDE-mediated degradation of insulin before performing dose response and kinetic studies.

EXPERIMENTAL

HPLC analyses

HPLC analyses were carried out using an Agilent HPLC 1100 system (Santa Clara, CA). Samples were loaded onto a Vydac® low trifluoroacetic acid (TFA) silica C-18 column (Grace, Deerfield, IL) heated to 60 °C, and $A\beta_{1\text{-}40}$ was detected at 215 nm using gradient elution. Solvent A consisted of 95% water and 0.075% TFA, and solvent B consisted of 95% acetonitrile and 0.075% TFA. The $A\beta_{1\text{-}40}$ standard curve was created by injecting varying amounts of peptide into the system (0-20 μg). Reactions (50 μl) contained *Rn*IDE (10 μg/ml), $A\beta_{1\text{-}40}$ (50 μM), and DMSO or compound (100 μM) in 0.1 M KPi buffer, pH 7.6. All samples were diluted 2X with solvent A before injecting into the column. Peak areas were determined using the analysis tools on the Agilent ChemStation software.

Purification of recombinant RnIDE

Recombinant 6X-His-*Rn*$IDE_{M42\text{-}L1019}$ was expressed in and purified from BL21 (DE3) cells using immobilized metal affinity chromatography. The cultures were induced with 150 μM IPTG and incubated overnight at 20 °C with shaking at 80 rpm. Cell lysates containing the protein of interest were loaded onto a column packed with BD Talon™ metal affinity resin (BD Biosciences, Sparks, MD) to a bed volume of 10 ml. Protein bound to the column was eluted using 250 mM imidazole following washes with lysis buffer (50 mM Na-K phosphate, 300 mM NaCl, pH 8.0) to remove unbound cell components. After several dialysis steps to decrease the imidazole concentration, the protein solution was concentrated to 13.2 mg/ml using Centriprep Centrifugal filter units (EMD Millipore, Billerica, MA) with a 30 kDa molecular weight cut-off.

Aliquots of the concentrated protein solution were flash frozen in liquid nitrogen and stored at -80 °C.

Crystallization experiments

Crystallization screens were set up using the hanging drop method and Crystal Screen™, Crystal Screen 2™, PEG/Ion Screen™, PEG/Ion 2 Screen™ and PEG/Rx™ 2 (Hamptom Research Inc; Aliso Viejo, CA) screening kits. Ammonium sulfate and phosphate grid screens were performed according to methods provided by Hampton Research Inc.

DLS, Thermofluor and NMR analyses

To determine particle size distribution, solutions containing the three samples of compound **3** obtained from NCI, TCI America, and Calbiochem (100 μM) were prepared in 0.1 M KPi buffer, pH 7.6 in a volume of 50 μl. The samples were centrifuged at 14,000 rpm for 15 mins. DMSO was used as a control since it was the solvent in which the compounds were stored. A volume of 15 μl from the supernatant of each sample was transferred to a clean cuvette and incubated at 30 °C for 1 min and hydrodynamic radius data collected in a DynaPro-LSR 99-E-15 instrument (Proterion Corporation, Piscataway, NJ). Thermal melt profiles were obtained in a manner similar to that described in Chapter 2 except that the samples contained 100 μM compound **3** obtained from NCI, TCI, and Calbiochem. ^{1}H NMR spectra were obtained by dissolving powdered forms of the three samples in deuterated DMSO and analyzed in a Varian Mercury Plus 400 NMR spectrometer.

REFERENCES

1. Noinaj, N., et al., *Identification of allosteric regulatory site of insulysin.* PLoS One, 2011. **6**(6): p. e20864.
2. Organization, W.H. and I.D. Federation, *Definition and diagnosis of diabetes mellitus and intermediate hyperglycemia*. 2006, World Health Organization: Geneva, Switzerland.
3. Farris, W., et al., *Insulin-degrading enzyme regulates the levels of insulin, amyloid β-protein, and the β-amyloid precursor protein intracellular domain in vivo.* Proc Natl Acad Sci USA, 2003. **100**(7): p. 4162-4167.
4. Leissring, M.A., et al., *Designed inhibitors of insulin-degrading enzyme regulate the catabolism and activity of insulin.* PLoS One, 2010. **5**(5): p. e10504.

Table A.1. *Conditions conducive to the growth of RnIDE crystals.*

Salt/Additive	Buffer	Precipitant/Polymer	Screen
Conditions obtained from crystal screens			
0.2 M $CaCl_2.2H_2O$	0.1 M $CH_3COONa.3H_2O$, pH 4.6	20% v/v 2-Propanol	Crystal Screen™
0.02 M ZnCl2	None	20% w/v PEG 3350	PEG/Ion 2 screen™
Near optimum conditions			
-	0.1 M HEPES, pH7.0	15% v/v 1,2-Propanediol, 10% PEG 8000	-
	1.8 M Na-KPO_4, pH5.6 and 6.9		-
10% glycerol, 100 mM NaCl	-	15% v/v 1,2-Propanediol, 10% PEG 8000	-
15% glycerol, 100 mM NaCl	-	15% v/v 1,2-Propanediol, 10% PEG 8000	-

Table A.2. *Hydrodynamic radii of particles in solutions of RnIDE activator compound 3.*

Solutions of compound **3** (C3) obtained from the three sources were prepared in 0.1 M KPi buffer to a final concentration of 100 μM. 1-anilinonaphthalene-8-sulfonic acid (ANS, 1 mM) served as a negative control whereas Congo Red (750 μM) and Triton X-100 (0.5%) served as positive controls for distinct particle sizes. NCI: National Cancer Institute; TCI: TCI America; CB: Calbiochem.

Compound	**Radius (nm)**
ANS	0.33 ± 0.06
Congo Red	20.5 ± 7.25
Triton X-100	4.93 ± 0.15
Kpi	0.27 ± 0.15
DMSO	0.25 ± 0.07
C3 (NCI)	5.97 ± 1.59
C3 (TCI)	0.325 ± 0.05
C3 (CB)	0.37 ± 0.06

Table A.3. *Thermal melt profiles of solutions containing compound 3.*

Compound	Tm (°C)
DMSO	45.01 ± 2.9
C3 (NCI)	54.44 ± 1.04
C3 (TCI)	57.18 ± 1.68
C3 (CB)	57.33 ± 0.06

Table A.4. *List of HsIDE inhibitor hits.*

% activity	Observed hits
31 - 40%	13
21 - 30%	12
11 - 20%	15
6 - 10%	7
0 - 5%	6

Figure A.1. *Effect of RnIDE activators on $A\beta_{1\text{-}40}$ degradation.*

HPLC analyses were carried out using an Agilent HPLC 1100 system (Santa Clara, CA). Samples were loaded onto a Vydac® low trifluoroacetic acid (TFA) silica C-18 column (Grace, Deerfield, IL) heated to 60 °C, and $A\beta_{1\text{-}40}$ was detected at 215 nm using gradient elution. Solvent A = 95% water, 0.075% TFA; Solvent B = 95% acetonitrile, 0.075% TFA. All samples were diluted 2X with Solvent A before injecting into the column.

A) Standard curve for $A\beta_{1\text{-}40}$ generated using varying amounts of peptide (0-20 μg). Data obtained was plotted in Microsoft Excel and an equation derived for the linear fit.

B) Reactions (50 μl) contained *Rn*IDE (10 μg/ml), $A\beta_{1\text{-}40}$ (50 μM), and DMSO or compound (100 μM) in 0.1 M KPi buffer, pH 7.6. D - DMSO.

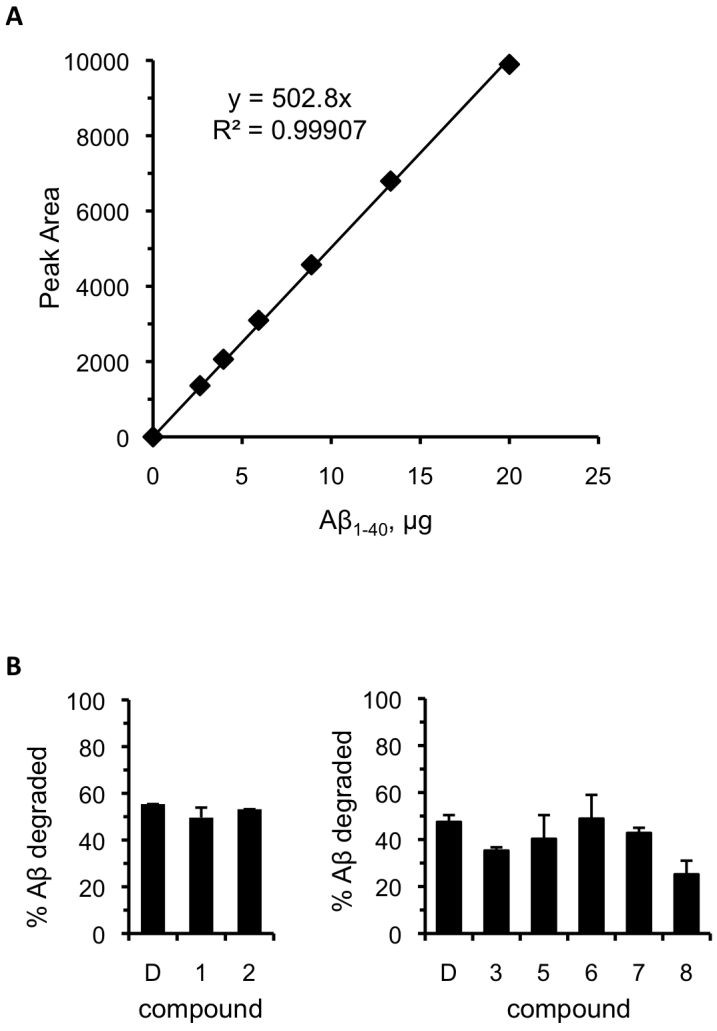
A
y = 502.8x
R² = 0.99907
Peak Area
10000
8000
6000
4000
2000
0
0
5
10
15
20
25
Aβ1-40, µg
B
% Aβ degraded
100
80
60
40
20
0
D
1
2
compound
% Aβ degraded
100
80
60
40
20
0
D
3
5
6
7
8
compound

Figure A.2. *Purification of recombinant RnIDE.*

Recombinant 6X-His-*Rn*IDE$_{M42\text{-}L1019}$ was expressed and purified from *E. coli* using immobilized metal affinity chromatography. Two-fold serial dilutions of the enzyme preparation were analyzed by SDS-PAGE and stained using Coomassie^{TM} Brilliant Blue R-250 solution. Lane 1 contains 10 μg total protein. *Rn*IDE migrated at its predicted molecular weight of 114 kDa. Bands marked with an arrow indicate *Rn*IDE and those marked with an asterisk indicate degradation products.

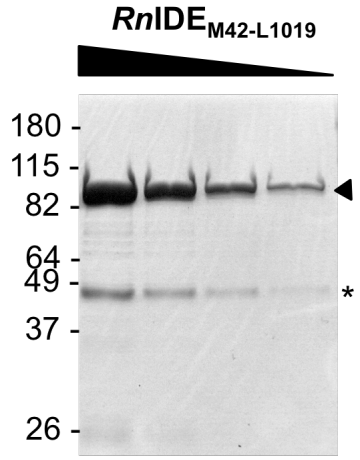
*RnIDE*M42-L1019
180
115
82
64
49
37
26
*

Figure A.3. *Effect of compound **3** from different sources on RnIDE activity.*

Samples of compound **3** obtained from various sources (100 μM) were evaluated using fluorescence-based *in vitro* assays. All activities were normalized to that of the appropriate DMSO-treated control, which was set at 100%. In addition to compound **3**, reactions contained *Rn*IDE (10 μg/ml) and the fluorogenic **a**-factor-based substrate (50 μM).

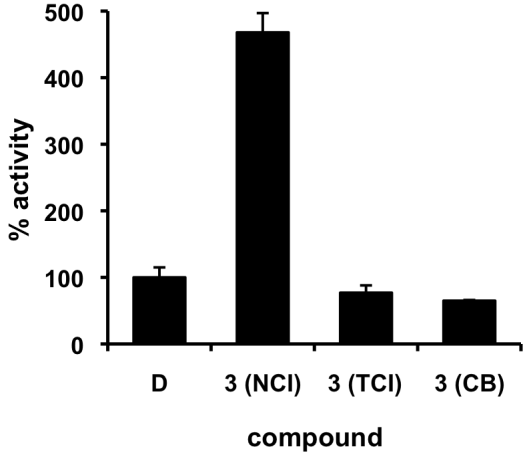
500
400
300
200
100
0
% activity
D
3 (NCI)
3 (TCI)
3 (CB)
compound

Figure A.4. *NMR spectra for compound **3** obtained from different sources.*

^{1}H NMR spectra of samples from NCI **(A)**, TCI America **(B)**, and Calbiochem **(C)** obtained using a Varian Mercury Plus 400 NMR spectrometer. Powdered samples were resuspended in deuterated DMSO for analysis.

A

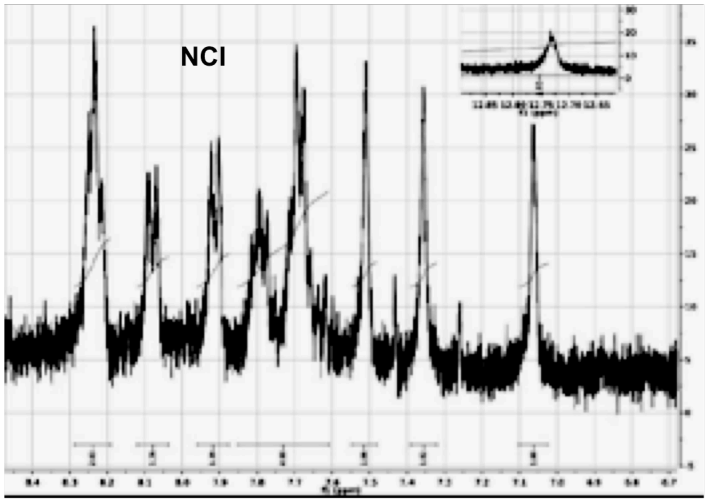

B

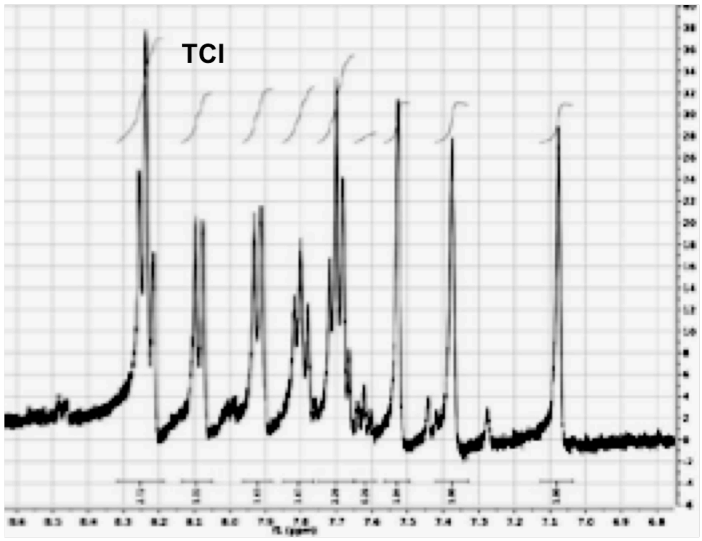

C

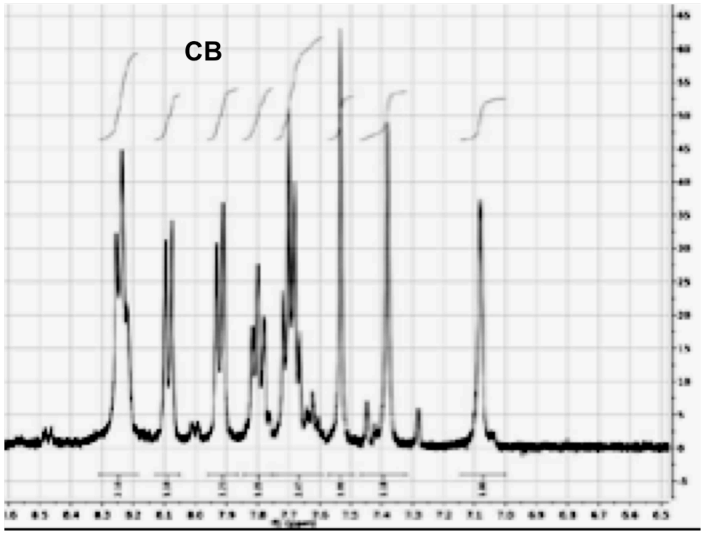

Figure A.5. *Structures of HsIDE inhibitors*.

The chemical structures of six primary hits from the high-throughput screen are shown. These inhibitors reduced *Hs*IDE activity to <5%. Structures were obtained from the NCI Developmental Therapeutics Program database and re-drawn using ChemDraw (CambridgeSoft, Perkin Elmer, Cambridge, MA).

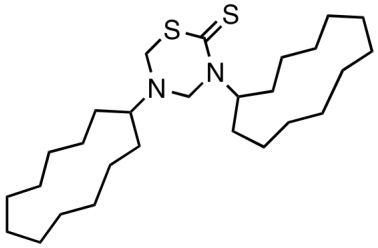

NSC 209910

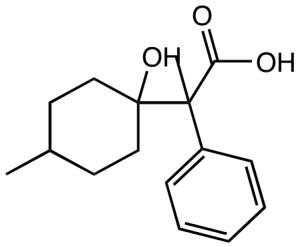

NSC 41431

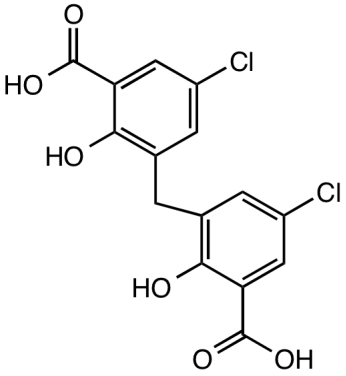

NSC 48684

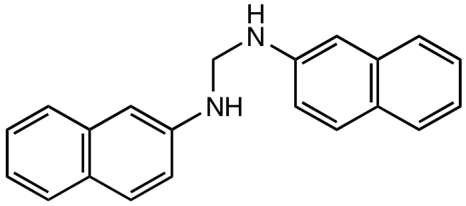

NSC 57975

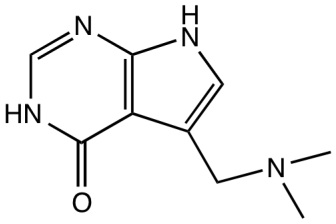

NSC 62749

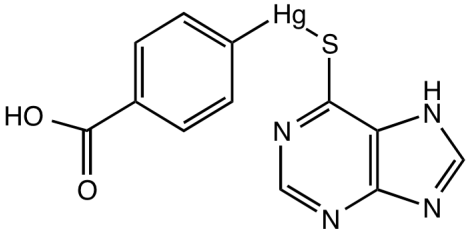

NSC 92585

APPENDIX B

PROTEOLYTIC PROCESSING OF CERTAIN CAAX MOTIFS CAN OCCUR IN THE ABSENCE OF THE RCE1P AND STE24P CAAX PROTEASES[3]

[3] Kukday, S.S.*, Krishnankutty, R.K.*, Castleberry, A.J., Breevoort, S.R. and W.K. Schmidt. 2009. *Yeast*. 26(8): 451-463. Reprinted here with permission of the publisher.
*Equal contribution by these authors.

ABSTRACT

The CaaX motif directs C-terminal protein modifications that include isoprenylation, proteolysis, and carboxylmethylation. Proteolysis is generally believed to require either Rce1p or Ste24p. While investigating the substrate specificity of these proteases using the yeast **a**-factor mating pheromone as a reporter, we observed Rce1p and Ste24p-independent mating (RSM) when the CKQQ CaaX motif was used in lieu of the natural **a**-factor CVIA motif. Uncharged or negatively charged amino acid substitutions at the a_1 position of the CKQQ motif prevented RSM. Alanine substitutions at the a_2 and X positions enhanced RSM. Random mutagenesis of the CaaX motif provided evidence that RSM occurs with approximately 1% of all possible CaaX motif permutations. Combined mutational and genetic data indicates that RSM-promoting motifs have a positively charged amino acid at the a_1 position. Two of nine naturally occurring yeast CaaX motifs conforming to this pattern promoted RSM. The activity of the isoprenylcysteine carboxyl methyltransferase Ste14p was required for RSM, indicating that RSM-promoting CaaX motifs are indeed proteolyzed. RSM was enhanced by the over-expression of Axl1p or Ste23p, suggesting a role for these M16A subfamily metalloproteases in this process. We have also determined that an N-terminal extension of the **a**-factor precursor, which is typically removed by the yeast M16A enzymes, is required for optimal RSM. These observations suggest a model that involves targeting of the **a**-factor precursor to the peptidosome cavity of M16A enzymes where subsequent interactions between RSM-promoting CaaX motifs and the active site of the M16A enzyme lead to proteolytic cleavage.

INTRODUCTION

The CaaX motif is a C-terminal tetrapeptide sequence generally described as having an invariant cysteine (*C*), two aliphatic amino acids (a_1 and a_2), and one of several amino acids in the terminal position (*X*). Eukaryotic proteins having a CaaX motif (CaaX proteins) typically undergo three ordered post-translational modifications (reviewed in [1, 2]) (**Figure B.1**). The first is isoprenylation of the cysteine by either the C15 farnesyl transferase (FTase) or the C20 geranylgeranyl transferase I (GGTase I). The context of the CaaX motif can dictate which isoprenoid is attached, with geranylgeranylated proteins often having Leu and Phe at the *X* position. Isoprenylation is followed by an endoproteolytic cleavage that removes the last three amino acids of the motif (i.e. aaX). Two proteases, Rce1p and Ste24p, have been identified that can perform CaaX proteolysis [3, 4]. CaaX proteolysis is followed by carboxylmethylation of the farnesylated cysteine by an isoprenylcysteine carboxyl methyltransferase (ICMT). Collectively, these modifications modulate the activity, membrane partitioning, subcellular localization, stability, and/or protein-protein interaction properties of the modified protein [3, 5-11].

CaaX proteins have diverse, biologically important functions. Pertinent examples of CaaX proteins include signaling molecules (*i.e.,* Ras and RhoB), nuclear proteins (*i.e.,* CENP-E, CENP-F, and nuclear lamins), Hsp40 chaperones (*i.e.,* Ydj1p and DNJ3), and fungal mating pheromones (*e.g., Saccharomyces cerevisiae* **a**-factor). Because of the prominence of CaaX proteins in association with disease (e.g. Ras and cancer), it is generally hypothesized that interfering with CaaX modifications could be incorporated into disease intervention strategies. This hypothesis has led to the development of FTase inhibitors (FTIs) that are currently being

investigated for the treatment of cancer and progeroid syndromes [12, 13]. Inhibitors of the CaaX proteases and ICMT hold similar therapeutic potential and are being investigated [14-17]. A problematic issue in this research area is the ability of CaaX proteins to be processed by partially redundant activities. For example, several proteins are known to be isoprenylated by GGTase I in the presence of FTIs [18, 19]. Likewise, it is possible that targeted inhibition of Rce1p can lead to alternative processing by Ste24p, and *vice versa*. This issue is less of a concern for targeted inhibition of the ICMT because there appears to be no alternative enzyme that can perform the carboxyl methylation of CaaX proteins.

The two CaaX proteases are both ER-localized membrane proteins, but are otherwise unrelated by primary sequence [20]. Ste24p is a zinc-dependent metalloprotease that has been purified and demonstrated to posses *in vitro* CaaX proteolytic activity [4]. The mechanism of Rce1p remains undefined. Several lines of evidence support the function of Rce1p as a CaaX protease, including genetic and over-expression studies [3, 4, 10, 21]. Bioinformatic and inhibitor profiles suggest that it is a metalloprotease [15, 22].

Rce1p and Ste24p have partially overlapping substrate specificity, meaning that each enzyme has specific substrates and also shared ones. For example, Rce1p specifically modifies Ras GTPases, Ste24p specifically modifies prelamin A, and both enzymes modify the yeast **a**-factor precursor [3, 23, 24]. Yeast **a**-factor has been a convenient reporter for investigating CaaX modifications because defects in any of the three post-translational events results in a sterile mating phenotype and because it can be used to readily monitor either Rce1p or Ste24p activity [3]. The yeast system is also useful for the evaluation of CaaX proteases from other eukaryotic species because they all have the ability to recognize yeast **a**-factor precursor as a substrate [25-28].

While investigating the substrate specificities of the yeast CaaX proteases using **a**-factor as a reporter, we observed the ability of certain CaaX motifs to promote yeast mating in the absence of Rce1p and Ste24p. This study compares Rce1p and Ste24p-independent mating (RSM) with mating promoted by the established CaaX proteases and provides evidence that a substantial number of CaaX motifs, including naturally occurring yeast motifs, can promote RSM. Moreover, we provide evidence that the yeast M16A metalloproteases Axl1p and Ste23p, which normally cleave an N-terminal extension found on the **a**-factor precursor, can enhance RSM, suggesting that these enzymes may be responsible for this activity.

EXPERIMENTAL

Yeast strains

The yeast strains used in this study are listed in **Table B.1**. yWS829 was created by disrupting the *STE14* gene in yWS164 using the *Bam*HI-ClaI fragment from pSM284 [7]. The disruption was specific as confirmed by PCR using appropriate primers flanking the sites of integration and Southern analysis using the *URA3* cassette to probe a *BamH*I digest of genomic DNA prepared from the candidate disruption strain. Yeast strains were routinely grown at 30 °C on rich media (YEPD) or appropriate synthetic dropout media (SC-) when propagating plasmid-transformed strains [29]. Yeast DNA transformations were carried out according to published methods [30].

Yeast plasmids

The yeast plasmids used in this study are listed in **Table B.2**. pWS610 and pWS612 were constructed by subcloning the appropriate *Not*I-*Xho*I fragment encoding **a**-factor from

pSM1605 and pWS196, respectively, into pRS415. pWS817 was created similarly but with pWS654 and pRS315. pWS196 and all other **a**-factor encoding plasmids bearing altered CaaX motifs were created by PCR-directed plasmid-based recombination [31]. The parent plasmid (i.e. pSM1605, pWS438 or pWS610) was treated with *Mlu*I and, in most instances, *Sph*I to generate a gap in the 3′untranslated region (UTR) of the *MFA1* gene very near the 3′ end of the open reading frame (ORF). The digested plasmid was co-transformed into yeast with a PCR product having sequence homology to the plasmid in regions flanking the restriction site(s) to allow for gap repair. The PCR product was generated using a mutagenic forward oligo that contained 39 bases of homology to the parent plasmid, nine bases encoding the desired aaX sequence, and an 18-21 base extension for annealing to a template (i.e. pSM1605, pWS438 or pWS610). The reverse oligo was complementary to the vector outside the polylinker into which the *MFA1* encoding fragment was subcloned; its use generates homology to the plasmid on the *Sph*I side of the digested plasmid. Following co-transformation of the digested plasmid and PCR product, individual yeast colonies surviving appropriate selection (SC-Ura or SC-Leu) were screened for those containing a plasmid encoding the altered *MFA1* gene, as determined by restriction enzyme mapping and subsequent sequencing of isolated plasmids; a silent site (e.g. *Sph*I or *Pst*I) was typically incorporated along with the desired mutation. All plasmids derived from pWS438 were converted to low-copy plasmids by subcloning the *Not*I-*Xho*I MFA1-encoding fragment into pRS315 at the same sites. pWS196 was the only plasmid derived from pSM1605, and it was manipulated as described above.

pWS601 and pWS602 were also created by PCR-directed plasmid-based recombination. These plasmids encode *AXL1* and *STE23*, respectively, behind the constitutive phosphoglycerate kinase

(*PGK*) promoter. pSM703 was the recipient vector used in the construction of these plasmids, which was gapped within its polylinker prior to use.

Constructs encoding ubiquitin fusions were created by PCR-directed plasmid-based recombination essentially as described above for the creation of **a**-factor CaaX motif mutants. A PCR fragment encoding the CKQQ motif was derived from pWS718 and recombined into *Mlu*I linearized pSM1368 and pSM1369 to create pWS892 and pWS893, respectively. To create pWS894, a PCR fragment also derived from pWS718 was produced that would incorporate the DNA sequence encoding mature **a**-factor upon recombination into *Mlu*I linearized pWS892.

Serial dilution mating assay

The ability of the various CaaX motifs to promote **a**-factor maturation was judged using a genetic assay that scores diploid formation resulting from the mating of haploid mating partners. The *MAT***a** haploid strain used (yWS164) lacks both CaaX protease-encoding genes and both **a**-factor-encoding genes [27]. Mating competence was restored in this strain by co-transformation with plasmids encoding an **a**-factor species and a CaaX protease. Transformation with the latter was not necessary in the case of certain **a**-factor CaaX variants.

In brief, the serial dilution mating assay involves the mixing of *MAT***a** and *MAT*α cell suspensions on medium selective for diploid growth [28]. The cultures are prepared by first growing the *MAT***a** yeast in selective media and the *MAT*α yeast in non-selective YEPD for 24 hrs, then normalizing the cultures to a cell density of A_{600} 1.00 ± 0.05 with appropriate sterile media. A portion of each normalized *MAT***a** culture was diluted ten-fold with a normalized *MAT*α culture such that the final volume of the mating mixture was 100 µl. This primary mixture was subjected to several additional ten-fold dilutions using normalized *MAT*α cells as the diluent until a set of 5 samples was prepared. A portion of each serially diluted mixture (5

μl) was spotted onto solid SD medium. Growth of diploid cells on SD medium was scored after 3-4 days growth at 30 °C. The results of the mating test were digitally recorded by scanning the plates using a standard flat bed scanner. Unless otherwise noted, images are representative of mating results observed within one experiment where the indicated yeast strains were evaluated as a set to facilitate better assessment of relative mating efficiencies.

Quantitative mating assay

Assays were performed essentially as previously described [29]. In brief, *MAT***a** yeast were cultured for 36 hours to saturation in SC-ura-leu medium; *MAT*α yeast were cultured for 24 hours in YEPD liquid. Ten-fold serial dilutions of *MAT***a** yeast were prepared in SC-ura-leu liquid in triplicate, and a portion (100 μl) of an empirically determined dilution was mixed with an equal volume (100 μl) of undiluted *MAT*α yeast. The mixtures were spread onto SD solid minimal medium. In parallel, a portion (100 μl) of the *MAT***a** 10^{-5} dilution was spread onto SC-ura-leu solid medium to derive the titer of viable cells in the sample. The number of colonies observed on the SD plate after three days growth was recorded, adjusted for the dilution factor, and normalized for the titer of viable cells. Normalized values were used to determine mating efficiencies relative to a wild type strain (IH1783 containing pRS315 and pRS316) that was defined as having 100% mating efficiency. The *MAT***a** dilutions were chosen such that the resultant number of diploid colonies was typically in the range of 10-100 per plate, or in the case of non-maters, an undiluted sample was used.

Genetic screen to identify* CaaX *motifs that permit RSM

A library of plasmids encoding all possible permutations of the CaaX motif appended to yeast **a**-factor was created in yWS164. The individual plasmid-bearing colonies were assessed by replica methods for the ability to produce **a**-factor. Both mating and halo assays were used

[32]. In brief, the population of transformants was replica plated onto separate lawns of IH1793 and RC757. The lawns were prepared by scraping freshly grown strains from a YEPD plate (i.e. 48 hrs growth at 30 °C), diluting the cells into liquid YEPD, adjusting the density to A_{600} 1.00 ± 0.05, pouring the cell suspension onto a plate of SD (IH1793) or YEPD (RC757) (~3-5 ml/plate), immediately decanting the majority of the surface liquid, and allowing the residual liquid to absorb for 30 min at room temperature. The replica printed plates were incubated at 30 °C for 120 hours (IH1793 lawn) or 16 hrs (RC757 lawn) to allow for growth of diploids and formation of halos, respectively. Plasmids were isolated from colonies exhibiting mating competence and the ability to growth arrest RC757 cells [33]. The plasmids were retransformed into yWS164, phenotypes reconfirmed, and plasmids sequenced.

The plasmid library was created by plasmid-based PCR-directed recombination. pWS654 was gapped with *Pst*I, which cuts within the sequence encoding the aaX portion of the *MFA1* gene, and *Mlu*I, which cuts 3′ of the *MFA1* ORF. The forward oligo used to generate the PCR fragment had 39 bases of homology to the *MFA1* gene (5′ to *Pst*I cut site), a nine base sequence that was randomized for every possible nucleotide combination (i.e. the randomized aaX sequence), and 24 bases for annealing of the primer to the pWS438 plasmid used for target amplification; the first codon of the 24 base sequence encoded a stop codon. The reverse primer was homologous to DNA just outside the polylinker of pWS438 into which the *MFA1* gene was subcloned. This sequence is also present on pWS654. The plasmid-derived DNA fragments and the PCR-generated DNA fragments were co-transformed into yWS164 to facilitate recombination events that formed plasmids allowing for selective growth of the yeast on SC-Leu medium.

RESULTS

a-factor-CKQQ promotes Rce1p and Ste24p-independent mating (RSM)

The specificities of the yeast Rce1p and Ste24p CaaX proteases can been monitored using the yeast **a**-factor mating pheromone as a reporter molecule. During such an investigation, we observed mating by a strain expressing the **a**-factor-CKQQ variant in the absence of the established CaaX proteases (**Figure B.2A**). The CKQQ motif was derived from Pex19p and is also present on the mammalian Ser/Thr kinase Lkb1, a known tumor suppressor. Both proteins are known to be isoprenylated and thus substrates for CaaX proteolysis [34, 35]. RSM was not observed when either wildtype **a**-factor (CVIA) or a variant known to be Ste24p-specific (CASQ) was expressed.

Through close inspection of diploid colony densities, we predicted that Ste24p, and to a lesser extent Rce1p, could enhance CKQQ-dependent RSM. This prediction was confirmed through quantitative mating tests (**Figure B.2B**) [29]. We also confirmed that the CVIA motif was readily cleaved by Rce1p and to a lesser extent by Ste24p in a manner consistent with the reported properties of these enzymes [36, 37]. We also determined that the Ste24p/CKQQ and Ste24p/CASQ pairings had approximately equal mating efficiencies. Overall, our analysis revealed that RSM mating efficiency was low (<1%), but within an order of magnitude for that observed for CASQ and CKQQ motifs in the presence of CaaX proteases.

Other CaaX *motifs also support RSM*

To investigate the extent of motifs that support RSM, the a_1, a_2 and X positions of the CKQQ motif were independently altered to Ala. This analysis revealed that Lys at the a_1 position was a critical determinant for RSM (**Figure B.3A**). Alterations at the a_2 and X position

did not abolish RSM. Both CKAQ and CKQA appeared to support more efficient mating than the CKQQ motif. The possibility of a charge requirement at the a_1 position was investigated in more detail by substituting various polar amino acids (**Figure B.3B**). Of the motifs evaluated, CRQQ and CHQQ promoted RSM while CDQQ and CEQQ did not. The CRQQ motif appeared to support more efficient mating than CKQQ, while the CHQQ motif appeared to support less efficient mating. This observation was confirmed by quantitative mating tests (**Figure B.2B**).

Given our findings, we hypothesized that the C(K/R/H)aX motif might be a good predictor of RSM substrates. To test this hypothesis, we examined additional natural yeast CaaX motifs and several synthetic sequences (i.e. not occurring in yeast) corresponding to this consensus. Only a subset of these motifs promoted mating when appended to **a**-factor (**Figure B.3C** and **Table B.3**). These observations indicate that C(K/R/H)aX can be used to identify candidate substrates for RSM, but that this consensus sequence is not an absolute predictor of RSM substrates. Our result was somewhat expected since the consensus-matching CKIA motif has been previously identified as not promoting mating activity [37].

A relatively large number of CaaX *motifs can support RSM*

To broadly investigate the propensity of CaaX motifs to promote mating in the absence of Rce1p and Ste24p, we set up a genetic screen to identify motifs capable of producing biologically active **a**-factor in an *rce1 ste24* null background. For the screen, a degenerate PCR oligonucleotide was used to create a population of plasmids encoding yeast **a**-factor with randomly appended aaX sequences. Theoretically, 8000 aaX permutations were possible. The plasmid library was created in yeast through recombination-mediated methods. Evaluation of over 3000 yeast colonies by replica-based mating tests revealed a substantial number having the ability to mate and induce growth arrest of *MAT*α *sst2-1* yeast. RSM was observed at a rate of

0.93% ± 0.61% suggesting that approximately 75 CaaX motifs can promote RSM. Six plasmids capable of promoting RSM were recovered and sequenced. This limited analysis revealed sequences having either Lys or Arg at the a_1 position but no consistent pattern at the a_2 and X positions (**Table B.3**). Future investigations to identify additional RSM motifs will be required to fully define the RSM consensus.

RSM is dependent on Ste14p

Two hypotheses were developed to explain our observations for RSM. The most straightforward was that a third CaaX proteolytic activity is responsible for RSM (**Figure B.4A**). Alternatively, it was possible that certain RSM-promoting motifs were uncleaved, and that the uncleaved motifs somehow mimicked the biophysical properties of a carboxylmethylated C-terminus such that cellular export and receptor binding by the pheromone were now possible. To distinguish between these possibilities, we predicted that a proteolytic-dependent mechanism would require the isoprenylcysteine carboxyl methyltransferase (ICMT) for activation of the biological activity of **a**-factor, whereas a carboxylmethyl mimic would not. We thus evaluated the dependence of RSM on the Ste14p ICMT. Using **a**-factor-CKAQ as a reporter, we observed that RSM was indeed dependent on Ste14p (**Figure B.4B**). This observation strongly implicates involvement of a proteolytic activity in promoting RSM.

Our interpretation, however, is subject to the concern that another CaaX protein might have impaired function in the absence of *STE14*, and that this impairment contributes to the negative mating phenotype observed. Unlike **a**-factor, however, no other CaaX protein has been identified whose function is fully impaired in the absence of carboxylmethylation. Nevertheless, it remains formally possible that the function of some CaaX protein, perhaps one involved in cell fitness (e.g. Ras2p) or the mating response (e.g. Ste18p), is partially compromised in the absence

of *STE14* such that the weak mating observed with **a**-factor-CKQQ is now below the detection threshold of our methods.

RSM is enhanced by the yeast M16A proteases Axl1p and Ste23p

To further advance the hypothesis that RSM is promoted by a proteolytic activity, we sought to identify protease gene(s) involved. Using a candidate approach, we first examined other proteases associated with **a**-factor maturation, specifically the M16A subfamily proteases Axl1p and Ste23p. These proteases independently cleave an N-terminal extension found on the **a**-factor precursor during **a**-factor biogenesis, with Axl1p being responsible for the majority of this activity [38]. When over-expressed, each protease was capable of enhancing RSM associated with **a**-factor-CKQQ (**Figure B.5A**). Protease over-expression did not promote RSM in the presence of wildtype **a**-factor or a charge switch mutant (CVIA and CDQQ, respectively) (**Figure B.5B**). This observation suggests that the effect of protease over-expression is linked to recognition of a specific subset of CaaX motifs. Our results are consistent with Axl1p and Ste23p contributing to the proteolytic activity that promotes RSM but do not exclude the possibility of the M16A proteases activating a secondary protease having this role.

The N-terminal extension of a-factor is important for RSM

Given the possible and likely involvement of M16A enzymes in cleaving RSM-promoting CaaX motifs, we hypothesized that the N-terminal extension of **a**-factor would somehow be involved in regulating RSM. The first third of this N-terminal extension is removed by Ste24p to yield a partial extension, which is subsequently fully removed by the activity of a yeast M16A enzyme [39]. By analogy to substrates of other M16A enzymes, the partial N-terminal extension presumably binds an exosite on the M16A enzyme [40].

First, we examined whether the N-terminal extension shields the natural **a**-factor CaaX motif but not RSM-promoting CaaX motifs from M16A recognition. To test this possibility, **a**-factor was expressed with and without its N-terminal extension using a ubiquitin fusion approach that allows expression of very short peptides [39, 41]. The fusions incorporated the full-length **a**-factor precursor sequence (Ubi-P1), a truncated sequence reflecting partial loss of the N-terminal extension (Ubi-P2), or the mature sequence of **a**-factor (Ubi-M) (**Figure B.6A**). The fusions had an associated CaaX motif, either CVIA or CKQQ. None of the fusions containing the wildtype CaaX motif CVIA were capable of promoting RSM despite encoding functional **a**-factor products (**Figure B.6B**), indicating that the N-terminal extension does not simply shield CaaX motifs from M16A recognition. Of note, Ubi-M appeared less effective at promoting mating in the presence of CaaX proteases relative to its longer counterparts, which is consistent with its rapid turnover in cells [39].

We next examined whether the N-terminal extension is needed to recruit the **a**-factor precursor to the 'peptidosome' cavity of the M16A enzyme where CaaX motifs with appropriate biophysical properties (i.e. RSM promoting motifs) would be cleaved. To test this possibility, ubiquitin-**a**-factor fusions having a CKQQ motif were evaluated (**Figure B.6C**). In the presence of CaaX proteolytic activity, all of the ubiquitin fusions had reduced ability to promote mating relative to their CVIA counterparts, with Ubi-M(CKQQ) being completely incapable of promoting mating. RSM was observed with Ubi-P1(CKQQ) and Ubi-P2(CKQQ) but not with Ubi-M(CKQQ). The lack of recognition of Ubi-M(CKQQ) by both Rce1p and Ste24p suggests that the N-terminal extension is a recognition and/or a targeting determinant that may facilitate interaction with these CaaX proteases. The fact that Ubi-P2(CKQQ) promotes mating somewhat better than Ubi-P1(CKQQ) is consistent with our assertion that the N-terminal extension of **a**-

factor, specifically the partial extension present on the P2 intermediate, is important for RSM. However, the fact that Ubi-M(CKQQ) cannot promote mating in the presence of CaaX proteases, precludes our ability to conclusively demonstrate an essential recruitment role for the N-terminal extension in RSM.

DISCUSSION

We have identified multiple CaaX motifs that, when used in lieu of the natural **a**-factor CVIA motif, can promote yeast mating in the absence of the established CaaX proteases Rce1p and Ste24p. Rce1p and Ste24p independent mating (RSM) can be promoted by several CaaX motifs naturally present in the yeast genome as well as multiple synthetic sequences (**Table B.3**). Our genetic analysis allows us to project that approximately 75 motifs can promote RSM. These motifs represent approximately 1% of all possible CaaX permutations. The fact that RSM-promoting motifs have been previously overlooked is probably not surprising given that only about 1% of CaaX motifs have been previously evaluated in the context of the **a**-factor reporter. [3, 28, 37]. Moreover, with the exception of CKIA, none of the previously evaluated motifs were matches for the consensus sequence C(K/R/H)aX, which we have derived as a good but not absolute predictor of an RSM-promoting motif. Sequencing of all the RSM-promoting motifs identified by our unbiased genetic screen may provide additional insight into whether there is an RSM consensus motif. Evaluation of existing motifs suggests that a charged residue at the X position may not be compatible with RSM.

Our observations are consistent with RSM involving proteolysis of the susceptible motifs and identify the yeast M16A metalloproteases Axl1p and Ste23p as having involvement in this

process. We do not know whether these proteases act indirectly or directly. Indirect action could be as simple as M16A enzymes activating a distinct protease having RSM activity or as complex as M16A enzymes serving as scaffolds to help recruit such an activity or to properly present substrates to this activity. Determining whether a direct or indirect scenario is more likely will require purification of the yeast M16A enzymes and the synthesis of a compatible substrate. The hypothesis that yeast M16A enzymes can directly cleave CaaX motifs, however, is supported by additional observations. Three yeast activities, one membrane-associated and two soluble, have been previously identified that are able to cleave the **a**-factor CaaX motif *in vitro* [42, 43]. The membrane-associated activity is likely a combination of Rce1p and Ste24p activities, and neither can be responsible for RSM due to their absence in our test strain. One of the soluble activities is a *PEP4*-dependent carboxypeptidase, most likely carboxypeptidase Y. This enzyme is a compartmentalized vacuolar protease and is not expected to come in contact with **a**-factor intermediates, which are hypothesized to be modified by enzymes having cytosol-oriented active sites; mature **a**-factor is exported directly from the cytosol and across the plasma membrane by the Ste6p ABC-type transporter [44]. The second soluble *in vitro* activity is associated with an undefined 110 kDa enzyme and is phenanthroline-sensitive. Axl1p and Ste23p are approximately this size and are both predicted to be phenanthroline-sensitive based on their functional homology to other M16A proteases, such as the human insulin-degrading enzyme (IDE) [38]. Thus, they are likely responsible for the *in vitro* activity reported. However, one major inconsistency remains between our *in vivo* observations and the reported 100 kDa *in vitro* activity that cleaves CaaX motifs. We do not observe cleavage of the CVIA CaaX motif *in vivo* whereas this is observed *in vitro*. A major difference between the two types of experiments

is, respectively, the use of a full-length biologically active reporter vs. a shorter peptide-based biologically inactive reporter, and this could underlie the specificity differences observed.

Another issue that remains to be resolved is the physiological impact of M16A enzymes on the maturation of CaaX proteins having RSM-promoting motifs. We believe that M16A enzymes cleave RSM-promoting motifs only in the specific context of the yeast **a**-factor reporter. This conclusion is based on the observation that the **a**-factor CKQQ variant, when produced without its N-terminal extension, is an unsuitable substrate for RSM. The N-terminal extension, by analogy to M16A other substrates, is likely involved in binding to the exosite of M16A enzymes. This extension helps anchor the substrate in the so-called "peptidosome" cavity of the M16A enzyme. We thus hypothesize that certain CaaX motifs, once drawn into the cavity of an M16A enzyme, have the propensity to compete against the ideal M16A cleavage sequence for binding to the active site, perhaps by their ability to form extended beta sheet interactions with the M16A enzyme. The ability of other substrates to behave similarly would be limited to those having an exosite binding sequence and being small enough to fit within the M16A enzyme cavity, which is predicted to hold proteins less than 50 amino acids in size [40]. None of the naturally occurring yeast proteins having RSM promoting motifs are small enough to fit in an M16A cavity. Hence, we believe that these proteins are not modified to any appreciable extent by M16A enzymes. However, we cannot discount the possibility that small CaaX proteins with RSM promoting motifs exist in other systems that would be suitable M16A substrates in those systems. If such candidates exist in humans, IDE might be able to help mature these proteins under conditions where CaaX protease inhibition is a therapeutic strategy.

ACKNOWLEDGEMENTS

We are grateful to members of the Schmidt and Sabatini labs (University of Georgia) for technical advice and critical discussions. This work was supported in part through a Georgia Cancer Coalition Distinguished Cancer Clinician/Scientist Scholar award (to WKS) and a grant from the National Institutes of Health (to WKS; R01 GM67092).

REFERENCES

1. Spence, R. and P.J. Casey, *Mechanism of catalysis by protein farnesyltransferase.*, in *The Enzymes*, F. Tamanoi and D. Sigman, Editors. 2001, Academic Press: New York, NY. p. 1-18.
2. Young, S.G., et al., *Postisoprenylation protein processing: CXXX (CaaX) endoproteases and isoprenylcysteine carboxyl methyltransferase.*, in *The Enzymes*, F. Tamanoi and D.S. Sigman, Editors. 2001, Academic Press: New York, NY. p. 155-213.
3. Boyartchuk, V.L., M.N. Ashby, and J. Rine, *Modulation of Ras and **a**-factor function by carboxyl-terminal proteolysis.* Science, 1997. **275**(5307): p. 1796-800.
4. Tam, A., W.K. Schmidt, and S. Michaelis, *The multispanning membrane protein Ste24p catalyzes CAAX proteolysis and NH2-terminal processing of the yeast a-factor precursor.* J Biol Chem, 2001. **276**(50): p. 46798-806.
5. Hrycyna, C.A., et al., *The Saccharomyces cerevisiae STE14 gene encodes a methyltransferase that mediates C-terminal methylation of **a**-factor and RAS proteins.* EMBO J., 1991. **10**: p. 1699-1709.
6. Marcus, S., et al., *Significance of C-terminal cysteine modifications to the biological activity of the Saccharomyces cerevisiae **a**-factor mating pheromone.* Mol. Cell. Biol., 1991. **11**(7): p. 3603-12.
7. Sapperstein, S., C. Berkower, and S. Michaelis, *Nucleotide sequence of the yeast STE14 gene, which encodes farnesylcysteine carboxyl methyltransferase, and demonstration of its essential role in **a**-factor export.* Mol. Cell. Biol., 1994. **14**(2): p. 1438-1449.

8. Kim, E., et al., *Disruption of the mouse Rce1 gene results in defective Ras processing and mislocalization of Ras within cells.* J. Biol. Chem., 1999. **274**(13): p. 8383-8390.

9. Bergo, M.O., et al., *Targeted inactivation of the isoprenylcysteine carboxyl methyltransferase gene causes mislocalization of K-Ras in mammalian cells.* J. Biol. Chem., 2000. **275**(23): p. 17605-10.

10. Bergo, M.O., et al., *Absence of the CAAX endoprotease Rce1: effects on cell growth and transformation.* Mol Cell Biol, 2002. **22**(1): p. 171-81.

11. Manandhar, S.P., et al., *Chemical inhibition of CaaX protease activity disrupts yeast Ras localization.* Yeast, 2010. **27**(6): p. 327-43.

12. Young, S.G., L.G. Fong, and S. Michaelis, *Prelamin A, Zmpste24, misshapen cell nuclei, and progeria--new evidence suggesting that protein farnesylation could be important for disease pathogenesis.* J Lipid Res, 2005. **46**(12): p. 2531-58.

13. Basso, A.D., P. Kirschmeier, and W.R. Bishop, *Lipid posttranslational modifications. Farnesyl transferase inhibitors.* J Lipid Res, 2006. **47**(1): p. 15-31.

14. Winter-Vann, A.M. and P.J. Casey, *Post-prenylation-processing enzymes as new targets in oncogenesis.* Nat Rev Cancer, 2005. **5**(5): p. 405-12.

15. Manandhar, S.P., E.R. Hildebrandt, and W.K. Schmidt, *Small-molecule inhibitors of the Rce1p CaaX protease.* J Biomol Screen, 2007. **12**(7): p. 983-93.

16. Wang, M., et al., *A small molecule inhibitor of isoprenylcysteine carboxymethyltransferase induces autophagic cell death in PC3 prostate cancer cells.* J Biol Chem, 2008. **283**(27): p. 18678-84.

17. Blum, R., A.D. Cox, and Y. Kloog, *Inhibitors of chronically active ras: potential for treatment of human malignancies.* Recent Patents Anticancer Drug Discov, 2008. **3**(1): p. 31-47.

18. Sebti, S.M. and A.D. Hamilton, *Farnesyltransferase and geranylgeranyltransferase I inhibitors and cancer therapy: lessons from mechanism and bench-to-bedside translational studies.* Oncogene, 2000. **19**(56): p. 6584-93.

19. Fiordalisi, J.J., et al., *High affinity for farnesyltransferase and alternative prenylation contribute individually to K-Ras4B resistance to farnesyltransferase inhibitors.* J Biol Chem, 2003. **278**(43): p. 41718-27.

20. Schmidt, W.K., et al., *Endoplasmic reticulum membrane localization of Rce1p and Ste24p, yeast proteases involved in carboxyl-terminal CAAX protein processing and amino-terminal **a**-factor cleavage.* Proc Natl Acad Sci USA, 1998. **95**(19): p. 11175-80.

21. Otto, J.C., et al., *Cloning and characterization of a mammalian prenyl protein-specific protease.* J. Biol. Chem., 1999. **274**(13): p. 8379-82.

22. Pei, J. and N.V. Grishin, *Type II CAAX prenyl endopeptidases belong to a novel superfamily of putative membrane-bound metalloproteases.* Trends Biochem Sci, 2001. **26**(5): p. 275-7.

23. Bergo, M.O., et al., *Zmpste24 deficiency in mice causes spontaneous bone fractures, muscle weakness, and a prelamin A processing defect.* Proc Natl Acad Sci U S A, 2002. **99**(20): p. 13049-54.

24. Pendas, A.M., et al., *Defective prelamin A processing and muscular and adipocyte alterations in Zmpste24 metalloproteinase-deficient mice.* Nat Genet, 2002. **31**(1): p. 94-9.

25. Bracha, K., M. Lavy, and S. Yalovsky, *The Arabidopsis AtSTE24 is a CAAX protease with broad substrate specificity.* J Biol Chem, 2002. **277**(33): p. 29856-64.

26. Cadinanos, J., et al., *Identification, functional expression and enzymic analysis of two distinct CaaX proteases from Caenorhabditis elegans.* Biochem J, 2003. **370**(Pt 3): p. 1047-54.

27. Cadinanos, J., et al., *AtFACE-2, a prenylated-protein protease from Arabidopsis thaliana related to Ras converting enzymes.* Journal of Biological Chemistry, 2003. **278**(43): p. 42091-7.

28. Plummer, L.J., et al., *Mutational analysis of the ras converting enzyme reveals a requirement for glutamate and histidine residues.* J Biol Chem, 2006. **281**(8): p. 4596-605.

29. Michaelis, S. and I. Herskowitz, *The **a**-factor pheromone of Saccharomyces cerevisiae is essential for mating.* Mol. Cell. Biol., 1988. **8**(3): p. 1309-18.

30. Elble, R., *A simple and efficient procedure for transformation of yeasts.* BioTechniques, 1992. **13**: p. 18-20.

31. Oldenburg, K.R., et al., *Recombination-mediated PCR-directed plasmid construction in vivo in yeast.* Nucleic Acids Res, 1997. **25**(2): p. 451-452.

32. Nijbroek, G.L. and S. Michaelis, *Functional assays for the analysis of yeast ste6 mutants.* Methods Enzymol, 1998. **292**: p. 193-212.

33. Robzyk, K. and Y. Kassir, *A simple and highly efficient procedure for rescuing autonomous plasmids from yeast.* Nucleic Acids Research, 1992. **20**(14): p. 3790.

34. Gotte, K., et al., *Pex19p, a farnesylated protein essential for peroxisome biogenesis.* Mol Cell Biol, 1998. **18**(1): p. 616-28.

35. Collins, S.P., et al., *LKB1, a novel serine/threonine protein kinase and potential tumour suppressor, is phosphorylated by cAMP-dependent protein kinase (PKA) and prenylated in vivo.* Biochem J, 2000. **345 Pt 3**: p. 673-80.

36. Boyartchuk, V., et al. *Roles of CAAX proteases in **a**-factor and Ras maturation*. in *Yeast Cell Biology*. 1997. Cold Spring Harbor, NY.

37. Trueblood, C.E., et al., *The CaaX proteases, Afc1p and Rce1p, have overlapping but distinct substrate specificities.* Mol. Cell. Biol., 2000. **20**(12): p. 4381-92.

38. Kim, S., et al., *Yeast as a tractable genetic system for functional studies of the insulin-degrading enzyme.* J Biol Chem., 2005. **280**(30): p. 27481-27490.

39. Tam, A., et al., *Dual roles for Ste24p in yeast **a**-factor maturation: NH_2-terminal proteolysis and COOH-terminal CAAX processing.* J. Cell Biol., 1998. **142**(3): p. 635-49.

40. Shen, Y., et al., *Structures of human insulin-degrading enzyme reveal a new substrate recognition mechanism.* Nature, 2006. **443**(7113): p. 870-4.

41. Boyartchuk, V.L. and J. Rine, *Roles of prenyl protein proteases in maturation of Saccharomyces cerevisiae **a**-factor.* Genetics, 1998. **150**(1): p. 95-101.

42. Ashby, M., D. King, and J. Rine, *Endoproteolytic processing of a farnesylated peptide in vitro.* Proc. Natl. Acad. Sci. USA, 1992. **89**: p. 4613-17.

43. Hrycyna, C.A. and S. Clarke, *Maturation of isoprenylated proteins in Saccharomyces cerevisiae.* J. Biol. Chem., 1992. **267**(15): p. 10457-64.

44. Kuchler, K., R.E. Sterne, and J. Thorner, *Saccharomyces cerevisiae STE6 gene product: a novel pathway for protein export in eukaryotic cells.* EMBO J., 1989. **8**(13): p. 3973-3984.

45. Powers, S., et al., *RAM, a gene of yeast required for a functional modification of RAS proteins and for production of mating pheromone **a**-factor.* Cell, 1986. **47**(3): p. 413-22.

46. Chen, P., et al., *Biogenesis of the Saccharomyces cerevisiae mating pheromone **a**-factor.* J. Cell. Biol., 1997. **136**(2): p. 251-69.

47. Adames, N., et al., *Role of yeast insulin-degrading enzyme homologs in propheromone processing and bud site selection.* Science, 1995. **270**: p. 464-67.

48. Sikorski, R.S. and P. Hieter, *A system of shuttle vectors and yeast host strains designed for efficient manipulation of DNA in Saccharomyces cerevisiae.* Genetics, 1989. **122**(1): p. 19-27.

49. Zhang, Y., et al., *Hsp70 molecular chaperone facilitates endoplasmic reticulum-associated protein degradation of Cystic Fibrosis Transmembrane Conductance Regulator in yeast.* Mol Biol Cell, 2001. **12**(5): p. 1303-14.

50. Fujimura-Kamada, K., F.J. Nouvet, and S. Michaelis, *A novel membrane-associated metalloprotease, Ste24p, is required for the first step of NH_2-terminal processing of the yeast **a**-factor precursor.* J. Cell Biol., 1997. **136**(2): p. 271-85.

51. Schmidt, W.K., A. Tam, and S. Michaelis, *Reconstitution of the Ste24p-dependent N-terminal proteolytic step in yeast **a**-factor biogenesis*. J. Biol. Chem., 2000. **275**(9): p. 6227-33.

Table B.1. *Strains used in this study.*

STRAIN	GENOTYPE	REFERENCE
IH1783	*MAT***a** *trp1 leu2 ura3 his4*	ATCC#204278
IH1793	*MAT*α *lys1*	ATCC#204279
RC757	*MAT*α *sst2-1 rme his6 met1 can1 cyh2*	[45]
SM2331	*MAT***a** *trp1 leu2 ura3 his4 mfa1*Δ *mfa2*Δ	[46]
yWS164	*MAT***a** *trp1 leu2 ura3 his4 mfa1*Δ *mfa2*Δ *rce1::TRP1 ste24::KAN^R*	[27]
yWS829	*MAT***a** *trp1 leu2 ura3 his4 mfa1*Δ *mfa2*Δ *rce1::TRP1 ste24::KAN^R ste14::URA3*	This study

Table B.2. *Plasmids used in this study.*

PLASMID	GENOTYPE	REFERENCE
P80	*CEN URA3 AXL1*	[47]
pRS315	*CEN LEU2*	[48]
pRS316	*CEN URA3*	[48]
pRS415	*CEN LEU2*	[48]
pRS424	*2μ TRP1*	[48]
pSM284	*integrating ste14:URA3*	[7]
pSM703	*2μ URA3* P_{PGK}	[49]
pSM1107	*CEN URA3 HA::STE24*	[50]
pSM1153	*CEN TRP1 AXL1*	[20]
pSM1366	*CEN URA3 UBI-MFA1 M*	[39]
pSM1368	*CEN URA3 UBI-MFA1 P1*	[39]
pSM1369	*CEN URA3 UBI-MFA1 P2*	[39]
pSM1605	*2μ URA3 MFA1*	[51]
pSM1314	*CEN URA3 RCE1::HAc*	[20]
pWS196	*2μ URA3 MFA1-CASQ*	This study
pWS438	*2μ LEU2 MFA1*	[27]
pWS601	*2μ URA3* P_{PGK}*-AXL1*	This study
pWS602	*2μ URA3* P_{PGK}*-STE23-BglII*	This study
pWS610	*CEN LEU2 MFA1*	This study
pWS612	*CEN LEU2 MFA1-CASQ*	This study
pWS654	*2μ LEU2 MFA1-CALQ*	[28]
pWS718	*2μ LEU MFA1-CKQQ*	This study
pWS727	*CEN LEU2 MFA1-CKQQ*	This study
pWS737	*CEN LEU2 MFA1-CAQQ*	This study
pWS738	*CEN LEU2 MFA1-CKAQ*	This study
pWS739	*CEN LEU2 MFA1-CKQA*	This study
pWS817	*CEN LEU2 MFA1-CALQ*	This study
pWS844	*CEN LEU2 MFA1-CRQQ*	This study
pWS845	*CEN LEU2 MFA1-CKIS*	This study
pWS846	*CEN LEU2 MFA1-CKQS*	This study
pWS847	*CEN LEU2 MFA1-CKGE*	This study
pWS848	*CEN LEU2 MFA1-CKCI*	This study
pWS849	*CEN LEU2 MFA1-CKYI*	This study
pWS850	*CEN LEU2 MFA1-CKCT*	This study
pWS851	*CEN LEU2 MFA1-CEQQ*	This study
pWS852	*CEN LEU2 MFA1-CHQQ*	This study
pWS853	*CEN LEU2 MFA1-CDQQ*	This study
pWS854	*CEN LEU2 MFA1-CRVK*	This study
pWS855	*CEN LEU2 MFA1-CRNR*	This study
pWS856	*CEN LEU2 MFA1-CRMV*	This study
pWS883	*2μ LEU2 MFA1-CKVA*	This study
pWS884	*2μ LEU2 MFA1-CRVA*	This study
pWS885	*2μ LEU2 MFA1-CRMS*	This study

pWS886	*2μ LEU2 MFA1-CRVN*	This study
pWS887	*2μ LEU2 MFA1-CKMT*	This study
pWS891	*2μ LEU2 MFA1-CKIT*	This study
pWS892	*CEN URA3 UBI-MFA1 P1 (CKQQ)*	This study
pWS893	*CEN URA3 UBI- MFA1 P2 (CKQQ)*	This study
pWS894	*CEN URA3 UBI- MFA1 M (CKQQ)*	This study
pWS912	*CEN LEU2 MFA1-CRME*	This study

Table B.3. *Summary of ability of CaaX motifs to promote Rce1p and Ste24p-independent mating (RSM).*

MOTIF	RSM OBSERVED	SOURCE[a]
CALM	No[b]	synthetic
CALQ	No[b]	synthetic
CAMQ	No[b]	synthetic
CAQQ	No	synthetic
CASQ	No	*YDJ1*
CDQQ	No	synthetic
CEQQ	No	synthetic
CHQQ	Yes	synthetic
CKAQ	Yes	synthetic
CKCI	No	POP8
CKCT	No	*YBL049w/MOH1*
CKGE	No	*YMR197c/VTI1*
CKIS	Yes	*YPR092w*[c]
CKIT	Yes	RSM screen
CKMT	Yes	RSM screen
CKQA	Yes	synthetic
CKQQ	Yes	*PEX19, LKB1, NAP1*
CKQS	Yes	*NAP1*
CKVA	Yes	RSM screen
CKYI	No	*YMR060c/SAM37/TOM37*
CRME	No	*YJL059W/YHC3*
CRMS	Yes	RSM screen
CRMV	Yes[b]	synthetic
CRNR	No	*YML041C/VPS71*
CRQQ	Yes	synthetic
CRVA	Yes	RSM screen
CRVK	No	*YMR158W/MRPS8*
CRVN	Yes	RSM screen
CVIA	No	*MFA1, MFA2*

[a] All of the indicated genes are those of *S. cerevisiae* except for LKB1 and NAP1which are human.

[b] Krishnankutty and Schmidt, unpublished observation; see also [28]

[c] Reported as a dubious ORF in the *Saccharomyces* Genome database (www.yeastgenome.org).

Figure B.1. *CaaX proteins are extensively modified post-translationally*.

The C-terminal tetrapeptide CaaX motif directs three ordered post-translational modifications, including isoprenylation, proteolysis and carboxylmethylation. Interfering with these steps can disrupt the activity and/or localization of the protein being modified.

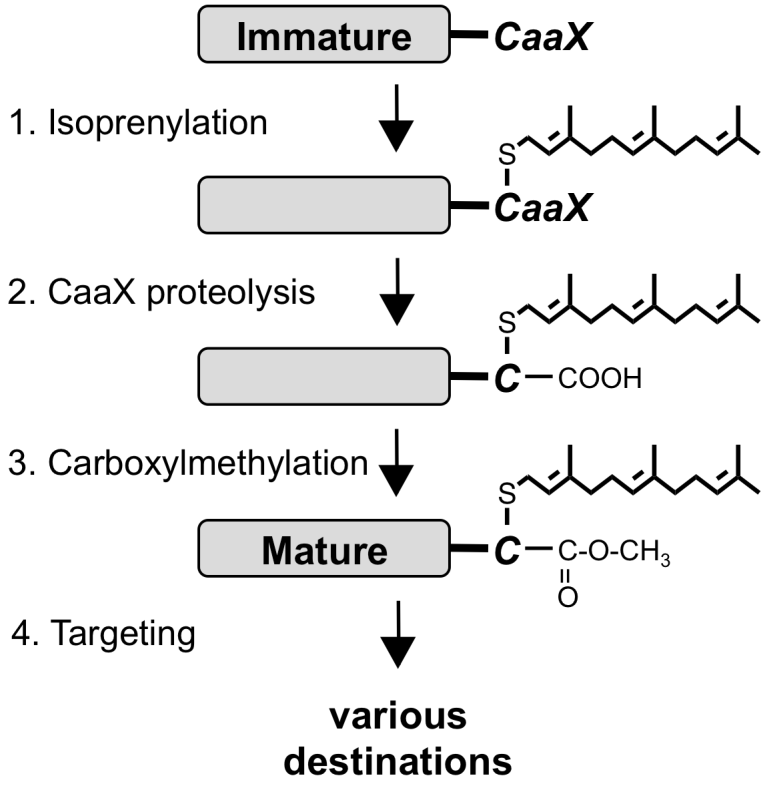
Immature
CaaX
1. Isoprenylation
S
CaaX
2. CaaX proteolysis
S
C
COOH
3. Carboxylmethylation
S
Mature
C
C-O-CH3
O
4. Targeting
various
destinations

Figure B.2. *Evidence for Rce1p and Ste24p-independent mating (RSM).*

A) The **a**-factor-CKQQ variant promotes mating in a yeast strain lacking endogenous copies of the CaaX proteases and **a**-factor genes (yWS164). This phenotype is not associated when **a**-factor is appended with its natural CaaX motif (CVIA) or one that is Ste24p-specific (CASQ). When co-expressed with Ste24p, but not Rce1p, the CKQQ variant promotes more efficient mating. The plasmids used were pRS316, pSM1107, pSM1314, pWS610, pWS612, and pWS727.

B) Quantitative mating tests were conducted to quantifiably compare the amount of mating promoted by **a**-factor CaaX motif variants. Mating efficiencies are reported relative to a wildtype control (IH1783) containing both CaaX protease genes, both **a**-factor genes, and empty vectors (pRS315 and pRS316) to maintain the same plasmid markers as the tested strains. The plasmids used were pSM1314 (*RCE1*), pSM1107 (*STE24*), pWS610 (CVIA), pWS612 (CASQ), pWS727 (CKQQ), pWS844 (CRQQ), and pWS852 (CHQQ), which were evaluated alone and in combination. In instances where plasmids were evaluated alone, an appropriate empty vector was included to maintain markers. ND – not determined.

A

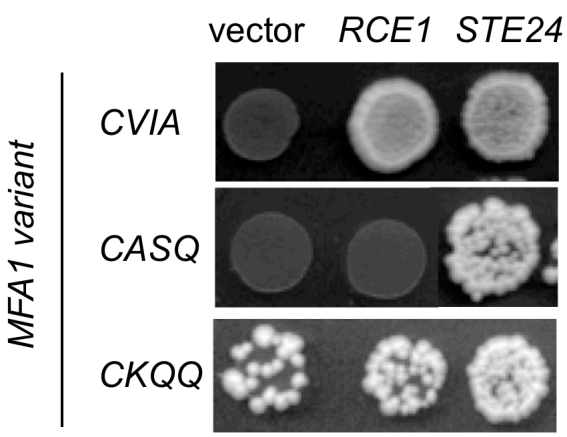

B

Mating Efficiency (% relative to WT control)

CaaX motif	vector	*RCE1*	*STE24*
CVIA	0	115.43 ± 8.83	35.14 ± 4.30
CASQ	0	0	1.01 ± 0.77
CKQQ	0.22 ± 0.01	0.91 ± 0.44	1.35 ± 0.25
CRQQ	0.65 ± 0.18	ND	ND
CHQQ	0.01 ± 0.00	ND	ND

Figure B.3. *Multiple CaaX motifs promote RSM.*

Serial dilution mating tests were conducted as described in Figure 2 using yWS164 and plasmids encoding the indicated **a**-factor CaaX variants. Only the first dilution spot is shown for each mating test.

A) Ala substitutions at the a_1, a_2 and X positions of the CKQQ motif. The plasmids used were pWS610, pWS727, pWS737, pWS738, and pWS739.

B) Charged amino acid substitutions at the a_1 position. The plasmids used were pWS610, pWS727, pWS844, pWS851, pWS852, and pWS853.

C) Naturally occurring motifs that correspond to the consensus C(K/R/H)aX. See **Table B.3** for the source gene of the natural CaaX motifs. The plasmids used were pWS845, pWS846, pWS847, pWS848, pWS849, pWS850, pWS854, pWS855, and pWS912.

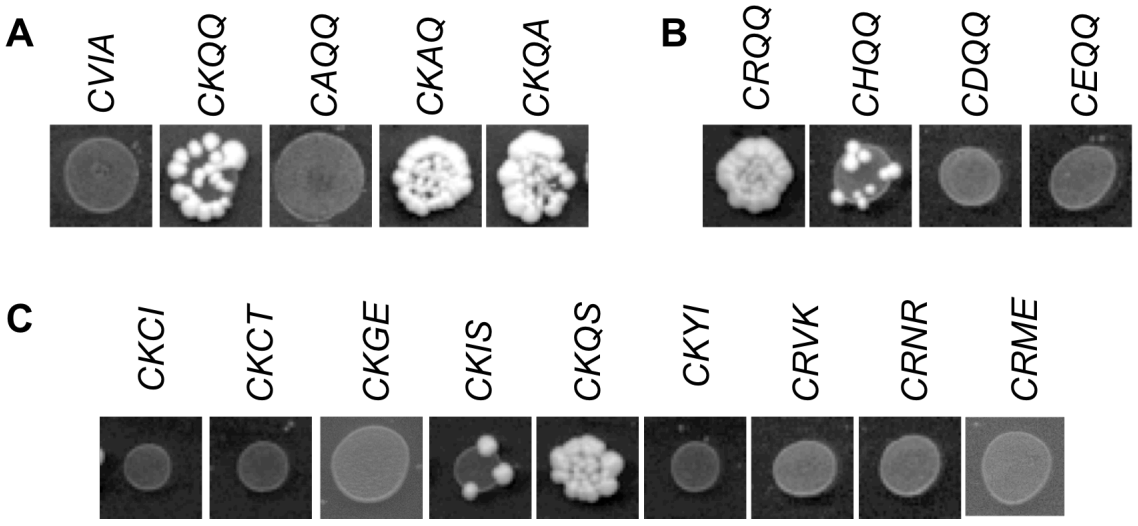
A
CVIA
CKQQ
CAQQ
CKAQ
CKQA
B
CRQQ
CHQQ
CDQQ
CEQQ
C
CKCI
CKCT
CKGE
CKIS
CKQS
CKYI
CRVK
CRNR
CRME

Figure B.4. *RSM requires carboxylmethylation.*

A) Models for RSM. In the absence of Rce1p and Ste24p, CaaX proteolysis of **a**-factor-CKQQ is mediated by either an ER (1) or non-ER-localized (2) protease (Rsm1p). If the latter, the dependence of RSM on Ste14p indicates that a trafficking step is required to return proteolyzed **a**-factor to the Ste14p ICMT that resides at the ER. Alternatively, non-proteolyzed **a**-factor could promote mating (3). In this scenario, RSM would be independent of Ste14p. ER – endoplasmic reticulum; PM – plasma membrane.

B) Loss of Ste14p in a CaaX protease deficient strain prevents RSM. The plasmids used were pWS610 and pWS738, which were separately transformed into yWS164 and yWS829. yWS164-derived strains were additionally transformed with pRS316 to provide a comparable set of auxotrophic markers to that of the yWS829-derived strains.

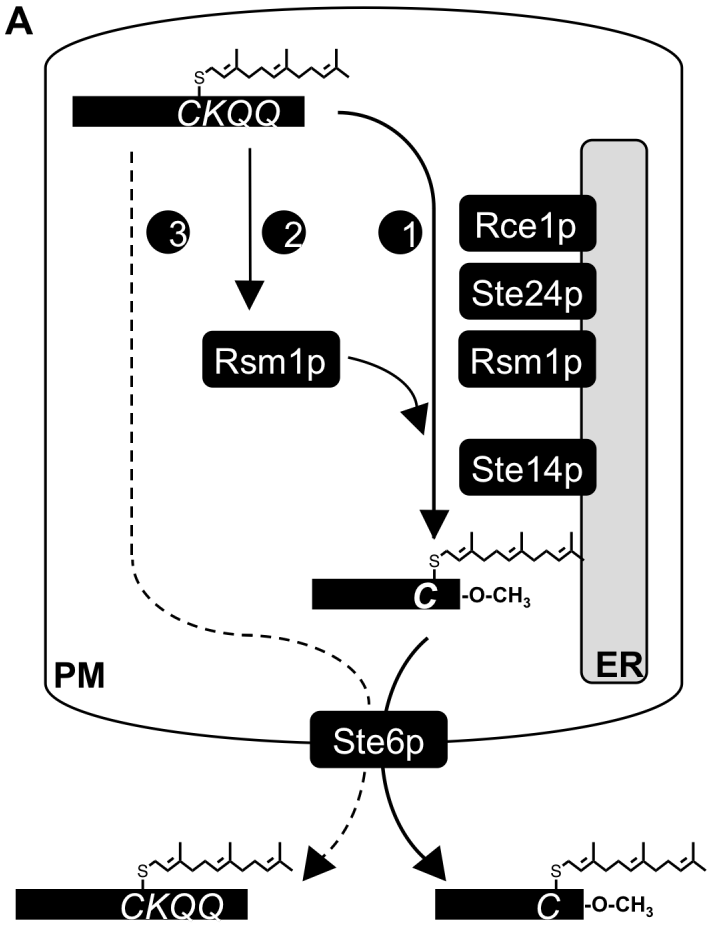
A
CKQQ
3
2
1
Rce1p
Ste24p
Rsm1p
Rsm1p
Ste14p
C
-O-CH3
PM
ER
Ste6p
CKQQ
C
-O-CH3

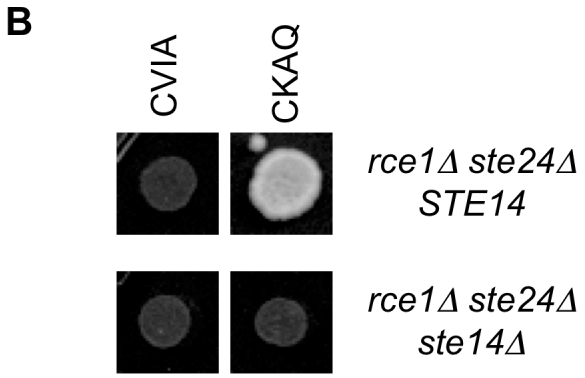
B
CVIA
CKAQ
rce1Δ ste24Δ
STE14
rce1Δ ste24Δ
ste14Δ

Figure B.5. *RSM is enhanced by M16A proteases.*

A) Axl1p and Ste23p were independently over-expressed in yWS164 in the presence of the **a**-factor CKQQ variant, and the strains were subjected to a serial dilution mating test as described in Figure 2. The first two dilution spots are shown. The plasmids used were pRS316, pWS601, pWS602, and pWS727.

B) The ability of over-expressed Ste23p to enhance RSM was evaluated for CaaX motifs that were previously identified as either not promoting (e.g. CVIA and CDQQ) or promoting RSM (e.g. CKQQ). The plasmids used were pWS602, pWS610, pWS727, and pWS853. The experiments shown in Panels A and B were performed on separate days and a slight variation in mating efficiency is apparent for the same strain, which is labeled *STE23* in Panel A and CKQQ in Panel B.

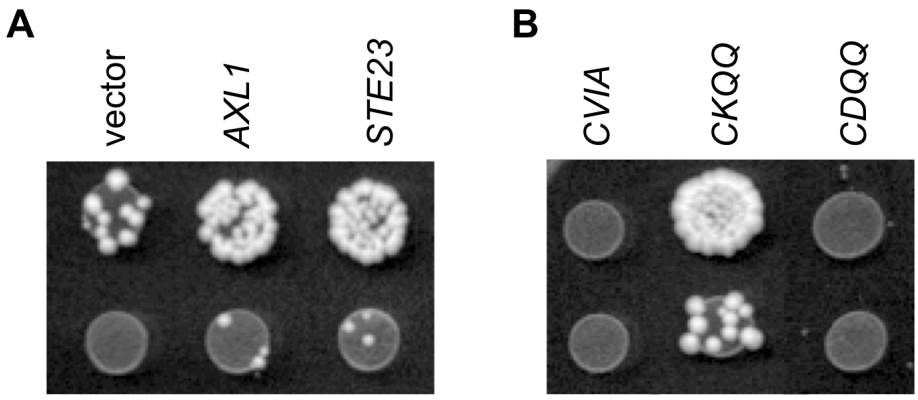
A
vector
AXL1
STE23
B
CVIA
CKQQ
CDQQ

Figure B.6. *The N-terminal extension of **a**-factor modulates RSM.*

A) Cartoon depicting the proteolytic cleavage sites in the **a**-factor precursor and ubiquitin fusions created to bypass certain proteolytic steps associated with **a**-factor biogenesis. See text for additional details on the ubiquitin fusions.

B) Ubiquitin fusions to various lengths of the **a**-factor precursor were expressed in either SM2331 or yWS164, and the strains subjected to a serial dilution mating test as described in Figure 2. The plasmids used were pRS316, pSM1366, pSM1368, and pSM1369.

C) A mating test was performed as described in panel B using ubiquitin-**a**-factor fusions appended with the CKQQ motif. The plasmids used were pRS316, pWS892, pWS893, and pWS894.

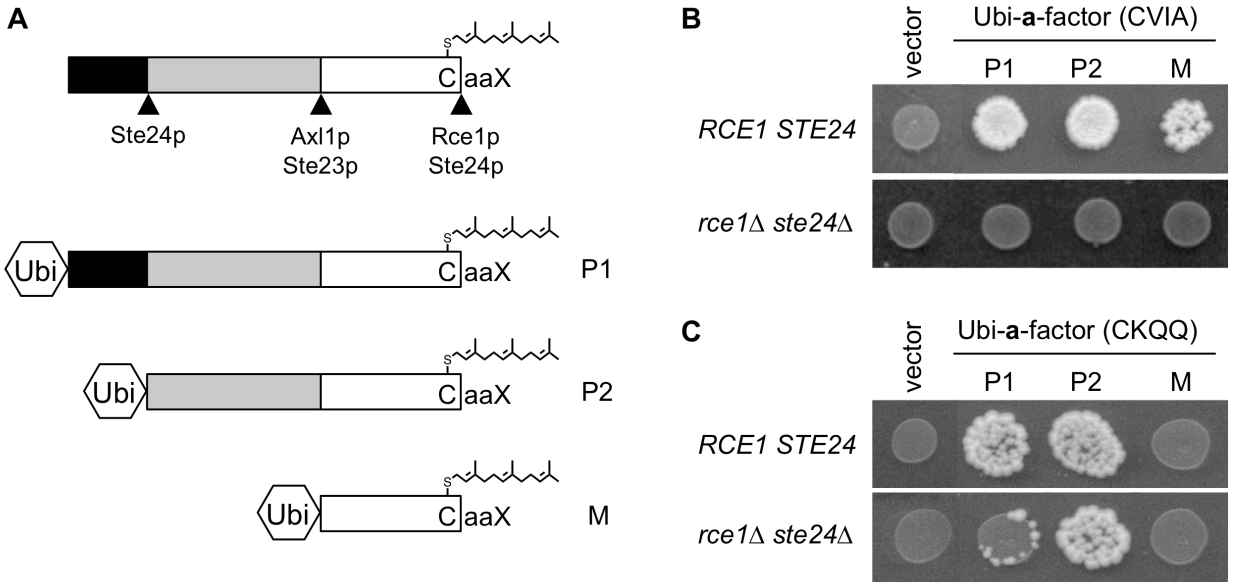
A
C aaX
Ste24p
Axl1p
Ste23p
Rce1p
Ste24p
Ubi
P1
P2
M
B
vector
Ubi-a-factor (CVIA)
P1
P2
M
RCE1 STE24
rce1Δ ste24Δ
C
vector
Ubi-a-factor (CKQQ)
P1
P2
M
RCE1 STE24
rce1Δ ste24Δ